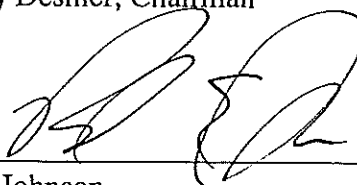


To The Graduate School:

The members of the committee approve the dissertation of David Delene presented on December 10, 1998.



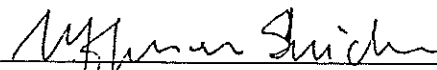
Terry Deshler, Chairman



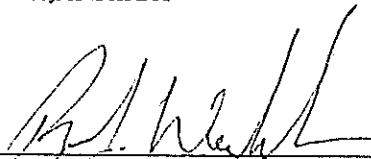
Paul Johnson



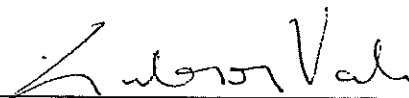
Alfred Rodi



Jefferson Snider

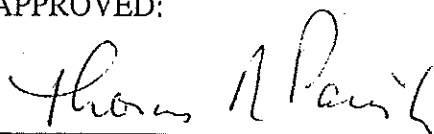


Perry Wechsler



Gabor Vali

APPROVED:



Thomas R. Parish, Head, Department of Atmospheric Science

Stephen E. Williams, Dean, The Graduate School

Delene, David J., Vertical Profiles of Cloud Condensation Nuclei at Midcontinental Sites Through the Development and Use of a Balloon-borne Instrument, Ph. D., Department of Atmospheric Science, December, 1998.

A balloon-borne instrument was developed for observations of vertical profiles of cloud condensation nuclei (CCN) number concentration. The CCN concentration is deduced from measurements of the laser light scattered by water droplets that activated on CCN within a cloud chamber. The amount of light scattering is proportional to the number of droplets that form within the chamber. The instrument is calibrated by correlating the number of droplets within a sample volume with the amount of scattered light. The balloon-borne CCN counter has been flown on 12 balloon flights at Laramie, Wyoming (41 °N) and 2 balloon flights at Lauder, New Zealand (45 °S). The instrument gondola for each of these flights also contained a condensation nuclei (CN) counter and an optical particle counter to measure aerosols with diameter greater than 0.3 μm ($D_{0.3}$). The vertical profile measurements from the 14 flights have been summarized by classifying them into five distinct atmospheric layers: surface, lower tropospheric, upper tropospheric, stratospheric and regions of high humidity. Laramie summer and winter profiles show that the mean CCN concentration decreases between the lower and upper tropospheric layers (445 cm^{-3} to 126 cm^{-3} in summer; 146 cm^{-3} to 64 cm^{-3} in winter). Variations in the vertical profile of CCN concentration were typically positively correlated with changes in CN and $D_{0.3}$ concentrations, and often corresponded with changes in relative humidity, typically being positively correlated but sometimes negatively correlated. The CCN/CN ratio typically increases between the lower and upper troposphere. The summer CCN concentrations at Lauder, New Zealand (45 °S) were about twice the summer CCN concentrations measured at Laramie, Wyoming (41 °N) while the CN and $D_{0.3}$ concentrations were about the same.

VERTICAL PROFILES OF CLOUD CONDENSATION
NUCLEI AT MIDCONTINENTAL SITES THROUGH
THE DEVELOPMENT AND USE OF A BALLOON-
BORNE INSTRUMENT

By
David J. Delene

A dissertation submitted to the Department of Atmospheric Science and Graduate School
of the University of Wyoming in partial fulfillment of requirements for the degree of

DOCTOR OF PHILOSOPHY
in
ATMOSPHERIC SCIENCE

Laramie, Wyoming
December, 1998

Acknowledgments

Lyle Womack and Jason Gonzales provided engineering support in conducting balloon flights and assistance in laboratory work. Special thanks to Fred Brechtel of Colorado State University for sharing his computer programs to obtain aerosol size spectrums and CN concentrations. Fred Brechtel also provided advice in using the differential mobility analyzer to generate monodisperse aerosols. Greg Roberts profiled a copy of his AAAR poster and valuable discussions about his experience in calibrating a photometric CCN counter. Diane LeBlanc from the University's Writing Center helped with editing the dissertation. Committee members, Terry Deshler, Paul Johnson, Alfred Rodi, Jefferson Snider, Perry Wechsler, and Gabor Vali provided support, suggestion, and comments throughout my dissertation research. Thanks to fellow graduate students Bill Bellon and Bill Hoffman for stimulating discussing about my research. This research was supported by a grant from the National Aeronautics and Space Administration.

Table of Contents

Acknowledgments.....	ii
Table of Contents.....	iii
List of Figures	iv
List of Tables	vi
CHAPTER 1: Introduction	
1. Overview	1
2. Cloud Condensation Nuclei.....	2
3. Review of Cloud Condensation Nuclei Measurements.....	4
4. Modeling the Climate Affects of Cloud Condensation Nuclei	6
5. Sources of Cloud Condensation Nuclei	7
6. Research Objectives	10
CHAPTER 2: Calibration of a Photometric Cloud Condensation Nucleus Counter Designed for Deployment on a Balloon Package	
Abstract	13
1. Introduction	14
2. Standard Calibration Procedure	15
3. Testing the Standard Calibration Procedure	18
4. Calibration Dependence on Supersaturation	19
5. Calibration Dependence on Aerosol Type	21
6. Calibration Error	24
7. Conclusions	26
CHAPTER 3: Vertical Profiles of Cloud Condensation Nuclei Above Wyoming and New Zealand	
Abstract	37
1. Introduction	38
2. Atmospheric Aerosol Layers.....	42
3. Summary of Laramie, Wyoming Aerosol Profiles	47
4. Comparison between Wyoming and New Zealand Profiles.....	50
5. Conclusions	51
CHAPTER 4: Conclusions	
1. Summary.....	59
2. Future Work	61
References	67
Appendix I:	
1. Aerosol Volatility Measurements.....	73
Appendix II	
1. CCN Counter Calibration Procedure.....	76
2. Balloon-borne CCN Counter's Calibration History.....	80
Appendix III:	
1. CCN Counter Data Processing	82
2. Standard Plot of all Balloon Flights	83

List of Figures

- Figure 1.** Continental CCN profiles obtained from aircraft measurements. The measurement location and percent supersaturation are given for each profile. The Miles City, Montana profiles are from *Hobbs et al.* [1985], the Arizona, Alaska and Southern Florida profiles are from *Hoppel et al.* [1973], and the Southern Germany profile is from *Schafer and Georgii* [1994]. 12
- Figure 2.** The photodetector voltage peak versus the number of droplets counted within the video sample volume and the corresponding droplet concentration. Droplets are counted at the time of the photodetector voltage peak. The droplets nucleated on polydisperse NaCl aerosols produced using a solution of 0.1 g/L of NaCl in an ultrasonic vaporizer. The calibration slope (solid line) is the least squares linear fit to the data with a forced zero y-intercept. 28
- Figure 3.** Measurements of the concentration of 120 nm monodisperse NaCl aerosols using the CCN counter at 1% supersaturation (circles) and CN counter (solid line). The CCN concentration is measured using the video camera to count droplets over a predetermined video sample volume. The CCN concentration is averaged over approximately 20 samples (10 min) with the standard deviation given by the error bars. The decrease in concentration with time is the result of aerosol being removed to the walls of the sampling bag. Filtered air was continuously added to the sampling bag after 115 minutes. 29
- Figure 4.** The CCN counter's calibration slope dependence on supersaturation. The data are fitted using the equation, $C = \text{Alpha} + \text{Beta}/SS$, where Alpha and Beta are calibration constants, SS is the chamber supersaturation, and C is the calibration slope. Error bars represent one standard derivation in the calculated calibration slope. 30
- Figure 5.** Time versus the average ratio of the droplet number (dashed line) and the average ratio of the photodetector voltage (solid line). The definition of the average ratio is given in the text. The legends give the average and standard deviation times for the peak number of droplets and peak photodetector voltage. Time zero is at the beginning of a 5 s chamber flush. Following the chamber flush, an air sample is captured within the chamber, CCN active and droplets form, grow and begin to fall. 31
- Figure 6.** Supersaturation of the CCN counter versus the average time to reach the peak. The error bars on the photodetector voltage time are one standard deviation of the average. Error bars (not shown) on the average time to reach the droplet number peak are similar. The left axis and solid triangles denote the time between the droplet number peak and photodetector voltage peak. 32
- Figure 7.** Examples of the aerosol size spectrum generated using a solution of 0.1 g/L of NaCl in an ultrasonic vaporizer. Legend gives the total number concentration (in cm^{-3}) for each aerosol size spectrum. 33
- Figure 8.** CCN counter calibration data using aerosol from the ambient atmosphere outside the laboratory building in Laramie, Wyoming. The photodetector voltage peak versus the number of droplets counted within the video sample volume and the corresponding droplet concentration are shown. Droplets are counted at the time of the photodetector voltage peak. The calibration slope (solid line) is the least squares linear fit to the data with a forced zero y-intercept. 34

Figure 9. Aerosol profiles that include the smallest size channel of the optical particle counter ($D > 0.3 \mu\text{m}$, thin line), the CCN concentration (1% supersaturation, circles), and the CN concentration ($D > 0.01 \mu\text{m}$, thick line). Open circles represent measurements below the detection limit of the CCN counter. The concentration measured by each aerosol instrument has been corrected to standard temperature and pressure (STP). Equivalent potential temperature (thick line) and relative humidity (thin line) are shown in the right-hand panel. The left axis denotes the measured atmospheric pressure and the far right axis denotes the altitude above mean sea level. The surface at Laramie, Wyoming is at approximately 2.2 km above mean sea level. The horizontal lines on the far right of the equivalent potential temperature plots denote the lower (solid lines) and upper (dashed lines) tropospheric layers. 54

Figure 10. Summer and winter measurement of an optical particle counter ($D > 0.3 \mu\text{m}$, circles), a CCN counter (1% supersaturation, squares), and a CN counter ($D > 0.01 \mu\text{m}$, asterisks) for balloon flights at Laramie, Wyoming. The error bars represent one standard deviation for the measured concentrations within the layer. The aerosol concentrations have been corrected to standard temperature and pressure (STP). Due to instrument problems, some data are missing. The average and standard deviation for the balloon flight data presented in each plot is displayed within the plot. Only measurements above the detection limit of the CCN counter are included, so the upper troposphere CCN concentration may be biased to higher concentration, especially for winter measurements. 55

Figure 11. Aerosol ratios for summer and winter flights at Laramie, Wyoming. The average and standard deviation for the lower tropospheric (top line) and upper tropospheric (bottom line) layers are displayed in the legends. The aerosol ratios are computed by averaging aerosol measurements within a layer and then taking the ratio of the aerosol averages. 56

Figure 12. Summer and winter $D_{0.3}$ (circles), CCN (squares), and CN (asterisks) gradients for the lower and upper tropospheric layers. Negative gradients indicate a percentage decrease in concentration with increasing height above the surface. The averages and standard deviations of the layer data presented in each plot are displayed in the legends. 57

Figure 13. Examples of the aerosol size spectrum generated using a solution of 0.1 g/L of NaCl in a model 3075 TSI constant output atomizer. Legend gives the total number concentration, in cm^{-3} , for each aerosol size spectrum. 66

Figure 14. Plot showing the average upper tropospheric $D_{0.3}$ (circles), CCN (squares), and CN (asterisks) concentrations for each summer balloon descent profile obtain in Laramie, Wyoming. Histograms showing the ratio of heated (160°C) descent to 40°C ascent aerosol concentration ratios for all summer flights at Laramie, Wyoming. 75

Figure 15. Calibration constants for the CCN counter using the peak calibration method. The old video camera calibration constant is based on a 0.0314 cm^{-3} video sample volume and the new video camera calibration constant is based on a 0.0707 cm^{-3} video sample volume. The legend indicates the concentration of the NaCl solution using in the vaporizer to produce the calibration aerosol. 81

List of Tables

- Table 1.** Calibration of the balloon-borne CCN counter at 1% supersaturation. The first column gives the calibration aerosol type: laboratory produced aerosol using a solution of 0.1 g/L NaCl in a vaporizer, monodisperse NaCl aerosol of different diameters, or aerosol from the ambient atmosphere outside the laboratory building. The second column gives the calibration slope using the photodetector voltage peak. The third column gives the calibration slope using a three-point sum around the photodetector voltage peak [Delene *et al.*, 1998]. The fourth column gives the average time to reach the number peak in seconds since the beginning of the sample. The last column gives the average time to reach the voltage peak in seconds since the beginning of the sample. The first 3 rows give the results of the standard calibration of the CCN counter in March, June, and, October 1998. The CCN counter was removed from the laboratory calibration bench between each standard calibration of the CCN counter and used elsewhere. The calibrations presented in rows 3-10 were preformed using the same focus and video camera alignment with the CCN counter..... 35
- Table 2.** Time to reach the photodetector voltage peak for field measurements in Laramie, Wyoming (41 °N), Lauder, New Zealand (45 °S), and Fairbanks, Alaska (65 °N). Due to a clear difference in aerosol concentration, the field measurements are divided into summer and winter seasons. The third column gives the average and standard deviation of the time to reach the photodetector voltage peak. The fourth column gives the number of samples used to compute the average..... 36
- Table 3.** Average aerosol concentrations and standard deviations in the lower and upper troposphere for summer balloon flights at Laramie, Wyoming (7 flights) and Lauder, New Zealand (2 flights). The aerosol ratios are computed by averaging measurements within a layer and then taking the ratio of the aerosol averages. Negative aerosol gradients indicate a decrease in concentration with increasing height above the surface..... 58

CHAPTER 1: Introduction

1. Overview

This dissertation focuses on conducting measurements of the vertical structure of cloud condensation nuclei (CCN) concentrations from the surface to the top of the troposphere, and relating these CCN measurements to coincident aerosol measurements of different sizes. The dissertation is divided into six parts. Chapter 1 provides background information on CCN measurements and defines the research objectives. Chapter 2 describes results of laboratory calibration work on the balloon-borne CCN counter. Chapter 3 summarizes results from 14 high-resolution CCN profiles. Chapter 4 summarizes the conclusions of the dissertation and suggests future research. Appendix I discuss aerosol volatility measurements. Appendix II and III provide technical information concerning the calibration of the CCN counter and the processing of the balloon flight CCN measurements.

The calibration results presented in Chapter 2 and the summary of the balloon flight measurements presented in Chapter 3 extends research I published in the Journal of Geophysical Research [Delene *et al.*, 1998]. Chapters 2 and 3 are written as stand-alone documents for submission to peer reviewed journals. Chapter 2 is planned for a technical journal such as the Journal of Atmospheric and Oceanic Technology. Chapter 3 is planned for the Journal of Geophysical Research. Since Chapters 2 and 3 are stand-alone documents, they each have an abstract, introduction and conclusion and may repeat some information that is presented elsewhere in this dissertation. The figures and tables for each chapter are placed at the end of the chapter, as required for journal submissions. All references contained within this dissertation are listed in the reference section on page 67.

2. Cloud Condensation Nuclei

Cloud droplets in the atmosphere form via heterogeneous nucleation involving aerosol particles. Aerosol particles that are capable of initiating cloud droplet formation at supersaturations observed in the atmosphere are called cloud condensation nuclei (CCN). All aerosol particles are capable of initiating droplet formation if the supersaturation of water vapor in the environment is high enough. Aerosol particles that form droplets at supersaturations of several hundred percent are called condensation nuclei (CN). The CN concentration is the total number of droplets per unit volume observed in a cloud chamber at supersaturations of several hundred percent. Similarly, the CCN concentration is the total number of droplets per unit volume observed in a cloud chamber at a supersaturation typically observed in the atmosphere. Characteristic supersaturations within the atmosphere are most often below 1%. Therefore, the CCN concentration is always less than the CN concentration, and aerosol particles that act as CCN are a subset of the aerosol particles that act as CN.

The size and chemical composition of an aerosol particle determine if it will activate and produce a cloud droplet. Larger-sized aerosols activate at lower supersaturations than smaller-sized aerosols. Hygroscopic aerosols (soluble aerosols that have an affinity for water) activate at lower supersaturations than aerosols that are insoluble. The effects of aerosol size and chemical composition is incorporated into the Kohler equation which predicts if an aerosol will activate to produce a cloud droplet in a supersaturated environment [*Pruppacher and Klett, 1997*]. Good agreement was obtained between modeled and measured CCN concentrations during a recent field campaign [*Covert et al., 1998*]. Kohler theory was used to model the CCN concentration using the aerosol number distribution and data on the aerosol's hygroscopic growth. *Chylek and Wong [1998]* recently showed that the original Kohler equation, with a variable van't Hoff factor,

agrees with experimental data of the condensational growth of a single levitated ammonium sulfate solution droplet.

CCN measurements determine the concentration of aerosols that have a size and composition to activate and produce cloud droplets at a certain environmental supersaturation. CCN measurements at several supersaturations can be obtained to construct a CCN spectrum. CCN spectra often can be expressed in the form (Twomey, 1959):

$$n = cS^k \quad (1)$$

Equation (1) shows that the CCN concentration, n , in units of cm^{-3} , can be related to the supersaturation, S , by two parameters, c and k . Parameter c is the CCN concentration at 1% supersaturation, and parameter k indicates how CCN concentration depends on supersaturation. The cloud droplet concentration resulting from lifting an air parcel is predicted by (1) if c and k are known or assumed. As an air parcel is lifted, the parcel's temperature decreases resulting in an increase in relative humidity. When the relative humidity increases above 100%, a supersaturated environment is created and a subset of the aerosol population activates to serve as CCN. As CCN activate and grow by the condensation of water vapor, they increasingly offset the increase in supersaturation caused by lifting an air parcel [Hobbs, 1993]. This competition between supersaturation increasing due to lifting an air parcel and supersaturation decreasing due to uptake of water vapor by droplets results in the supersaturation reaching a peak value and then declining. The peak supersaturation depends on the CCN spectrum and updraft speed [Rogers and Yau, 1989]. Forest fires [Eagan *et al.*, 1974] and paper mills [Hindman *et al.*, 1977] have been shown to produce large amounts of CCN and thus change the droplet concentration of clouds. Chuang *et al.* [1992] found agreement between a microphysical entrainment model and measurements of the cloud droplet spectra for the initial stage of cloud development over large

fires. *Hegg et al.* [1991] presented observations showing a relationship between CCN concentration at 1% supersaturation and mean concentration of droplets in marine stratus clouds.

Since the number concentration and activity of CCN have a large influence on cloud droplet spectra, CCN affect precipitation processes, cloud albedo, and global climate [*Hobbs*, 1993; *Jennings*, 1993; *Charlson and Heintzenberg*, 1995]. Increases in CCN concentration, resulting from increased SO₂ emissions, has been suggested as possibly offsetting global temperature change expected from increased CO₂ concentrations [*Wigley*, 1989; *Twomey*, 1991]. CCN directly affect climate by scattering and absorbing radiation and indirectly affect climate by altering the scattering characteristics of clouds [*Charlson et al.*, 1992]. Increases in CCN concentrations may alter global scale radiative characteristics by increasing cloud albedo and by increasing cloudiness. Global scale analysis of cloud droplet effective radii found systematic differences between continental and maritime environments and hemispheric contrasts that are indicative of differences in CCN concentration [*Han et al.*, 1994]. Statistical analysis of the change in total oceanic cloud amount between 1930 and 1981 shows a significant positive trend of increased cloudiness which may be the result of an increase in SO₂ emissions [*Panrungo et al.*, 1994]. Decreases in precipitation efficiency, resulting from increases in CCN concentration, may be responsible for an increase in cloudiness [*Albrecht*, 1989].

3. Review of Cloud Condensation Nuclei Measurements

Several studies have measured CCN number concentration near the earth's surface [*Hudson and Squires*, 1978; *Hudson and Frisbie*, 1991; *Philippin and Betterton*, 1997], and field campaigns have used aircraft to measure CCN concentrations aloft [*Hobbs et al.*, 1985; *Hudson and Xie*, 1998]. *Twomey and Wojciechowski* [1969] reported the parameters in equation 1 as; $c = 600$ and $k = \frac{1}{2}$ for continental air and $c=100$ and $k = \frac{1}{2}$ for maritime air. Numerical cloud models

have shown that the dependence on k can be quite weak [Hegg *et al.*, 1991]. Therefore, the CCN concentration at 1 % supersaturation may be the most important parameter for predicting the cloud droplet concentration. Pruppacher and Klett [1997] summarize c and k values measured at different geographic locations. Currently the only long term CCN monitoring program is the Australian "Atmospheric Baseline" program at Cape Grim. Measurements at Cape Grim show that the CN concentration has increased by about 1.2% per year while the CCN concentration has decreased by about 3% per year [Gras, 1995]. Recently Philippin and Betterton [1997] began a CCN monitoring program at an isolated continental mountain site in Arizona.

The number of research projects that have measured CCN concentrations aloft is similar to the number of research projects that have measured CCN concentrations at the earth's surface. This is the result of the importance of CCN measurements to cloud microphysics studies. Figure 1 presents examples of vertical CCN profiles obtained using aircraft. The profiles consist of four to six measurements ranging from the surface to a maximum height of approximately 5 km. The profiles show a general decrease in CCN concentration with increasing height above the surface; however, due to the low vertical resolution of the profiles, it is difficult to discern if the source of CCN is near the surface or if there is a major source within the atmosphere. The CCN measurements in Figure 1 do not show a systematic decrease in concentration with decreasing supersaturation. This indicates that CCN concentrations are highly variable and that a few measurement locations are insufficient to determine the global scale distribution of CCN. Aircraft measurements of CCN (Figure 1) have almost exclusively been confined to the lower troposphere. Upper tropospheric CCN measurements conducted by Hudson and Xie [1998] found constant CCN concentrations with increasing altitude above the lower troposphere.

There is a great deal of research interest in marine CCN due to the larger susceptibility of marine clouds, compared with continental clouds, to increases in cloud albedo resulting from increases in CCN concentration [Twomey, 1991]. The larger susceptibility of marine clouds is the result of lower CCN concentrations over oceans than over continents [Hobbs, 1993]. Numerous CCN measurements in marine environments have been made to investigate how cloud droplet spectra, and hence cloud albedo, relate to CCN concentration [Hudson, 1993a; Hudson, 1995]. Lower tropospheric CCN measurements in the Arctic Ocean found concentrations of less than 100 cm^{-3} at 1% supersaturation [Hegg *et al.*, 1995]. Lower tropospheric CCN measurements in the summertime Southern Ocean found concentrations of approximately 200 cm^{-3} at 1% supersaturation [Hudson, 1998]

4. Modeling the Climate Affects of Cloud Condensation Nuclei

Direct climate forcing by aerosols has started to be incorporated into global climate models [Boucher and Anderson, 1995; Haywood and Shine, 1995]. Global climate models have been developed that predict the aerosol mass concentration of anthropogenic and natural sulfate [Langner and Rodhe, 1991; Langner *et al.*, 1992; Taylor and Penner, 1994]. The predicted aerosol mass is based on oxidation of gaseous dimethyl sulfide (DMS) and sulfur dioxide (SO_2). The predicted mass concentration is assumed to reside in the accumulation mode of the aerosol number distribution. The accumulation mode contains aerosols ranging in size from approximately $0.1 \text{ }\mu\text{m}$ to $1.0 \text{ }\mu\text{m}$ diameter [Singh, 1995]. Global climate models determine the direct forcing by aerosol by using the predicted aerosol mass and a parameterization of the aerosol's optical properties [Boucher and Anderson, 1995]. The direct anthropogenic climate forcing is determined by comparing the direct climate forcing by natural sulfate aerosols with the direct climate forcing resulting from natural and anthropogenic sulfate aerosol.

It is more difficult to incorporate indirect climate forcing by aerosols than direct climate forcing into global climate models since aerosol number distribution, not aerosol mass, is important. Climate models incorporate aerosol number distribution by parameterizing lognormal size distributions. A parameterization is then used to relate the aerosol number concentration to the cloud droplet number concentration [Pan *et al.*, 1998]. Chuang *et al.* [1997] recently addressed indirect anthropogenic forcing by using a coupled climate/chemistry model to predict changes in the aerosol number distribution due to anthropogenic sulfate. Pan *et al.*, [1998] investigated indirect forcing of CCN using the method of Charlson *et al.* [1992] to determine changes in aerosol number concentration due to anthropogenic sulfate and three different parameterizations [Twomey, 1977; Jones *et al.*, 1994; Ghan *et al.*, 1993] to relate changes in aerosol number concentration to changes in cloud droplet concentration. They concluded that refining the input parameters might be more important than improving models to minimize uncertainties. Penner *et al.*, [1994] stated that the limited understanding of the indirect forcing of aerosol requires more research before it is understood well enough to be fully incorporated into global climate models. Liu *et al.*, [1996] noted that further knowledge of the relationships between cloud condensation nuclei and the aerosol size distribution is necessary to support modeling of the indirect effect of aerosols.

5. Sources of Cloud Condensation Nuclei

The formation, growth, and transport processes of cloud condensation nuclei (CCN), along with their chemical composition, still pose unresolved questions. The main obstacle to answering these questions lies in identifying the sources of CCN, and the times and regimes in which they are important. Four potentially important sources of aerosols that act as CCN are: 1) direct emissions of anthropogenic aerosol, 2) surface derived aerosol, 3) aerosol resulting from

gas-to-particle conversion, possibly involving cloud processes, and 4) aerosol of stratospheric origin transported downward into the troposphere. Direct anthropogenic sources of CCN are certainly important in some cases [Hobbs, 1970, Hudson, 1991]; however, they are believed not to dominate the global CCN budget, and will thus be negligible at remote sites. Hudson [1993b] noted in a review of CCN that understanding the degree to which anthropogenic sources contribute to the increase in continental CCN concentrations, compared to marine CCN concentrations, is a major challenge for researchers.

Initial studies of CCN indicated that the Earth's surface is an important source [Hoppel *et al.*, 1973]. More recent studies have shown that decreases in CCN concentration with height are usually observed in association with more polluted environments, and only a slight decrease in concentration with height is observed in a clean environment [Raga and Jonas, 1995]. The large decrease with height in polluted environments is probably due to anthropogenic sources, while the slight decrease in concentration is the result of a natural source of CCN. Near surface CCN measurements show that deposition rather than production occurs at the earth's surface, which indicates that a near surface source would have to be a diffuse source within the surface layer [Hudson and Squires, 1978].

A large amount of recent research has focused on clouds as a possible important source for CCN as well as a sink [Hegg, 1990; Hegg, 1991; Lin *et al.*, 1992; Saxena and Grovenstein, 1994; Saxena, 1996]. Clouds are postulated to be a source of CCN by creating an environment where new particles can be produced by homogeneous-bimolecular nucleation of sulfuric acid solution droplets from H_2SO_4 and H_2O vapor molecules [Perry and Hobbs, 1994]. The recently nucleated particles grow by uptake of vapor and coagulation of aerosols [Salk *et al.*, 1986], to attain sizes large enough to act as CCN. The observations of Radke and Hobbs [1991] of high total particle

concentrations in regions of high humidity suggests that relative humidity plays an important role in new particle production. *Clarke's* [1992, 1993] observations in the remote Pacific midtroposphere show an inverse relationship between available aerosol surface area and new particle concentration. Furthermore, the aerosol volatility data suggests a sulfuric acid composition, which supports recent homogeneous-bimolecular nucleation of the aerosols. *Clarke* [1993] presented evidence of a latitudinal gradient in ultrafine CN concentration with a large increase above the strong convective region associated with the intertropical convergence zone. *Bigg et al.* [1984] presented evidence of a link between the amount of solar radiation and the concentration of total particles in remote regions of the Southern Hemisphere. Taken together, these observations make a case for the importance of gas phase nucleation of sulfuric acid, and subsequent growth, as an important source of CCN in the remote troposphere. Observation and model studies indicate that favorable conditions for the production of new particles are high relative humidity, low total aerosol surface area, low temperatures, high SO₂ concentrations, and high solar radiation.

Stratospheric aerosol may also be a source for tropospheric CCN. Stratospheric aerosols are composed of sulfuric acid and water [*Rosen*, 1971, *Deshler et al.*, 1992] and thus should act as effective CCN. Stratospheric-tropospheric exchange occurring in association with irreversible eddy exchange phenomena provides a transport mechanism [*Holton et al.*, 1995]. Although several vertical profiles of CCN have been obtained with aircraft [*Squires and Twomey*, 1966; *Hoppel et al.*, 1973; *Hobbs, et al.*, 1985; *Hegg et al.*, 1995; *Raga and Jonas*, 1995], none of the vertical profiles presented in the literature extend into the lower stratosphere. *Rogers et al.*, [1981] measured stratospheric CCN concentration, activated at 1% supersaturation, in the range of 100 to 1000 cm⁻³. These stratospheric CCN concentrations are higher than the CCN

concentration below the tropopause. Indirect evidence of a stratospheric source of CCN comes from satellite occultation measurements of $1.0\ \mu\text{m}$ extinction which exhibits contamination of the upper troposphere by stratospheric aerosol [Kent *et al.*, 1988; Kent *et al.*, 1991]. Recent observations suggest that volcanic eruptions may affect the microphysical properties of clouds by changing stratospheric aerosol concentrations which will subsequently affect tropospheric clouds [Minnis *et al.* 1993; Wang *et al.*, 1995]. Mohnen [1990] points out that stratospheric CCN may influence the microphysics of cirrus clouds due to the relatively low concentration of ice nuclei. Hofmann [1993] presented twenty years of balloon-borne aerosol measurements that show a decrease in CN but an increase in aerosols with a diameters larger than $0.3\ \mu\text{m}$ ($D_{0.3}$) above the tropopause. Since CCN comprise a subset of CN and $D_{0.3}$ are a subset of CCN, these measurements do not clearly suggest a gradient of CCN across the tropopause.

6. Research Objectives

The purpose of this research is to examine the vertical structure of CCN concentrations from the surface to the top of the troposphere and to relate these measurements to concurrent measurements of CN and aerosol larger than $0.3\ \mu\text{m}$ diameter. These measurements can be used to examine the source of CCN at clean continental sites. Balloon-borne instruments are used to obtain high-resolution vertical concentration profiles of CN, CCN, and large aerosols. The highest CCN concentration within the vertical profile suggests CCN source regions. Currently available CCN profiles (Figure 1) do not have the vertical resolution to clearly indicate if the largest concentration of CCN is near the surface or aloft. The second objective of this research is to investigate the vertical variation of CCN from the surface to the top of the troposphere. Small-scale changes in CCN concentration will be discernible in the CCN profiles. CCN measurements throughout the vertical extent of the troposphere will allow for the detection of layers with

constant CCN concentration. The third objective of this research is to determine the relationship between CCN measurements and other concurrent aerosol measurements. Other aerosol measurements are obtained concurrently with the CCN measurements by using a balloon-borne CN counter and optical particle counter. The optical particle counter measures the number concentration of aerosols with a diameter greater than $0.3\ \mu\text{m}$ ($D_{0.3}$). Ratios of CCN/CN and $D_{0.3}$ /CCN will be determined throughout the vertical extent of the troposphere. The temporal variability of CCN profiles will be illustrated by comparing at Laramie, Wyoming, at different times of the year. The fourth objective of this research is to compare measurements made above Laramie, Wyoming (41°N), to measurements made above Lauder, New Zealand (45°S). Central to obtaining the research objectives is the development of an accurate calibration procedure for the balloon-borne CCN counter at 1% supersaturation. An accurate calibration is critical to obtaining dependable CCN/CN and $D_{0.3}$ /CCN ratios. Furthermore, the calibration of the CCN counter is necessary to ensure consistency within the data set when fundamental changes to the CCN counter are performed.

Continental Profiles

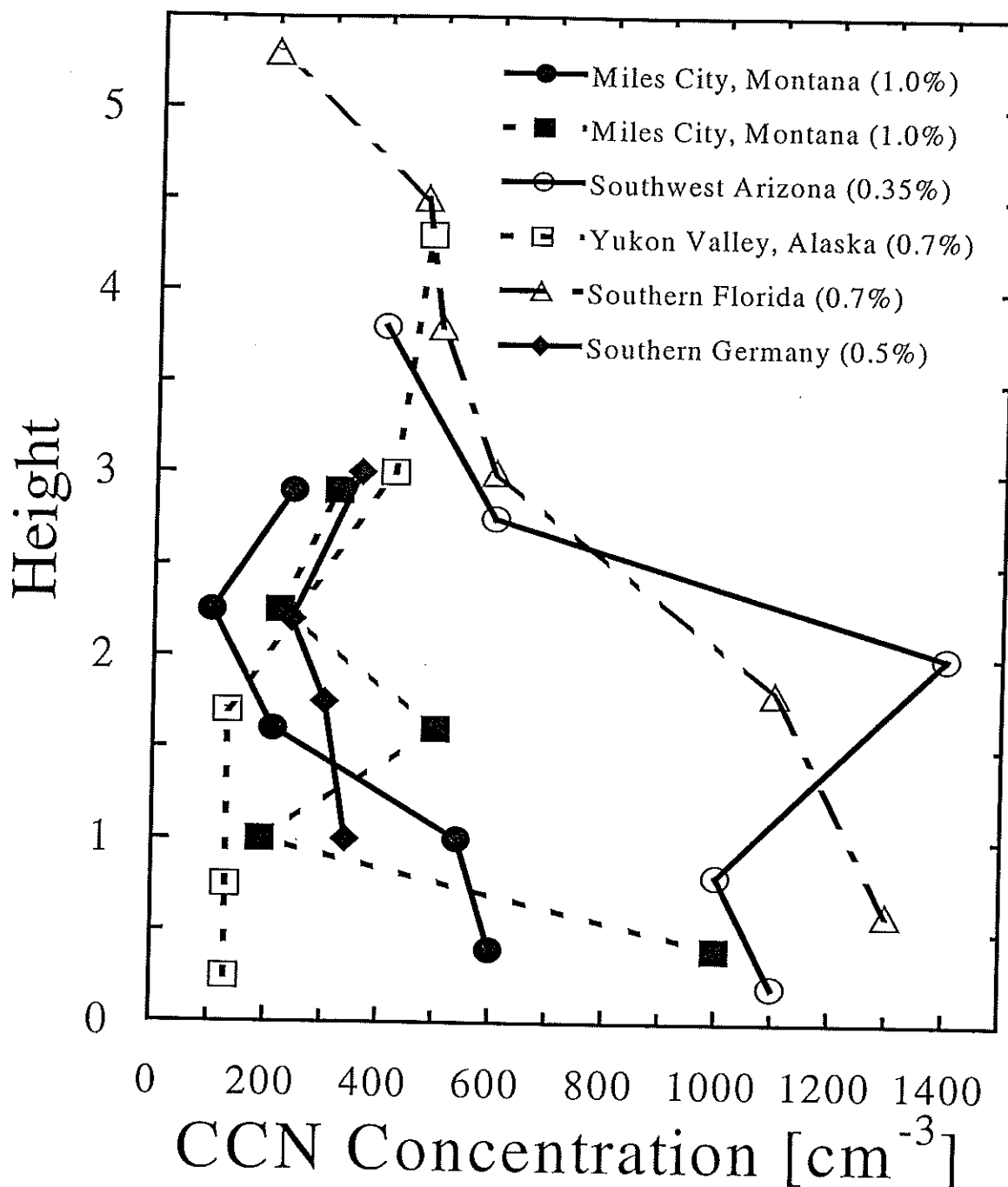


Figure 1. Continental CCN profiles obtained from aircraft measurements. The measurement location and percent supersaturation are given for each profile. The Miles City, Montana profiles are from *Hobbs et al.* [1985], the Arizona, Alaska and Southern Florida profiles are from *Hoppel et al.* [1973], and the Southern Germany profile is from *Schafer and Georgii* [1994].

CHAPTER 2: Calibration of a Photometric Cloud Condensation Nucleus Counter Designed for Deployment on a Balloon Package

Abstract

The importance of atmospheric aerosols in understanding global climate changes has renewed interest in measurements of cloud condensation nuclei (CCN). To obtain high-resolution (125 m) vertical profiles of CCN number concentration, a balloon-borne instrument was developed. The instrument deduces the CCN concentration from measurements of laser light scattered by water droplets that condense on CCN within a static thermal gradient-diffusion chamber. The amount of light scattering is linearly proportional to the number of droplets within the diffusion chamber. Correlating the number of droplets within the sample volume with the amount of light scattered by the droplets provides the instrument's calibration. The calibration was tested by comparisons between the CCN counter and a CN counter when sampling monodisperse aerosol larger than the CCN counter's critical activation size. The CCN counter's calibration depends on supersaturation and slightly on the size of CCN that activate to form droplets. The calibration dependence on CCN size is less than 10% at 1% supersaturation. Calibration on ambient atmospheric aerosol is similar to calibration on laboratory-generated polydisperse NaCl aerosol indicating that the laboratory calibration can be applied to field measurements. The activation and growth of droplets within the diffusion chamber is similar during field and laboratory measurements. The accuracy of the balloon-borne CCN counter's calibration is approximately 10% at 1% supersaturation.

1. Introduction

Cloud condensation nuclei (CCN) have a major influence on the cloud droplet number concentration and hence the radiative properties of clouds. Increases in CCN concentrations, resulting from increased SO₂ emissions, has been suggested as a mechanism which could modify clouds properties sufficiently to affect global climate [Wigley, 1989; Twomey, 1991]. The indirect affect of CCN on climate has started to be incorporated into global climate models [Meehl *et al.*, 1996; Chuang *et al.*, 1997; Pan *et al.*, 1998]. Pan *et al.*, [1998] concluded from comparisons of climate models that refining input parameters might be more important than improving models to minimize uncertainties. CCN measurements are an important link in relating changes in aerosol concentration to changes in cloud droplet number concentration [Boucher and Lohmann, 1995; Liu *et al.*, 1996]. A balloon-borne CCN counter has been developed to provide vertical profiles of CCN with a resolution of approximately 125 m. To relate these CCN measurements to concurrent aerosol measurements, an accurate calibration of the CCN counter is critical. The main objective here is to describe the calibration of the balloon-borne CCN counter and determine the accuracy of field measurements.

The balloon-borne CCN counter is similar to other static thermal-gradient diffusion chamber instruments [Lala and Jiusto, 1977; Bartlett and Ayers, 1981; Hoppel and Wojciechowski, 1981; Lala, 1981]. A 670 nm solid-state laser illuminates the center of the chamber where the supersaturation is held at a prescribed value. To keep the instrument lightweight, a photodetector, instead of a photographic or CCN camera, is used to measure the CCN concentration. The photodetector voltage relates the amount of scattered light to a known CCN concentration using the instrument's calibration. To obtain a CCN measurement at a single supersaturation requires 30 s. The temperature difference between the top and the bottom plate is

checked for 5 s to ensure that it is within the prescribed range (± 0.2 °C). The chamber is flushed for 5 s to remove air from the previous sample. A new air sample is captured and held within the chamber for 20 s. When a new air sample enters the chamber, CCN activate and droplets form, grow, and fall out. The top plate temperature is allowed to float with the enclosed temperature of the CCN counter, and the bottom plate temperature is controlled using thermoelectric coolers to achieve the prescribed supersaturation, which is calculated at the beginning of a measurement based on the top plate temperature. Following the suggestion of *Katz and Mirabel* [1975], the temperature and vapor pressure between the top and the bottom plates are assumed to be linear functions of the height above the bottom plate. Both the top and the bottom plates are kept wet for up to 3 hours using saturated blotter papers. *Delene et al.* [1998] provided an initial description of the balloon-borne CCN counter, described calibration at 1% supersaturation on NaCl aerosols, and presented some preliminary CCN profiles. The focus here is on dependence of the instrument's calibration on supersaturation, aerosol size, and aerosol type.

2. Standard Calibration Procedure

Calibration of the CCN counter is accomplished using the method of *Delene et al.* [1998]. The CCN concentration is determined by counting the number of water droplets in a measured portion of the laser beam using a video camera and personal computer (PC) frame grabber card. Concurrent with the video counts, the photodetector voltage is measured. A least squares linear fit between photodetector voltage and droplet count determines the calibration slope. The CCN counter's calibration constant is defined to be the calibration slope divided by the video sample volume. The calibration here differs from *Delene et al.*, [1998] by using a new video camera with higher resolution, greater magnification, lower noise, and greater light sensitivity. The new video camera counts more droplets within a 10 mm segment of the laser beam than does the old

video camera. Recent inquiries of the laser manufacturer indicated that the cross section of the laser beam was 5 x 1.8 mm instead of the 4 x 1 mm used by *Delene et al.* [1998]. Measuring the laser's cross section is uncertain due to blooming of the laser beam on the measurement apparatus. Our measurements of the laser beam width give 5.5 ± 0.5 mm comparing favorably to the laser manufacturer's width of 5.0 mm. Although the new video camera counts more droplets, a larger sample volume is used, which results in a reduction of the calibration constant by approximately 18% compared to the calibration constant determined with the old video camera.

The gain setting of the PC frame grabber card is used to test the sensitivity of the video camera. The number of droplets counted with the new video camera does not increase with gain increases on the frame grabber card. In contrast, the number of droplets counted with the old video camera does increase with gain increases on the frame grabber card. Therefore, the new camera seems sensitive enough to count all droplets within the field of view of the laser beam without over counting due to video noise.

Correctly setting the video camera's lens focus is critical for accurate calibrations; however, it is difficult to set the lens focus so that the whole depth of the laser beam is within focus. The focus of the lens is set by focusing on hairs of a Q-tip placed within the video sample volume. The focus is checked periodically during calibration by examining the video camera's output on a monitor to ensure that no large droplets with dim centers are present (out of focus droplets). The laser beam is at a 45-degree angle with respect to the lens and the sample length along the laser beam is 10 mm, thus the depth of field needs to be 14 mm. This is significantly larger than the 5 mm width of the laser beam. In an attempt to decrease the sensitive of the focus adjustment, the lens was moved back from the edge of the chamber, which increases in the depth of field but a reduces the magnification of droplets. Increasing the distance from the center of the chamber to

the lens from 46 to 52 mm results in a decrease of the 1% supersaturation calibration constant by approximately 10%. The reduced magnification resulting from this small increase in length probably resulted in under counting because some droplets were now too small to be detected. For all calibrations presented here the lens was placed at 46 mm from the center of the chamber to give the greatest magnification of droplet possible and the lens focus was carefully set to ensure that all droplets within the video sample were within focus.

Another important step for accurate calibrations is the alignment of the CCN counter's chamber with the video camera's lens. It is critical that the alignment be consistent for every laboratory calibration. This includes having the lens in the exact center of the chamber and ensuring that the video camera is level. The lens is placed in the center of the chamber by aligning the center of the video sample volume with the center of the air inlet. A vertical line overlay on the video camera's output denotes the center of the video sample volume and the center of the air inlet is on the direct opposite side of the diffusion chamber. The vertical placement of the video sample volume is set in the calibration software to ensure that the 1.8 mm height of the laser beam is enclosed within the video sample volume. The height of the laser beam is illuminated by placing a ruler along the laser beam and the video camera's output, with an overlay of the video sample volume, is examined on a monitor. After the video camera is aligned, a level is used to level the lens/video camera. The CCN counter and lens are fixed to the calibration bench to preserve the alignment setup during calibration. The alignment of the calibration system is checked before each calibration run to ensure that it has not changed.

Standard calibration of the CCN counter consists of obtaining several hundred comparisons of photodetector voltage and droplet concentration using laboratory aerosol produced from an ultrasonic vaporizer using a solution of 0.1 g/L of NaCl. The aerosol concentration is varied

during a measurement sequence by changing the amount of filtered air mixed with the generated aerosol. Figure 2 presents calibration data using the standard calibration method. The number of droplets, at the time of the photodetector voltage peak, and the video sample volume are used to determine the CCN concentration. The voltage peak method, instead of the voltage summation method of *Delene et al.* [1998], is used here because the resulting calibration constants are similar, and it simplifies examination of the calibration dependence on supersaturation.

3. Testing the Standard Calibration Procedure

The calibration of the CCN counter can be checked by comparing the CCN concentration against measurements made by a model 3010 TSI CN counter, when sampling monodisperse aerosol larger than the CCN counter's critical activation size. A differential mobility analyzer (DMA) [*Knutson and Whitby*, 1977] is used to produce monodisperse aerosol of different sizes. A conductive bag, partially filled with filtered air, is used to store the generated aerosols. Storing aerosols within a conductive bag is preferred to direct sampling from the DMA because there is no possibility that the counters will affect the flow rates through the DMA. When the concentration within the bag reaches the desired value, generation of aerosol is stopped, and the CCN and CN counters concurrently sample aerosols from the bag. During sampling from the conductive bag, the aerosol concentration decreases due to aerosols being collected by the walls of the bag. Coagulation of aerosols within the bag is less than 2% for the concentrations ($<1000 \text{ cm}^{-3}$) and times ($< 4 \text{ hr}$) of the laboratory comparisons (*Willeke and Baron*, 1993). Therefore, the size of the aerosols within the bag will remain constant throughout the laboratory tests.

Figure 3 presents an example of the CCN and CN counters measuring 125 nm monodisperse NaCl aerosol. The CCN concentration is determined using the video camera to count droplets, at the time of the photodetector voltage peak, over a predetermined video sample volume. Below a

concentration of 500 cm^{-3} , the averaged CCN concentrations agree with the CN concentrations. Above a concentration of 500 cm^{-3} , the CCN concentrations are low compared to the CN concentrations. The low CCN concentrations may be the result of under counting of droplets due to coincidence. Droplet coincidence results from one droplet being partially obscured by another droplet, resulting in two droplets being counted as one droplet. For the 3.5 hours required to generate Figure 3, the CCN counter was run continuously without rewetting the saturated blotter papers indicating that the saturated blotter papers on the top and the bottom plates will remain moist for over three hours.

4. Calibration Dependence on Supersaturation

The condensation growth rate of droplets is proportional to supersaturation [Rogers and Yau, 1989]; therefore, droplets will obtain sizes large enough to begin to fall in a shorter amount of time at higher supersaturations. Changes in droplet size will affect the calibration slope since the amount of scatter laser light is proportional not only to droplet number but also to droplet size. Changes in the CCN counter's supersaturation may change the size of droplets at the time of the photodetector voltage peak, and hence change the calibration constant. Observation of droplet fall velocities within the thermal-gradient diffusion chamber confirms that droplet size depends on the CCN counter's supersaturation. At lower supersaturations droplets are observed to fall slower than at higher supersaturations. Figure 4 illustrates the dependence of the calibration slope on supersaturation. The supersaturation dependence is fitted following the method of *de Oliveira and Vali* [1995]. The increase in the calibration slope as the supersaturations decreases indicates that droplets decrease in size as the supersaturation decreases.

The droplet size dependence on supersaturation is apparent in the shape of the average ratio of droplet number and the average ratio of photodetector voltage. Figure 5 shows the average

ratio values as the CCN counter's chamber is flushed (first 5 s) and droplets activate, grow, and fall out. The average ratios are calculated by dividing the measured droplet number or photodetector voltage by the maximum droplet number or photodetector voltage obtained during the sample to determine the ratio at each time interval and then averaging this ratio as a function of time for hundreds of samples. The average ratios never equal one since the peak ratio does not always occur at the same time for each sample. The peak in droplet number (solid lines) occurs before the peak in photodetector voltage (dashed lines). This indicates that droplets continue to grow larger, and hence scatter more light, after the occurrence of the droplet number peak. The average ratios at 1% supersaturation, compared to 0.3% supersaturation, have peaks that occur earlier in the measurement cycle and are narrower by a factor of 2. This difference is due to the droplet size dependence on supersaturation that results from the supersaturation dependence of the condensation growth rate of droplets [Rogers and Yau, 1989]. Broad peaks in the average ratio of the droplet number indicate that it does not make a significant difference exactly where the count of the droplet number peak is obtained. However, with narrow peaks in the droplet number it may make a significant difference. This may be the reason that in Figure 4 the data points when compared to the data fit show a slight under counting at high supersaturations and a slight over counting at lower supersaturations.

Figure 6 illustrates the time required to reach the droplet number and photodetector voltage peaks as a function of supersaturation. The standard deviation of the average time to reach the photodetector voltage peak increases with decreasing supersaturation. The increase in the variability in time to reach the peaks is due to broader peaks at lower supersaturation (Figure 5). The time between the average droplet number peak and the average photodetector voltage peak decreases linearly from 2.5 s at 0.3 % supersaturation to 1.0 s at 1.6% supersaturation (Figure 6).

This further illustrates the dependence of condensation growth rate on supersaturation. Droplets grow more quickly at higher supersaturations reducing the time between the droplet number and photodetector voltage peak.

5. Calibration Dependence on Aerosol Type

The size distribution and chemical composition of atmospheric aerosols is highly variable due to the complex interrelationships between several different sources and sinks [Singh, 1995]. Therefore, field measurements on atmospheric aerosols will have varying size distributions and chemical compositions. Figure 7 gives the aerosol size spectrum for the NaCl laboratory-generated aerosols produce with the vaporizer. The aerosol size spectrum is obtained using a TSI differential mobility analyzer and CN counter (Birmili *et al.*, 1997). The laboratory-generated aerosol has a bimodal, polydisperse size spectrum and it consists of totally soluble aerosols. Therefore, the calibration aerosol is quite different from ambient atmospheric aerosols.

Calibration of the CCN counter on different aerosol types was conducted to determine if the laboratory calibration can be applied to field measurements. Table 1 summaries several different calibrations of the CCN counter. The first three rows give the calibration results for the standard calibration method using polydisperse NaCl aerosol. Row one results are from March 1998, row two from June 1998, and row three from October 1998. No changes in the configuration of the CCN counter were made between these calibrations; however, the CCN counter was removed from the laboratory calibration bench between each of these calibrations and used elsewhere. The random errors of the calculated calibration slopes are given by the standard deviations in Columns 2 and 3. The change in the calibration slopes (Column 2 and 3) for the standard calibration method (Rows 1-3) is larger than the random errors for any one calibration. Systematic differences in the setup and alignment of the CCN counter with the video calibration

system are believed to cause the variability between calibrations. The observed variability in the standard calibration method (Rows 1-3) indicates that the calibration is repeatable to within 10%.

Roberts et al. [1997] observed a photodetector calibration dependence on the initial size of CCN in a static thermal-gradient diffusion chamber. To check for a calibration dependence on CCN size, the instrument was calibrated using monodisperse aerosol of several different sizes. The generation and sampling of monodisperse aerosol was described earlier. Results of calibrations on different monodisperse aerosol sizes are given in Rows 4-9 of Table 1. The aerosol size that activates droplets appears to have no detectable affect on the time to reach either the droplet number peak or the photodetector voltage peak (Columns 4 and 5). Furthermore, analysis of the measurements shows that there is no dependence between the time to reach the peaks and the aerosol concentration. An approximate 10% change in the calibration slope is observed between 35 nm NaCl and 120/160 nm NaCl aerosol.

The calibration slope dependence on CCN size indicates that the size of CCN that activate to produce droplets affects the amount of light scattered per droplet at the time of the photodetector voltage peak. This droplet dependence on initial CCN size is not intuitive. Droplets are a few micrometers in diameter at the photodetector voltage peak since they are observed to fall. Since the diffusional rate of growth of a droplet is proportional to the inverse of droplet radius, the droplet size spectrum becomes narrower as droplets grow to larger sizes [*Rogers and Yau*, 1989]. Intuitively, the narrowing of the droplet spectrum is expected to cause the droplets to be at approximately the same relative size at the photodetector voltage peak. Therefore, the calibration would not depend on the initial CCN size.

Due to the apparent dependence of the calibration on CCN size, the calibration may change if we calibrate on atmospheric aerosol instead of laboratory generated aerosol (Figure 7). Figure 8

shows calibration data using ambient atmospheric aerosols obtained from outside the laboratory building on three consecutive mornings in early October at Laramie, Wyoming. The measurements were made around sunrise under meteorological conditions of clear skies and high pressure, similar to a typical balloon flight. The ambient aerosol concentration was varied by diluting the aerosol sample with filtered air. Calibration on outside aerosol does not show a significant difference from the laboratory-generated NaCl aerosol. The slope obtained on the outside air is within the range of slopes obtained for the 3 different calibrations on polydisperse laboratory aerosol (Table 1, Rows 1-3). Furthermore, the average time to reach the peak values (Table 1, Columns 4 & 5) and shape of the average ratio peaks (not shown) are consistent with calibration on standard laboratory generated aerosol. The consistency between the calibration on laboratory-generated aerosol and atmospheric aerosol measured at the surface in Laramie, Wyoming suggests that the laboratory calibration can be applied to field measurements.

It is unknown if atmospheric aerosols in the upper troposphere or at different geographic locations are different enough to invalidate the calibration. While it is impossible to check the calibration on all types of aerosols, the average time to reach the photodetector voltage peak may indicate measurements that are not consistent with the laboratory calibration. Table 2 gives the time to reach the photodetector voltage peak for various field measurements. The surface and lower tropospheric time to reach the photodetector voltage peak are consistent with the laboratory calibrations (Table 1). The upper tropospheric time to reach the photodetector voltage peak shows more variability than the laboratory calibration data, but are still within the range of the laboratory calibrations. The increase in variability in the upper troposphere may be related to measurements being near the detection limit of the CCN counter. The peak is less well defined near the detection limit since only a few particles are within the photodetector sample volume.

6. Calibration Error

Accurate CCN measurements require accurate number concentrations of droplets using the scattered light signal and knowledge of the supersaturation within the thermal-gradient diffusion chamber. Accurately measuring and maintaining the temperature difference between the top and the bottom plates ensures a correct supersaturation. Measurements with a thermocouple placed on the top and the bottom saturated blotter papers, within the thermal-gradient diffusion chamber, confirm that the temperature difference is maintained to within ± 0.1 °C or $\pm 0.05\%$ supersaturation at a supersaturation of 1%. The supersaturation within the diffusion chamber could be incorrect due to the occurrence of transient supersaturations before steady-state temperature and moisture gradients are established [Fitzgerald, 1970; Saxena *et al.*, 1970]. To avoid transient supersaturations that exceed the steady-state peak value, it is advantageous to have air samples enter the diffusion chamber at the top plate temperature with a low relative humidity [Fitzgerald, 1970; Saxena *et al.*, 1970]. The balloon-borne CCN counter's top plate temperature is allowed to float with the box enclosure temperature. Before an air sample enters the chamber, it travels through 5 mm, inside diameter, stainless steel tubing within the CCN counter's box enclosure for approximately 0.3 s. Heat transfer calculations show that the air sample equilibrates with the enclosure temperature of the CCN counter before entering the chamber. Heat produced by the electronics ensures that the box enclosure temperature is higher than the ambient air temperature. Therefore, air entering at the enclosure temperature of the CCN counter also ensures that the relative humidity of the air sample is lower than the ambient relative humidity. Since air samples enter the CCN chamber at the enclosure temperature, transient supersaturations above the steady-state peak values are believed not to occur within the chamber under field measurement conditions.

The relative error in CCN concentration can be computed using Poisson counting statistics (Horvath *et al.*, 1990). The Poisson counting error can be significant at upper tropospheric concentrations since there are very few particles present in the laser beam. The counting error is larger for video counting of droplets than for photodetector counting of droplets due to the photodetector sample volume being approximately 2 times as large as the video sample volume used during the standard calibration procedure. The photodetector sample volume of 0.16 cm^3 determined by Delene *et al* [1998] was verified using measurements collected during laboratory calibrations on monodisperse aerosols. The Poisson counting error agrees with the standard deviation of 10 min averages of CCN concentration. Poisson counting statistics give a range of errors from 36 to 11% for CCN concentrations (at ambient pressure) of 50 to 500 cm^{-3} . The measurement threshold is approximately 20 cm^{-3} , which corresponds to 3 droplets being within the photodetector sample volume. Below this concentration, the photodetector peak is not discernible from the base line photodetector voltage determined during the chamber flush at the beginning of the sample.

The agreement between the CCN counter and a laboratory standard, commercially built TSI CN counter seen in Figure 3 indicates a good absolute calibration of the CCN counter. It also indicates that the video sample volume is correct, and the video camera/lens system is adequate to calibrate the CCN counter at 1% supersaturation. The variability, approximately 5-10%, between standard calibrations of the CCN counter (Table 1, Rows 1-3) is thought to result from systematic difference in the setup and alignment of the CCN counter with the video calibration system. Counting droplets using the photodetector to measure the scatter light signal, instead of counting droplets with a video camera system, has a small dependence on aerosol size. This size dependence is approximately the same as the systematic error in the standard laboratory

calibration. The calibration dependence on aerosol size does not seem to have a great affect in the real atmosphere since calibration on real atmospheric aerosol produces a calibration similar to the standard laboratory calibrations.

Considering all calibration results presented here, the calibration constant relating photodetector voltage to CCN concentration for the standard laboratory calibration of the balloon-borne CCN counter is believed to have an accuracy of 10% at 1% supersaturation. The video calibration of the CCN counter appears to work at supersaturations down to 0.2%. The calibration slopes fit nicely to a power law function (Figure 4); however, video counting of droplets is difficult at low supersaturation, due to the smaller droplets, and the dependence of the calibration constant on aerosol size may be more significant at supersaturations lower than at 1%. The video calibration method should be verified at low supersaturations.

7. Conclusions

A photometric CCN counter was calibrated using a video camera and PC frame grabber card to count droplets. Droplet number is linearly related to the amount of laser light scattered by the droplets. The standard calibration procedure for the CCN counter is repeatable to better than 10% accuracy. The calibration relationship between droplet number and photodetector voltage was verified by a comparison between the CCN counter and a CN counter when sampling monodisperse aerosol. Calibration of the CCN counter is found to depend on supersaturation and to have a slight dependence on the size of CCN that activate to form droplets. The dependence on supersaturation is easily accounted for by using a power law function to relate the calibration slope to supersaturation. The calibration dependence on CCN size is less than 10% at 1% supersaturation. Calibration on ambient atmospheric aerosol appears similar to the standard calibration procedure. Laboratory calibration measurements, compared to field measurements at

various locations and within different atmospheric layers, give average photodetector voltage peaks that occur at similar times after an air sample enters the thermal gradient-diffusion chamber. Therefore, it appears that within the diffusion chamber atmospheric CCN behave similar to laboratory produce CCN. Random errors in measured CCN concentration can be computed using Poisson counting statistics and range from 36 to 11% for CCN concentrations in the range of 50 to 500 cm^{-3} . The calibration constant that relates photodetector voltage to CCN concentration is believed to have an accuracy of 10% at 1% supersaturation.

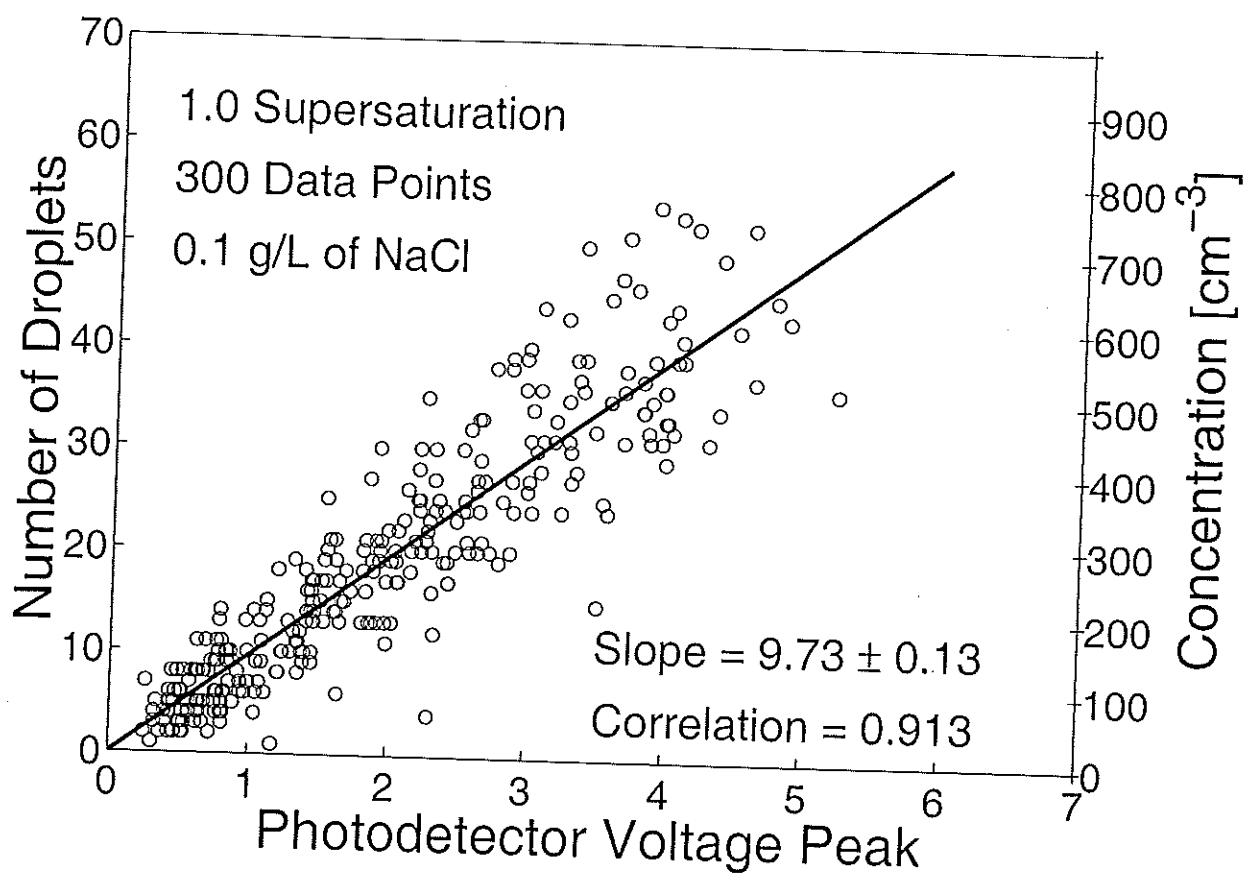


Figure 2. The photodetector voltage peak versus the number of droplets counted within the video sample volume and the corresponding droplet concentration. Droplets are counted at the time of the photodetector voltage peak. The droplets nucleated on polydisperse NaCl aerosols produced using a solution of 0.1 g/L of NaCl in an ultrasonic vaporizer. The calibration slope (solid line) is the least squares linear fit to the data with a forced zero y-intercept.

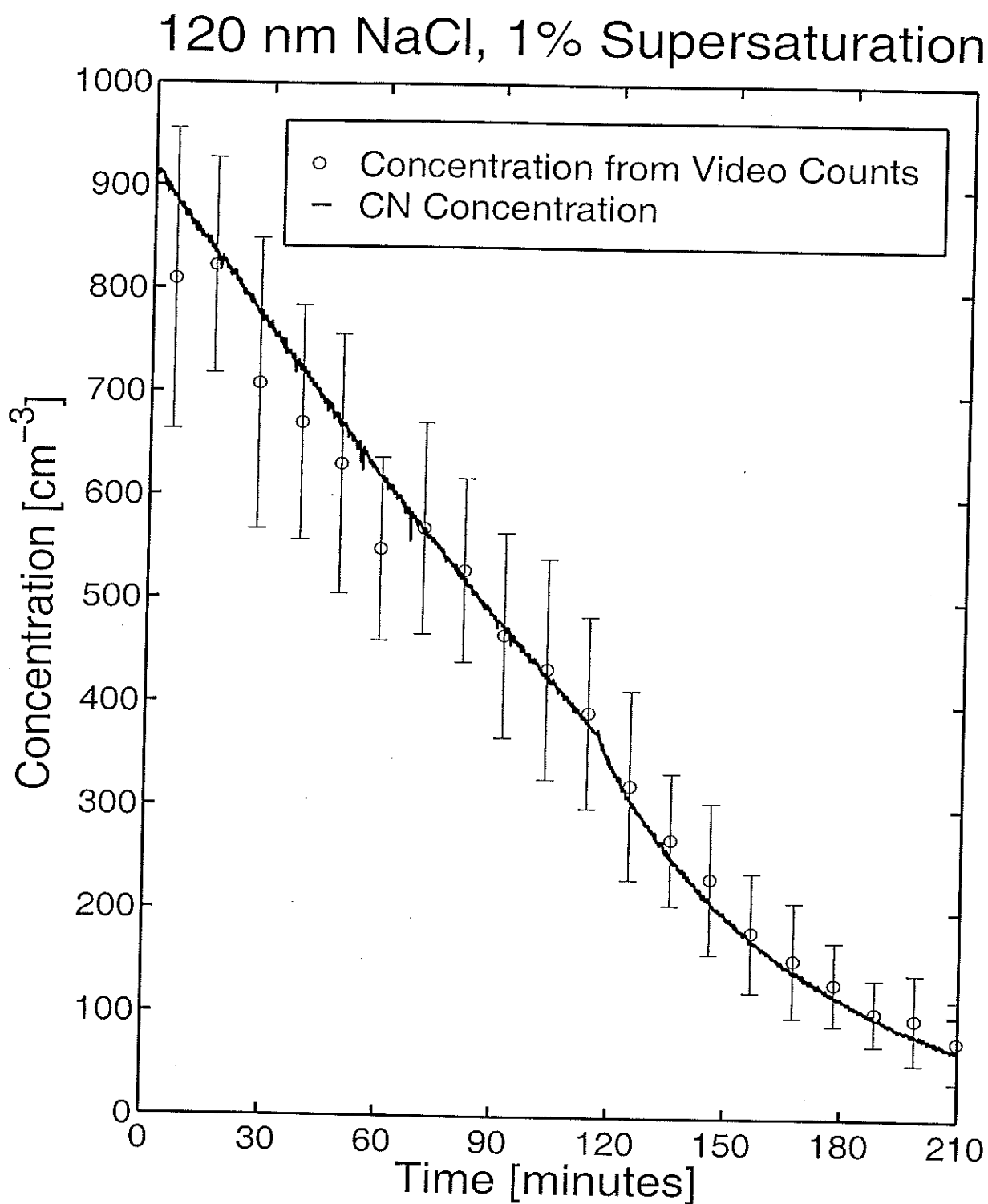


Figure 3. Measurements of the concentration of 120 nm monodisperse NaCl aerosols using the CCN counter at 1% supersaturation (circles) and CN counter (solid line). The CCN concentration is measured using the video camera to count droplets over a predetermined video sample volume. The CCN concentration is averaged over approximately 20 samples (10 min) with the standard deviation given by the error bars. The decrease in concentration with time is the result of aerosol being removed to the walls of the sampling bag. Filtered air was continuously added to the sampling bag after 115 minutes

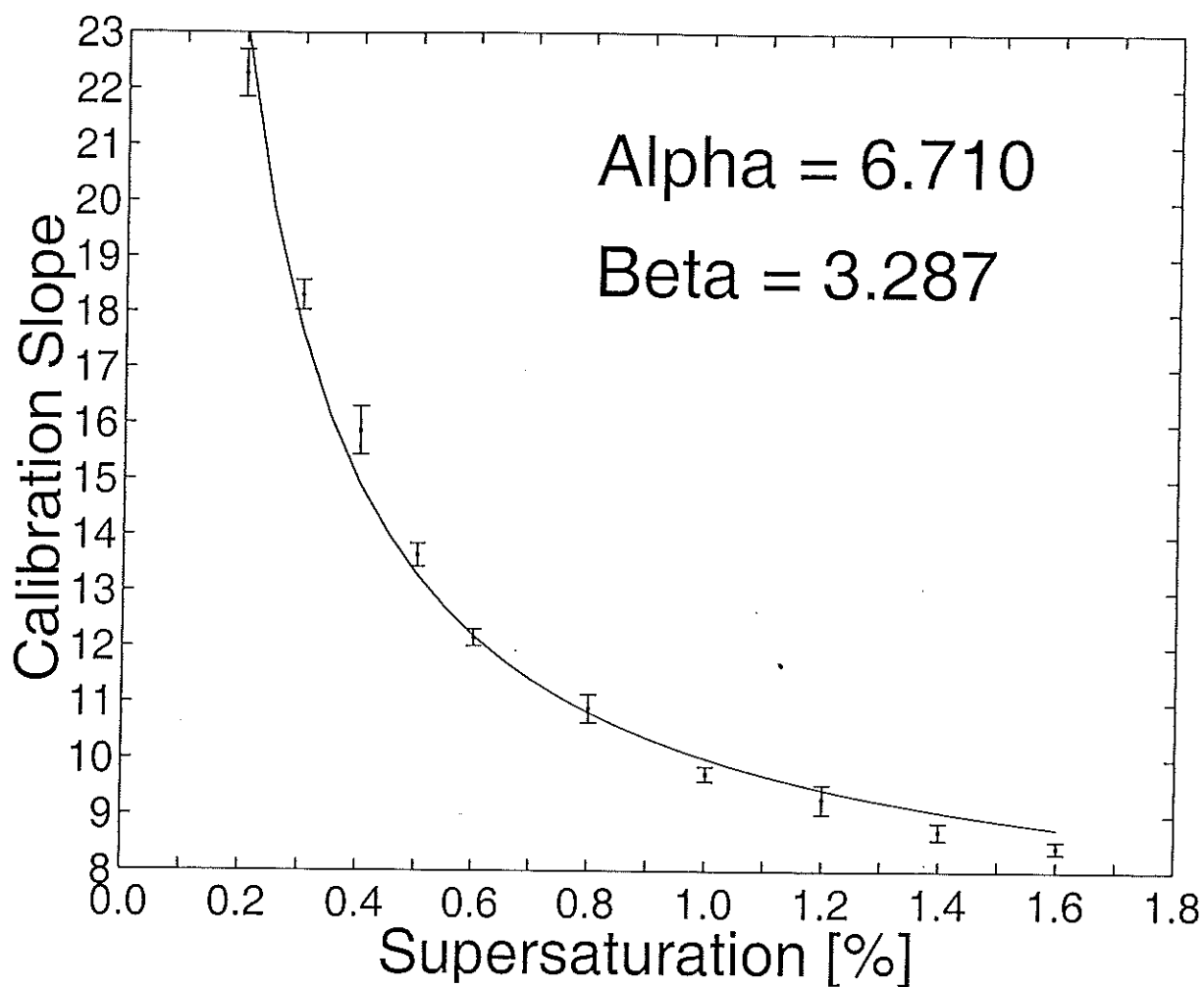


Figure 4. The CCN counter's calibration slope dependence on supersaturation. The data are fitted using the equation, $C = \text{Alpha} + \text{Beta}/\text{SS}$, where Alpha and Beta are calibration constants, SS is the chamber supersaturation, and C is the calibration slope. Error bars represent one standard derivation in the calculated calibration slope.

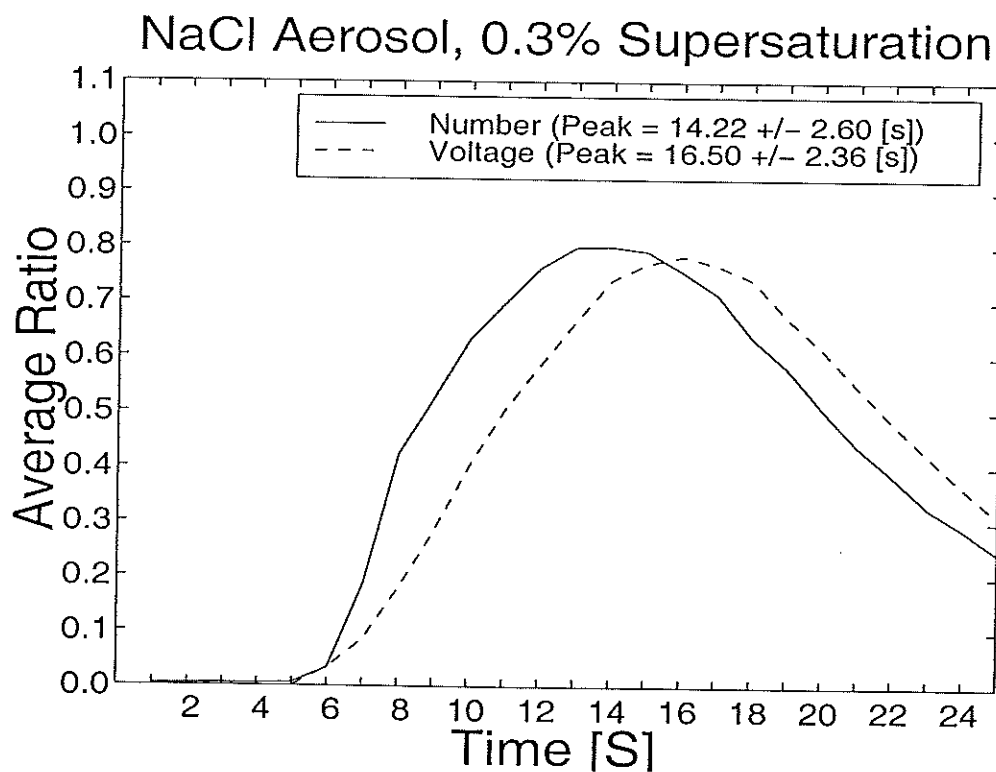
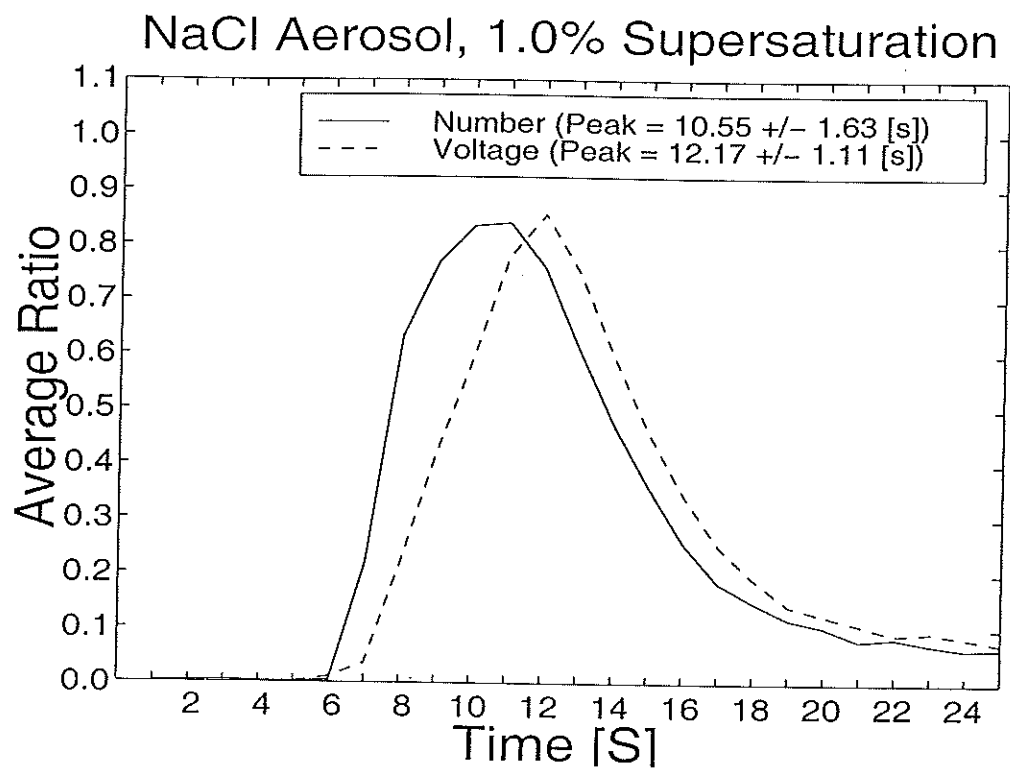


Figure 5. Time versus the average ratio of the droplet number (dashed line) and the average ratio of the photodetector voltage (solid line). The definition of the average ratio is given in the text. The legends give the average and standard deviation times for the peak number of droplets and peak photodetector voltage. Time zero is at the beginning of a 5 s chamber flush. Following the chamber flush, an air sample is captured within the chamber, CCN active and droplets form, grow and begin to fall.

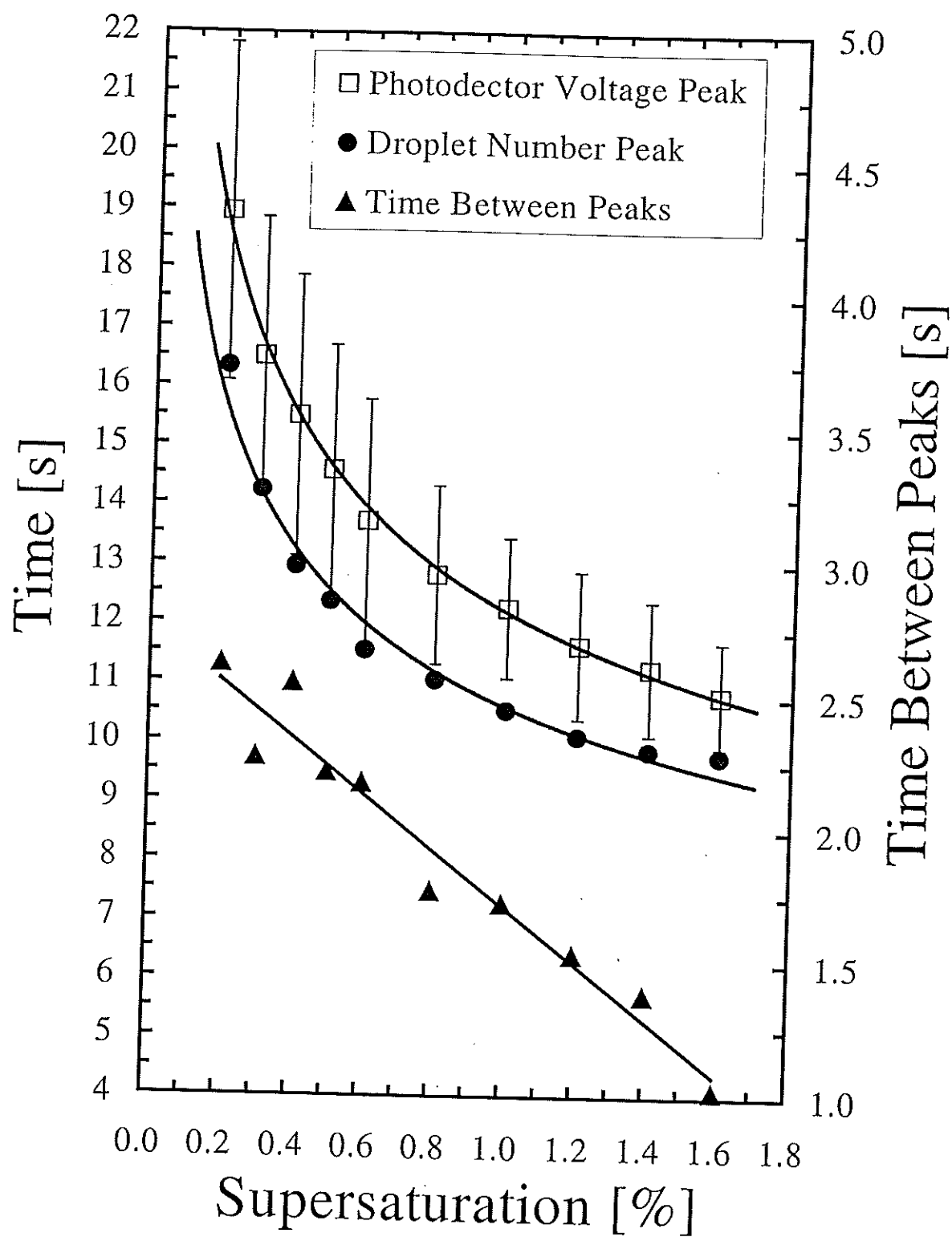


Figure 6. Supersaturation of the CCN counter versus the average time to reach the peak. The error bars on the photodetector voltage time are one standard deviation of the average. Error bars (not shown) on the average time to reach the droplet number peak are similar. The left axis and solid triangles denote the time between the droplet number peak and photodetector voltage peak.

Polydisperse NaCl Aerosol

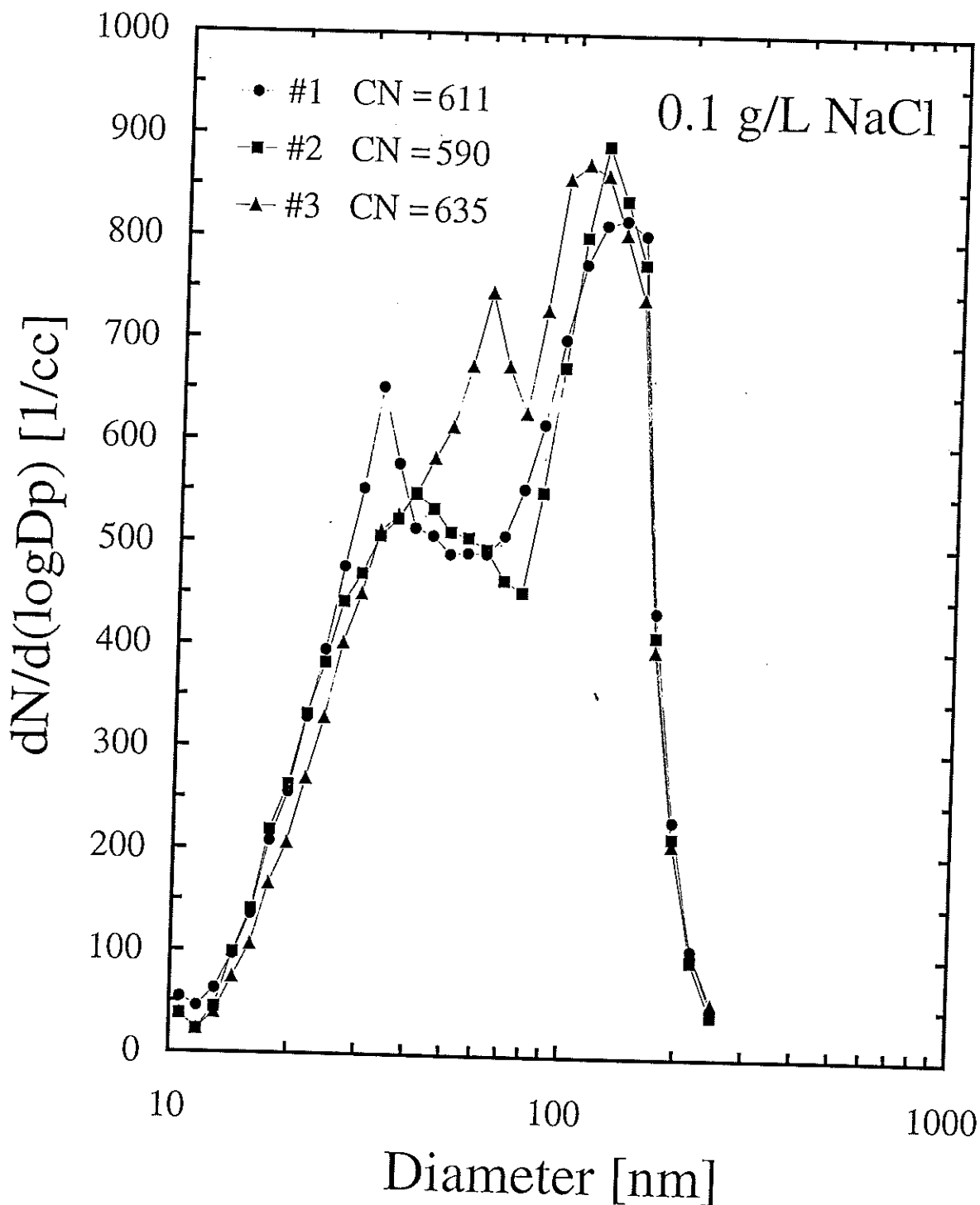


Figure 7. Examples of the aerosol size spectrum generated using a solution of 0.1 g/L of NaCl in an ultrasonic vaporizer. Legend gives the total number concentration (in cm^{-3}) for each aerosol size spectrum.

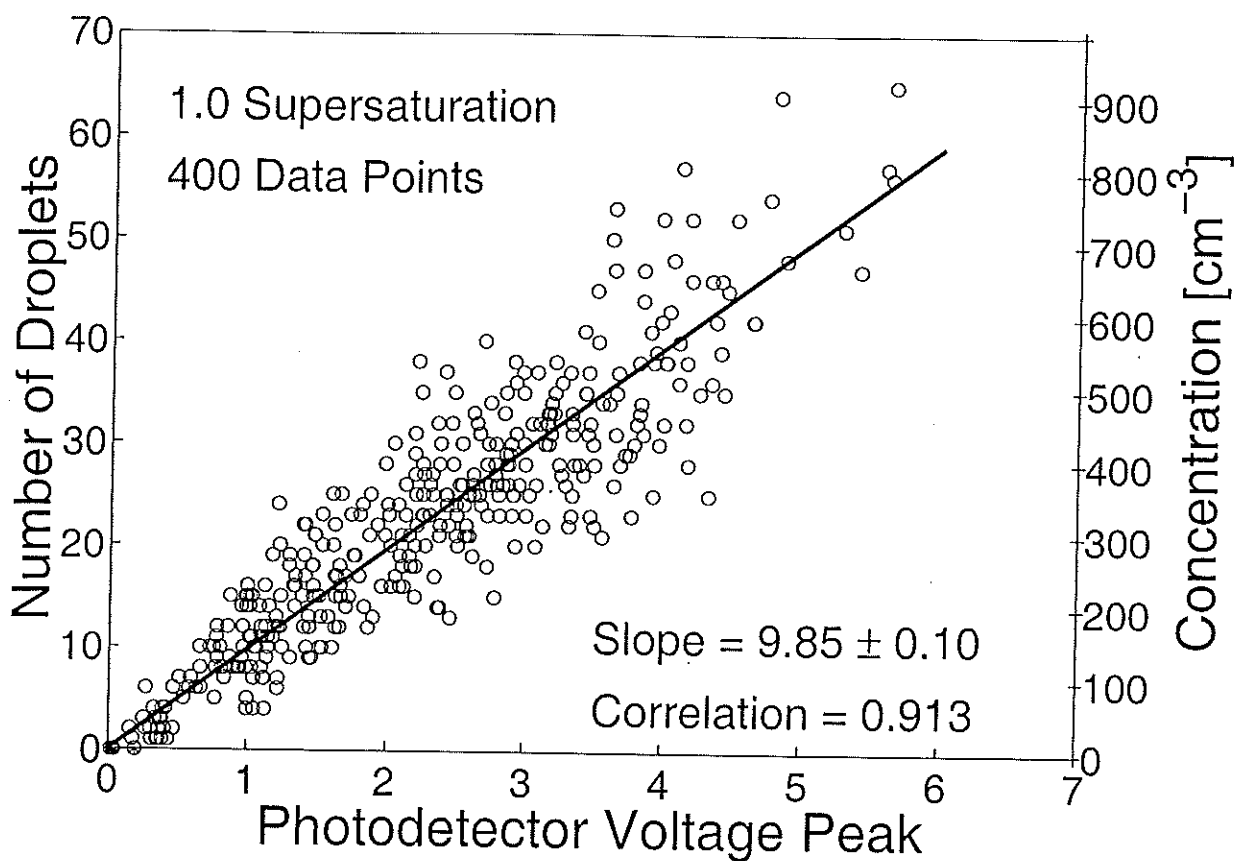


Figure 8. CCN counter calibration data using aerosol from the ambient atmosphere outside the laboratory building in Laramie, Wyoming. The photodetector voltage peak versus the number of droplets counted within the video sample volume and the corresponding droplet concentration are shown. Droplets are counted at the time of the photodetector voltage peak. The calibration slope (solid line) is the least squares linear fit to the data with a forced zero y-intercept.

Aerosol Type	Peak Method	Summation Method	Droplet Peak	Voltage Peak
0.1 g/L NaCl	9.44 ± 0.09	3.57 ± 0.03	10.6 ± 1.7	12.5 ± 1.5
0.1 g/L NaCl	10.08 ± 0.08	3.78 ± 0.02	10.5 ± 1.9	12.4 ± 1.4
0.1 g/L NaCl	9.73 ± 0.13	3.64 ± 0.03	10.6 ± 1.6	12.2 ± 1.1
35 nm	10.20 ± 0.18	3.94 ± 0.05	10.2 ± 1.2	12.1 ± 1.1
50 nm	9.84 ± 0.11	3.66 ± 0.03	10.5 ± 1.5	12.6 ± 1.1
60 nm	9.60 ± 0.13	3.55 ± 0.04	10.7 ± 1.5	12.5 ± 1.2
80 nm	9.21 ± 0.12	3.40 ± 0.03	10.5 ± 1.4	12.4 ± 1.2
120 nm	9.09 ± 0.08	3.39 ± 0.02	10.8 ± 1.7	12.5 ± 1.4
160 nm	9.12 ± 0.09	3.37 ± 0.03	10.4 ± 1.6	12.2 ± 1.2
Outside	9.84 ± 0.10	3.72 ± 0.03	10.4 ± 1.7	12.2 ± 1.4

Table 1. Calibration of the balloon-borne CCN counter at 1% supersaturation. The first column gives the calibration aerosol type: laboratory produced aerosol using a solution of 0.1 g/L NaCl in a vaporizer, monodisperse NaCl aerosol of different diameters, or aerosol from the ambient atmosphere outside the laboratory building. The second column gives the calibration slope using the photodetector voltage peak. The third column gives the calibration slope using a three-point sum around the photodetector voltage peak [Delene *et al.*, 1998]. The fourth column gives the average time to reach the number peak in seconds since the beginning of the sample. The last column gives the average time to reach the voltage peak in seconds since the beginning of the sample. The first 3 rows give the results of the standard calibration of the CCN counter in March, June, and, October 1998. The CCN counter was removed from the laboratory calibration bench between each standard calibration of the CCN counter and used elsewhere. The calibrations presented in rows 3-10 were performed using the same focus and video camera alignment with the CCN counter.

Layer	Location	Season	Voltage Peak	Samples
Surface	Laramie, Wyoming	Summer	12.2 ± 1.4	400
Surface	Fairbanks, Alaska	Winter	12.7 ± 1.8	144
Lower Troposphere	Laramie, Wyoming	Summer	12.5 ± 1.1	86
Lower Troposphere	Laramie, Wyoming	Winter	12.3 ± 1.0	18
Lower Troposphere	Lauder, New Zealand	Summer	12.4 ± 0.7	23
Upper Troposphere	Laramie, Wyoming	Summer	11.8 ± 1.6	117
Upper Troposphere	Laramie, Wyoming	Winter	13.1 ± 2.7	68
Upper Troposphere	Lauder, New Zealand	Summer	12.1 ± 1.3	67

Table 2. Time to reach the photodetector voltage peak for field measurements in Laramie, Wyoming (41 °N), Lauder, New Zealand (45 °S), and Fairbanks, Alaska (65 °N). Due to a clear difference in aerosol concentration, the field measurements are divided into summer and winter seasons. The third column gives the average and standard deviation of the time to reach the photodetector voltage peak. The fourth column gives the number of samples used to compute the average.

CHAPTER 3: Vertical Profiles of Cloud Condensation Nuclei Above Wyoming and New Zealand

Abstract

The importance of atmospheric aerosols in understanding global climate change has renewed interest in measurements of cloud condensation nuclei (CCN). To obtain high-resolution (125 m) vertical profiles of CCN number concentration, a balloon-borne CCN counter has been flown on 12 balloon flights at Laramie, Wyoming (41 °N) and 2 balloon flights at Lauder, New Zealand (45 °S). The instrument gondola for each of these flights also contained a condensation nuclei (CN) counter and an optical particle counter to measure aerosols with diameter greater than 0.3 μm ($D_{0.3}$). Variations in the vertical profile of CCN concentration were typically positively correlated with changes in CN and $D_{0.3}$ concentrations, and often corresponded with changes in relative humidity, typically being positively correlated but sometimes negatively correlated. Aerosol profiles generally show several distinct layers defined by the thermodynamic parameters of equivalent potential temperature and relative humidity. These layers are used to summarize the 14 vertical profiles by classifying aerosol measurements into five distinct atmospheric layers: surface, lower tropospheric, upper tropospheric, stratospheric and regions of high humidity. Laramie summer and winter profiles show that the mean CCN concentration decreases between the lower and upper tropospheric layers (445 cm^{-3} to 126 cm^{-3} in summer; 146 cm^{-3} to 64 cm^{-3} in winter). The summer CCN concentrations at Lauder, New Zealand (45 °S) were about twice the summer CCN concentrations measured at Laramie, Wyoming (41 °N) while the CN and $D_{0.3}$ concentrations were approximately the same. The average summer CCN/CN ratio in Wyoming shows an increase from 0.09 in the lower troposphere to 0.17 in the upper troposphere, while in New Zealand the average summer CCN/CN ratio shows an increase from 0.27 to 0.59.

1. Introduction

Increases in cloud condensation nuclei (CCN) concentration, resulting from increased SO_2 emissions, has been suggested as possibly offsetting global temperature change expected from increased CO_2 concentrations [Wigley, 1989; Twomey, 1991]. The number concentration and activity of CCN influences the cloud droplet spectra and hence precipitation processes, cloud albedo, and global climate [Hobbs, 1993; Jennings, 1993]. Aerosols directly affect climate by scattering and absorbing radiation and indirectly affect climate by altering the scattering characteristics of clouds [Charlson *et al.*, 1992]. The direct climate forcing of aerosols has started to be incorporated into global climate models [Boucher and Anderson, 1995; Haywood and Shine, 1995]; however, the limited understanding of the indirect forcing of aerosols requires more research before it is understood well enough to be fully incorporated into global climate models [Penner *et al.*, 1994]. Chuang *et al.* [1997] recently addressed indirect anthropogenic forcing by using a coupled climate/chemistry model to predict changes in the aerosol number spectrum due to anthropogenic sulfate. Using a microphysics model to improve the parameterization of Ghan *et al.* [1993], the change in the number concentration of cloud droplets is related to the change in the aerosol spectrum. Pan *et al.*, [1998] investigated indirect forcing of aerosols using the method of Charlson *et al.* [1992] to determine changes in aerosol number concentration due to anthropogenic sulfate and three different parameterizations [Twomey, 1977; Jones *et al.*, 1994; Ghan *et al.*, 1993] to relate changes in aerosol number concentration to changes in cloud droplet concentration. They concluded that refining the input parameters might be more important than improving models to minimize uncertainties.

Several studies have measured continental CCN number concentration near the earth's surface [Hudson and Squires, 1978; Hudson and Frisbie, 1991; Philippin and Betterton, 1997],

and field campaigns have used aircraft to measure continental CCN concentrations aloft [Hobbs *et al.*, 1985; Hudson and Xie, 1998]. Figure 1 presents examples of vertical CCN profiles obtained using aircraft. The profiles consist of four to six measurements ranging from the surface to a maximum height of approximately 5 km. The profiles show a general decrease in CCN concentration with increasing height above the surface; however, due to the low vertical resolution of the profiles, it is difficult to discern if the source of CCN is near the surface or if there is a major source within the atmosphere. The CCN measurements in Figure 1 also do not show a systematic decrease in concentration with decreasing supersaturation. This indicates that CCN concentrations are highly variable and that a few measurement locations are insufficient to determine the global scale distribution of CCN. Aircraft measurements of CCN have almost exclusively been confined to the lower troposphere. Recent upper tropospheric CCN measurements conducted by Hudson and Xie [1998] found constant CCN concentrations with increasing altitude above the lower troposphere.

To improve the vertical resolution and altitude range of existing CCN profiles, a balloon-borne CCN counter has been used to obtain 14 CCN profiles extending from the surface to 200 mbar at 2 continental sites. The CCN counter, operated at a constant supersaturation of 1%, was included on 12 flights at Laramie, Wyoming (41 °N) and 2 flights at Lauder, New Zealand (45 °S). The balloon flights typically start at dawn with clear skies and light winds. On each flight a condensation nucleus (CN) counter and optical particle counter (OPC) were included to obtain complementary measurements of CN and aerosols with diameter greater than 0.30 μm ($D_{0.3}$). Although the instrument package ascends to a pressure of 10 mb, the CCN counter is switched off at 200 mbar to avoid overheating resulting from reduced heat transfer at low pressures. A heater on the common inlet for the aerosol instruments raises the air temperature to 40 °C during

ascent and 160 °C during descent. After passing the heated inlet, the air sample temperature decreases as it flows through 0.6-1 m of stainless steel tubing to each instrument; however, the air entering each instrument remains above the ambient temperature. Thus, the humidity is low enough that the aerosol instruments measure dry particles. CCN measurements are obtained every 30 s providing a vertical resolution of approximately 125 m. The CN and $D_{0.3}$ measurements are made by counting individual aerosols with continuous flow instruments. The total aerosol count is recorded every 10 s so that the average concentration, determined using total aerosol count and instruments flow rate, has a vertical resolution of approximately 40 m. The high vertical resolution of the balloon profiles allows for the detection of small-scale changes in concentration. Several flights at a single location provide an indication of the common features of a CCN profile. Concurrent aerosol measurements allow for CCN concentrations and vertical profiles to be related to concentrations and profiles of both smaller (CN) and larger ($D_{0.3}$) aerosol.

The balloon-borne CCN counter uses a static thermal-gradient diffusion chamber to create a supersaturated environment where CCN active and water droplets form. The CCN concentration is deduced from the amount of laser light scattered by droplets within the diffusion chamber. *Delene et al.* [1998] provided a description of the balloon-borne CCN counter, described calibration at 1% supersaturation on NaCl aerosols, and presented some preliminary CCN profiles. The Poisson counting statistics for the CCN counter at concentrations (at ambient pressure) of 50 to 500 cm^{-3} are 36 to 11% and the minimum detectable concentrations (at ambient pressure) is approximately 20 cm^{-3} [Chapter 2].

The optical aerosol counters, which have been used for balloon-borne measurements by the University of Wyoming since 1971, are based on the measurement of scattered light by

individual particles passing through the instrument. The instruments were initially developed by *Rosen* (1964), and were most recently modified in 1989 to measure larger, more volatile particles, at lower concentrations [*Hofmann and Deshler*, 1991]. The aerosol size is determined from measurements of the intensity of white light scattered at 40 degrees from the forward direction using Mie theory and assuming spherical particles with an index of refraction of 1.45. For the midlatitudes the instruments now provide in situ observations of integral number densities for particles with diameter larger than 0.3 - 4.0 μm . For CN, the particles are forced to grow to optically detectable sizes with a growth chamber using ethylene glycol vapor. For aerosol $\geq 0.3 \mu\text{m}$ diameter, the Poisson counting statistics for concentrations of 0.001 to 1.0 cm^{-3} are 75 to 2%. For CN, the uncertainties for concentrations of 1.0 to 10.0 cm^{-3} are 8 to 3%. The minimum detectable concentrations from these aerosol counters are 0.0006 cm^{-3} .

The accuracy of each aerosol instrument is critical since we want to compare and combine the measurements. Careful evaluation of each aerosol instrument under tropospheric flight conditions has resulted in some data modifications since the preliminary results of *Delene et al.* [1998]. Connecting the inlet heater to the OPC with 5 mm (inside diameter) stainless steel tubing adds a pressure drop, which decreases the laboratory measured flow rate by 5%, resulting in a 5% increase in the aerosol concentration. The added pressure drop is negligible for the CN counter, which has a flow rate of 0.8 L min^{-1} , instead of the OPC's 10 L min^{-1} . Therefore, there was no correction to the CN concentration. To measure both tropospheric and stratospheric CN concentrations, it is necessary to dilute the tropospheric air before it enters the CN counter [*Rosen and Hofmann*, 1977]. Recent laboratory testing indicates that the actual dilution ratio is greater than used by *Delene et al.* [1998] leading to a correction of the tropospheric CN measurements reported by *Delene et al.* [1998] by a factor of 1.6. Laboratory calibrations of the

balloon-borne CCN counter using a higher resolution, greater magnification, lower noise, more light sensitive video camera and comparisons of the CCN counter to a model 3010 TSI CN counter resulted in a more accurate absolute calibration of the CCN counter. Thus, the CCN concentrations reported here are 18% lower than reported by *Delene et al.* [1998]. Calibrations with the new video camera have shown that the CCN counter has an accuracy of approximately 10% at 1% supersaturation [Chapter 2].

2. Atmospheric Aerosol Layers

Figure 9 presents 6 of our 14 aerosol profiles. The left-hand panels contain the $D_{0.3}$, CCN, and CN concentration, and the right-hand panels contain the equivalent potential temperature and relative humidity. Figure 9a is typical of the 8 aerosol profiles not shown. The equivalent potential temperature increases in the first 300 m above the surface, is nearly constant or slightly decreases until 5 km above mean sea level, and then increases in the upper troposphere. The relative humidity is nearly constant in the lower troposphere, decreases abruptly at approximately 5 km, and is relatively constant and less than 20% in the upper troposphere. The aerosol concentrations are relatively constant from the surface to approximately 5 km, decreases sharply at approximately 5 km, and are relatively constant in the upper troposphere. Figures 9b-9f differ from Figure 9a in showing variations in aerosol concentration which correspond to relative humidity changes, in addition to the typical decrease at approximately 5 km.

The aerosol profiles (Figure 9 and 8 profiles not presented) show several distinct layers defined by the thermodynamic parameters of equivalent potential temperature and relative humidity. These layers can be used to group the aerosol measurements, thus providing a broad organization to the data into five atmospheric layers: surface, lower troposphere, upper troposphere, stratosphere, and humidity. Different physical processes, described more fully

below, drive the mixing within each layer, resulting in different mixing time scales and affecting the distribution of atmospheric aerosols. Since the manifestation of these physical processes change from day to day and with time of year, the altitude boundaries of each layer were determined independently for each sounding using a clear and concise definition. Aerosol concentrations above Laramie, Wyoming are summarized by averaging measurements over the lower and upper tropospheric layers. These layer averages are then compared with layer averages obtained above Lauder, New Zealand. Measurements within the surface, stratospheric, and humidity layers are not extensive enough in the current data set to provide meaningful averages. These layers are useful to define so that measurements within the layers can be excluded from the lower and upper tropospheric layers.

Nighttime cooling of air near the earth's surface produces a temperature inversion resulting in a surface layer of approximately 300 m. The equivalent potential temperature strongly increases from the bottom to the top of the surface layer, which is clearly apparent in Figure 9a, 9c, and 9d and somewhat apparent in 9e and 9f. The top of the surface layer is located where the equivalent potential temperature starts to increase relatively slowly or is constant with height. The first horizontal solid line above the surface on the right hand side of the equivalent potential temperature profiles in Figure 9 indicates the top of the surface layer. Figure 9e shows that the aerosol concentration decreases through the surface layer; however, Figure 9a shows no change with height through the surface layer. By examining all of the aerosol profiles, it becomes evident that the surface layer is most apparent in the smaller sized aerosol. The CN concentration typically decreases sharply while the $D_{0.3}$ concentration decreases very slightly.

The contrast between the aerosol concentration at the surface, compared to the lower tropospheric layer, may be due to a strong temperature inversion trapping newly produced

aerosols. These newly produced aerosols could be natural or an anthropogenic effect of Laramie (population 26,000). *Hudson* [1991] points out that even a small coastal town produces a significant increase in CCN concentration. There seems to be some correlation between the strength of the temperature inversion and the degree to which the CN concentration changes from the surface to the bottom of the lower tropospheric layer; however, the current data set is too limited to arrive at any conclusions.

The lower tropospheric layer incorporates the atmospheric region where surface heating produces convection and cumulus cloud formation, which vertically mixes the atmosphere. The lower tropospheric layer extends upwards for several kilometers above the surface layer and is capped by the first sharp increase in equivalent potential temperature. If the first sharp increase in equivalent potential temperature is difficult to discern, then the first sharp decrease in relative humidity is used as an aid in defining the top of the lower tropospheric layer. The lower tropospheric layer is similar to a thermodynamically well-mixed layer; however, the lower tropospheric layer is more general. While the well-mixed layer would be defined by a strict criterion in the change of equivalent potential temperature, no such restriction is placed on the lower tropospheric layer. Consequently, a lower tropospheric layer can always be identified in our profiles. Figure 9a shows an example of the lower tropospheric layer, which runs from near the surface to approximately 5.1 km. The equivalent potential temperature slowly increases within the layer, followed by a relatively sudden increase above the layer. The relative humidity is nearly constant throughout the layer and decreases sharply above the layer. The lower tropospheric layer has slightly decreasing aerosol concentrations with a sharp decrease above the layer. Aerosol concentration does not always decrease with height in the lower tropospheric

layer as is evident by the slight increases in CCN and CN concentration observed in the lower tropospheric layer in Figure 9c.

The upper tropospheric layer incorporates the portion of the troposphere that has not been recently involved in cloud formation. Humidity layers (layers with high relative humidity; clearly defined later) are excluded from the upper tropospheric layer; therefore, layers that were possible involved in recent cloud formation are excluded from the upper tropospheric layer. The upper tropospheric layer extends from the stratosphere downward until the equivalent potential temperature decreases sharply. Within this layer, the equivalent potential temperature increases linearly with height, and the relative humidity is low and relatively constant. The upper tropospheric layer is evident in Figure 9a from approximately 6 to 12 km. The $D_{0.3}$ and CCN concentrations are constant throughout this layer, while the CN concentration decreases slightly.

The stratospheric layer is above the upper tropospheric layer and defined by increases in equivalent potential temperature and measured ozone. No stratospheric layers are present in Figure 9 since the tropopause is above 200 mbar; however, a definition of a stratospheric layer is necessary because winter flights may have tropopauses below 200 mbar and thus have the upper tropospheric layer stop at the bottom of the stratospheric layer instead of 200 mbar. Winter flights typically show increases in CCN concentrations above the upper tropospheric layer. The number of examples of stratospheric CCN layers however is too limited to warrant further discussion. Future measurements are planned to investigate stratospheric CCN.

In addition to the four general layers described above, which can be identified on all profiles, there are sometimes layers where the relative humidity changes abruptly. CCN concentration changes within humidity layers are usually mirrored by similar changes in $D_{0.3}$ and CN concentrations. Figure 9a presents no humidity layers, while Figures 9b-9f present all the

examples of humidity layers found in the data set. These examples can be divided into negative correlation or positive correlation between relative humidity and CCN concentration. Figure 9b at 4 km and Figure 9c at 10 km show negative correlation cases where relative humidity increases, to a maximum of approximately 70%, are associated with a decrease in aerosol concentration. Figure 9b at 4 km shows a two order of magnitude decrease in $D_{0.3}$ as compared with a one order of magnitude decrease in CN. Figure 9b is atypical of the balloon flights due to a trace amount of precipitation reported upwind on the previous day. The high relative humidity of the layer suggests that the air has been recently involved in the formation of precipitation where hydrometers could have removed aerosols from the layer. A more substantial decrease in the larger aerosols, which is observed to be the case in Figure 9b, is to be expected if precipitation is responsible for the aerosol decrease. Even if precipitation did not occur, CCN can still be removed due to Brownian capture [Hoppel *et al.*, 1990] and coalescence scavenging [Hudson and Frisbie, 1991]. The high relative humidity, with respect to water, observed in Figure 9c at 10 km suggests that the air was within or near a cirrus cloud which may be responsible for the observed decrease in aerosols. The OPC would not detect ice crystals present in a cirrus cloud due to the 40 °C heater on the inlet.

Figure 9d at 6.8 km, Figure 9e at 6.8 km, and Figure 9f at 6.5 km show changes in aerosol concentrations that are positively correlated with relative humidity. When these positively correlated humidity layers are present in the balloon ascent profiles they are not present in the balloon descent profiles. Therefore, they do not have a large horizontal extent (<50 km). These flights were conducted in fair weather conditions with the air mass probably not involved in the formation of precipitation for many days. Changes in the aerosol source between the different layers may be the cause for the observed variations. Different aerosol sources could be due to

distinctly different geographical origins of the air within the humidity layer; however, this seems unlikely because the humidity layers are thin and have a small horizontal extent. Another possibility is that the humidity level is an important factor in controlling the formation and/or growth of the aerosols [Salk *et al.*, 1986; Hegg, 1990; Perry and Hobbs, 1994]. Still another possibility is that clouds are responsible for elevating the CCN concentration within humidity layers [Saxena and Grovenstein, 1994]. Radke and Hobbs [1991] give some support to this idea with their observations of high CN concentration associated with high relative humidity around some small cumulus clouds. The observations for any one flight show that the relative humidity is correlated with the CCN concentration, however, there is little correlation between relative humidity and CCN concentration for measurement made on different balloon flights. This would indicate that relative humidity is only a contributing factor and not a controlling factor in determining the CCN concentration.

3. Summary of Laramie, Wyoming Aerosol Profiles

To summarize the measurements above Laramie, Wyoming, the aerosol measurements are grouped into the different atmospheric layers. Due to observed seasonal change in aerosol concentration, the balloon flights have been divided into summer and winter categories. Summer flights include June, July, August, and September balloon flights, and winter flights include November and January balloon flights. The October 22, 1997 balloon flight (Figure 9b) falls between the summer and winter season; therefore, it is not included in the summary. Figure 10 shows the variability of the lower and upper tropospheric measurements and gives aerosol seasonal averages and standard deviations. The summer averages indicate that between the lower and upper tropospheric layers the $D_{0.3}$ concentration decreases by more than an order of magnitude and the CN and CCN concentrations decrease by less than an order of magnitude.

The winter averages, compared to the summer averages, indicate that between the lower and upper tropospheric layers the $D_{0.3}$ and CCN concentration decrease is not as pronounced while the CN concentration decrease is similar. The difference in the concentration decrease for $D_{0.3}$ and CN between the lower and upper troposphere is probably related to differences in sources and sinks and hence aerosol residence times.

The CCN concentrations presented in Figure 10 seem reasonable when compare to previous measurements. *Pruppacher and Klett's* [1997] summary of continental CCN measurements give a range of 600 to 5000 cm^{-3} . The most extensive data to compare our measurements with is that collected by *Hobbs et al.* [1985] in the High Plains of the United States. Frequency distributions of the High Plains CCN measurements indicated two modes: a relatively low CCN concentration mode with mean concentration of 310 cm^{-3} and a higher CCN concentration mode with mean concentration of 2200 cm^{-3} . These concentrations are at 1% supersaturation at ambient pressure not STP. Converting these concentration to STP would cause a change in concentration by less than a factor of 2 assuming lower tropospheric measurements. *Hobbs et al.* [1985] postulate that the low concentration mode is the result of a background source of CCN and that the high concentration mode is due to additional natural and/or anthropogenic sources of CCN. The lower tropospheric CCN concentrations presented in Figure 10 agrees with the low "background" CCN concentration of 310 cm^{-3} .

The CCN/CN ratio and the $D_{0.3}$ /CCN ratio for summer and winter flights at Laramie, Wyoming are presented in Figures 11. The CCN/CN ratio is larger in the upper troposphere than in the lower troposphere (Figures 11a and 11b), while the $D_{0.3}$ /CCN ratio is larger in the lower troposphere than in the upper troposphere (Figures 11c and 11d). The CCN/CN ratio is relatively consistent between the summer and winter flights, whereas the $D_{0.3}$ /CCN ratio in the lower

troposphere decreases between the summer and winter flights. The increase in CCN/CN ratio in the upper troposphere would suggest that the aerosol size spectrum has shifted to larger sizes or that the aerosols are more hygroscopic. *Pruppacher and Klett [1997]* present results from three studies where the continental CCN/CN ratio is from 0.004 to 0.21. These ratios are comparable to the summer lower tropospheric ratio of 0.09 ± 0.07 and the upper tropospheric ratio of 0.16 ± 0.08 .

Figure 12 presents the percentage change in concentration per kilometer (aerosol gradient) for the lower and upper tropospheric layers. It is evident that even in the lower tropospheric layer the aerosol concentration typically decreases with height above the surface. Usually, the CN gradient is the largest indicating that the smaller sized aerosols have the largest decrease with height. The aerosol gradients for CN, CCN, and $D_{0.3}$ are similar in the upper summer troposphere but variable in the lower summer troposphere and in both the upper and lower winter tropospheric layers. The observed decrease of CCN with altitude indicates a source or gas precursor source near the earth's surface. The change in concentration with height within the lower troposphere may be related to the strength of the midlevel temperature inversion that caps the layer. Strong inversions may trap CCN near the top of the lower tropospheric layer, while weak inversions allow CCN to mix with air above the layer. Evidence of a relatively strong midlevel temperature inversion possibly trapping CCN is observed in Figure 9f. At approximately 5.3 km there is a temperature inversion present and the CCN concentrations has increased slightly from the surface to just below the inversion. The observed decrease in CN concentration in the summer and winter upper troposphere is inconsistent with previous observations of a CN maximum below the tropopause (*Hofmann, 1993*). The discrepancy between these observations may be due to the addition of the heated inlet to the CN counter.

Diffusion losses within the tubing connecting the heater and the CN counter are less than 20% in the upper troposphere, which are insufficient to account for the observed difference. Conditioning the air with the 40 °C heater may reduce the size of small sulfuric acid aerosols to the point where they are too small to be detected with the CN counter.

4. Comparison between Wyoming and New Zealand Profiles

To compare the northern midlatitude continental CCN measurements with a southern midlatitude site, 2 balloon flights were conducted at Lauder, New Zealand (45 °S). Lauder, New Zealand is a Southern Hemisphere, midlatitude site that has a landscape and climate similar to Laramie, Wyoming (41 °N). The site is 150 km downwind of the west coast of the south island where an abrupt north-south mountain barrier extends to over 3 km above mean sea level. Table 3 compares the average summer Wyoming and New Zealand measurements. The most striking difference between these measurements is that the CCN concentration is approximately twice as high in New Zealand as in Wyoming, whereas the concentration of $D_{0.3}$ and CN are similar in the New Zealand measurements as in Wyoming. The higher CCN concentrations in New Zealand are not the result of enhanced local pollution since the measured CN and ozone (not shown) concentrations were below the concentrations measured in Wyoming. The larger CCN concentration may be the result of obtaining New Zealand measurements at the height of the seasonal cycle in CCN concentration [Hobbs *et al.*, 1985]; however, none of the Wyoming profiles has CCN concentrations near those obtained in New Zealand. The higher CCN concentration is more likely due to differences in the aerosol spectrum or aerosol chemical composition.

The upper tropospheric CCN measurements above New Zealand agree well with late spring/early summer upper tropospheric measurements made by Hudson *et al.* [1998] of

approximately $200\text{--}300\text{ cm}^{-3}$ over the Southern Ocean. This agreement suggests that there is no major change in CCN concentration when upper tropospheric air passes over New Zealand. However, the CCN concentration substantially increases in the lower troposphere over New Zealand compared to the approximate 200 cm^{-3} measured in the marine boundary layer over the Southern Ocean [Hudson *et al.*, 1998]. A similar contrast between marine air and continental air over New Zealand is observed in the CN concentration. The upper tropospheric CN measurements above New Zealand agree with upper tropospheric measurements of approximately 600 cm^{-3} made by Hudson *et al.* [1998] over the Southern Ocean. The CN concentration substantially increases in the lower troposphere over New Zealand compared to measurements in the marine boundary layer. Hudson *et al.* [1998] obtained CN concentrations of less than 500 cm^{-3} in the marine boundary layer, which is a factor of 10 lower than the lower tropospheric CN concentration obtained above New Zealand (Table 3). The contrast in CN and CCN concentration between marine air and continental air has been observed in previous studies [Pruppacher and Klett, 1998;]. Hudson [1991] observed that the CN concentration is much higher 100 km inland while the CCN concentration at 0.7% supersaturation shows little change in concentration. Comparison between the balloon profiles and Hudson's [1998] measurements show that 150 km inland there is marked change in the CN and CCN concentrations in the lower troposphere, while the upper troposphere concentrations are similar.

5. Conclusions

Fourteen, unique, high vertical resolution, midlatitude, continental CCN profiles have been summarized. These CCN profiles were measured with a balloon-borne instrument and have a higher vertical resolution and a greater altitude range than previously available profiles. In addition to the CCN measurements, concurrent aerosol measurements were also made at smaller

(CN) and larger ($D > 0.3 \mu\text{m}$) sizes. The high vertical resolution of the balloon profiles shows that aerosol measurements can be classified into distinct atmospheric layers based on the thermodynamic properties of equivalent potential temperature and relative humidity. The profiles reveal that changes in CCN concentration are correlated with changes in the aerosol concentration at other sizes, and are associated with humidity changes. A typical profile consists of a relatively constant CCN concentration within the lower tropospheric layer typically from 0.3 to 2.5 km above the surface, a decrease above the lower tropospheric layer, and a relatively constant CCN concentration in the upper troposphere. This typical profile indicates that vertical mixing plays an important role in the distribution of CCN. Differences from this typical profile occur in the presence of humidity layers, which may be related to cloud processes. Humidity layers were observed on 5 out of 14 CCN profiles. Profile changes caused by humidity layers are evident in the three different aerosol size measurements, CN, CCN, $D_{0.3}$.

The average summer lower and upper tropospheric CCN concentration at Laramie, Wyoming (445 ± 157 and 126 ± 34 , respectfully) shows little variability between flights conducted under similar meteorological conditions. Two measurements of CCN profiles above New Zealand indicate concentrations, which are approximately twice as high, in both the lower and upper troposphere, as CCN concentrations in Wyoming. The comparison between Wyoming and New Zealand measurements suggests that geographic location is an important factor in determining CCN concentrations and there relationship to the smaller (CN) and larger size aerosols ($D_{0.3}$). The CCN/CN ratio increases between the lower and upper troposphere, which suggests that in the upper troposphere, the aerosol spectrum has shifted to larger sizes or aerosols are more soluble. The average summer CCN/CN ratio in Wyoming shows an increase from 0.09 in the lower troposphere to 0.17 in the upper troposphere, while in New Zealand the average summer

CCN/CN ratio shows an increase from 0.27 to 0.59. Aerosol gradients within the lower and upper tropospheric layers show relatively small changes within the layers and indicate that smaller sized aerosol decrease the greatest with increasing height above the surface. The decrease in CCN concentration between the lower and upper troposphere and the typical negative gradient in CCN concentration within the lower troposphere suggests a CCN source near the surface.

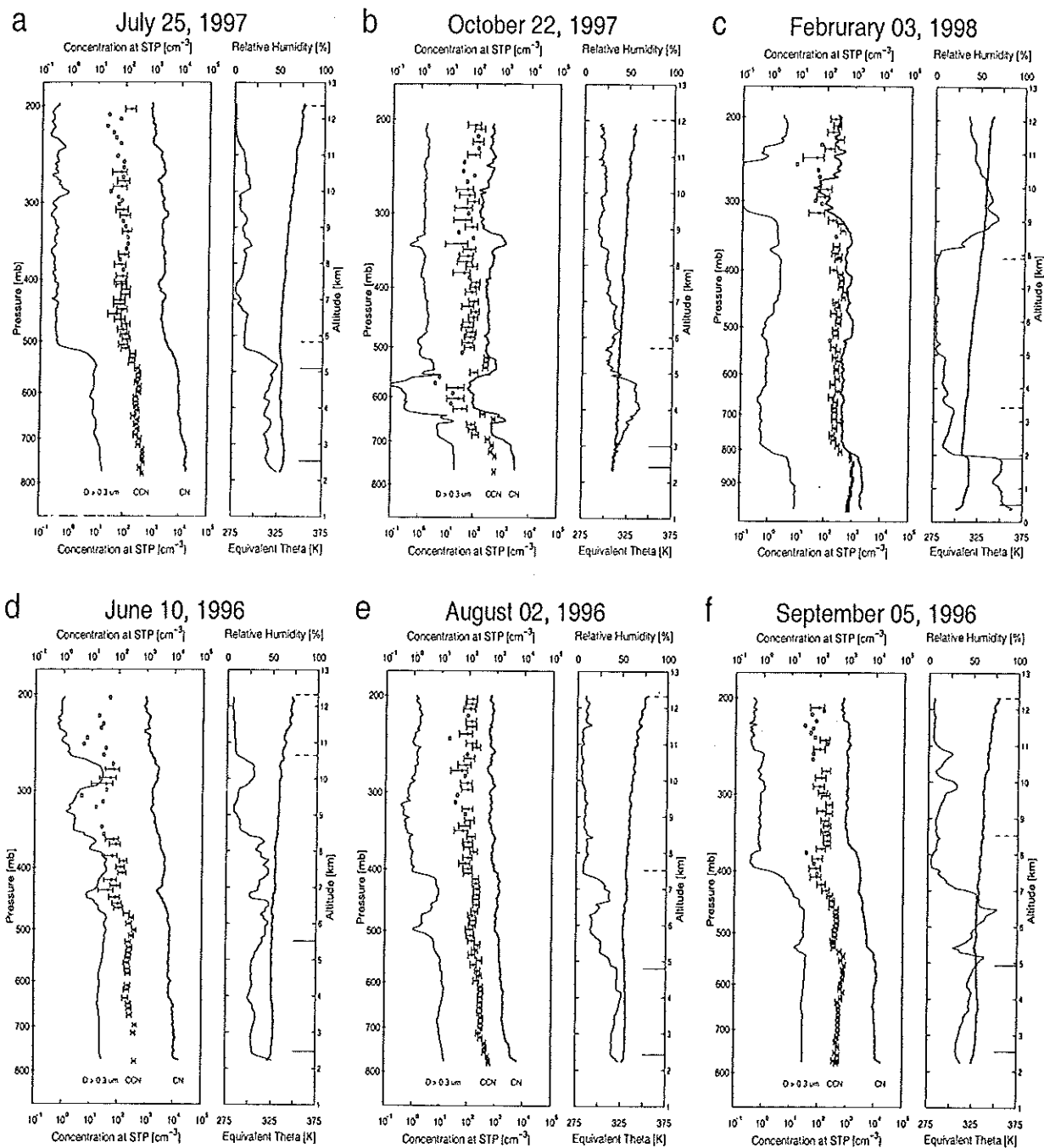
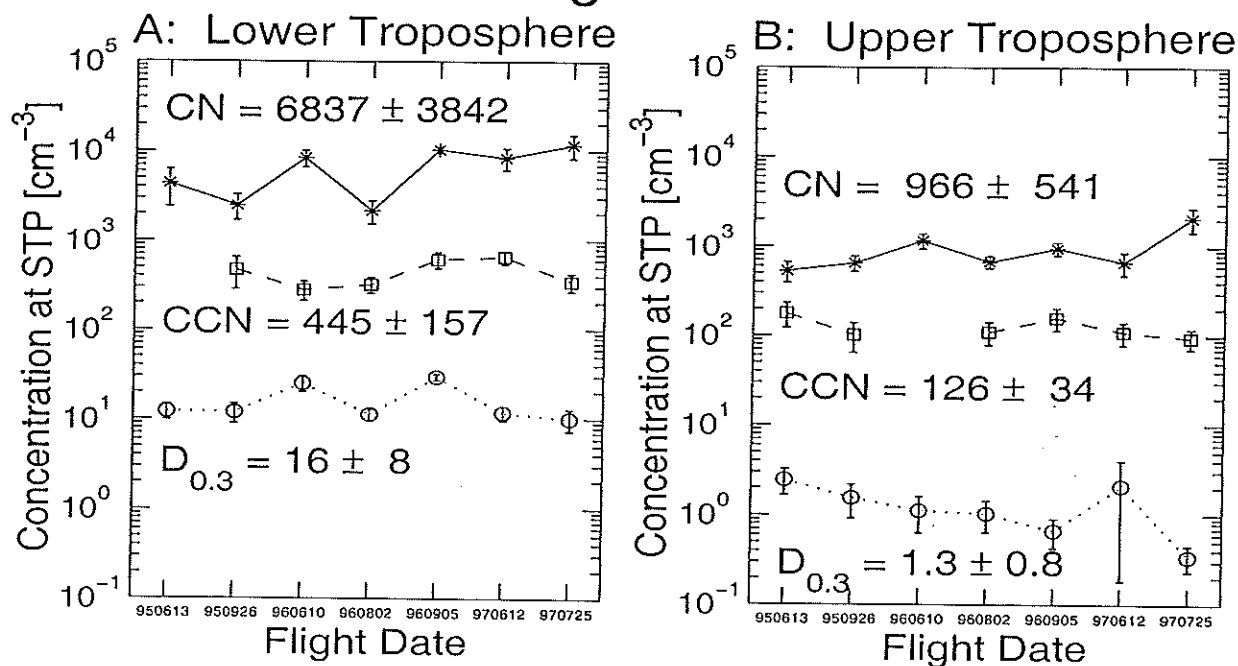


Figure 9. Aerosol profiles that include the smallest size channel of the optical particle counter ($D > 0.3 \mu\text{m}$, thin line), the CCN concentration (1% supersaturation, circles), and the CN concentration ($D > 0.01 \mu\text{m}$, thick line). Open circles represent measurements below the detection limit of the CCN counter. The concentration measured by each aerosol instrument has been corrected to standard temperature and pressure (STP). Equivalent potential temperature (thick line) and relative humidity (thin line) are shown in the right-hand panel. The left axis denotes the measured atmospheric pressure and the far right axis denotes the altitude above mean sea level. The surface at Laramie, Wyoming is at approximately 2.2 km above mean sea level. The horizontal lines on the far right of the equivalent potential temperature plots denote the lower (solid lines) and upper (dashed lines) tropospheric layers.

Summer Flights at Laramie



Winter Flights at Laramie

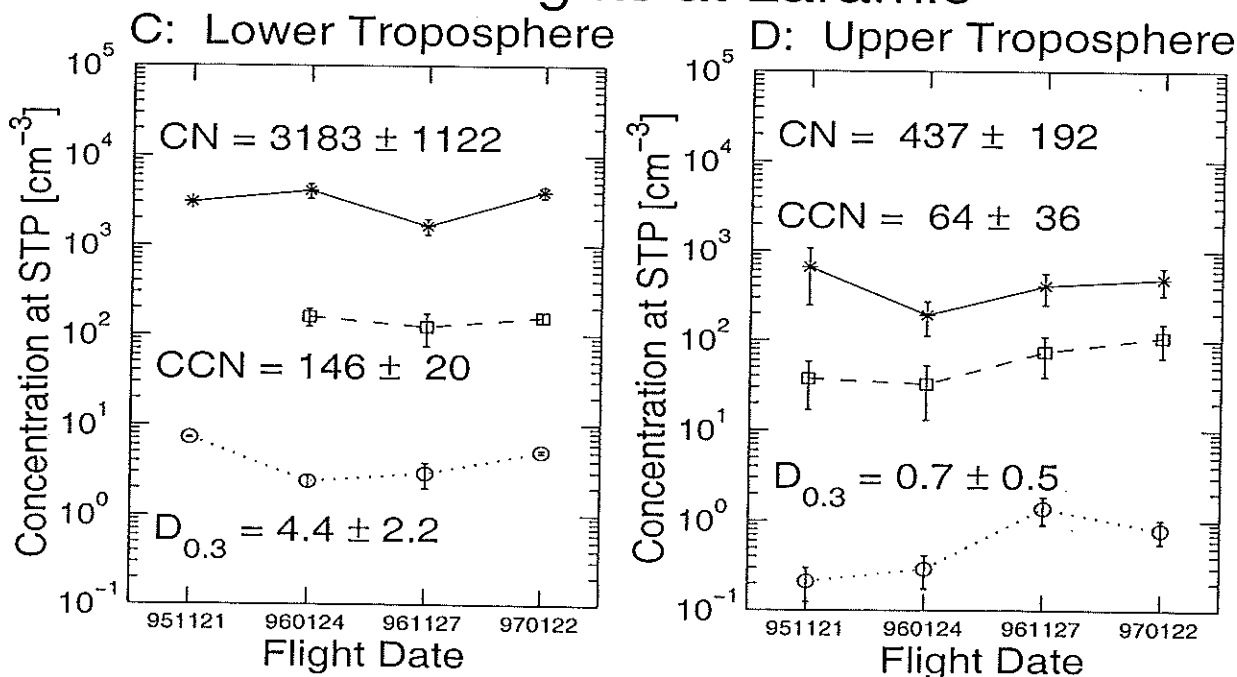


Figure 10. Summer and winter measurement of an optical particle counter ($D > 0.3 \mu\text{m}$, circles), a CCN counter (1% supersaturation, squares), and a CN counter ($D > 0.01 \mu\text{m}$, asterisks) for balloon flights at Laramie, Wyoming. The error bars represent one standard deviation for the measured concentrations within the layer. The aerosol concentrations have been corrected to standard temperature and pressure (STP). Due to instrument problems, some data are missing. The average and standard deviation for the balloon flight data presented in each plot is displayed within the plot. Only measurements above the detection limit of the CCN counter are included, so the upper troposphere CCN concentration may be biased to higher concentration, especially for winter measurements.

Balloon Flights at Laramie

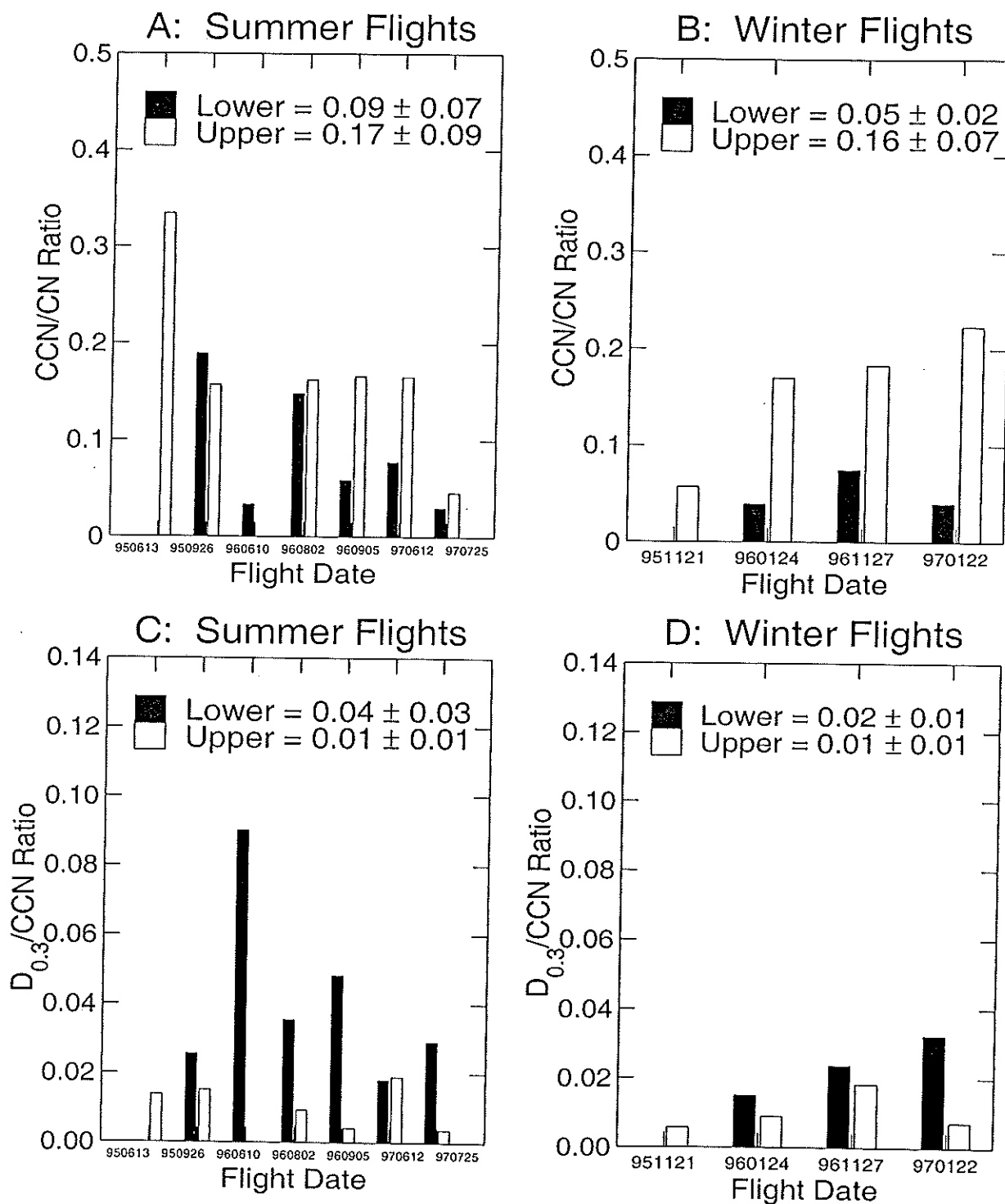
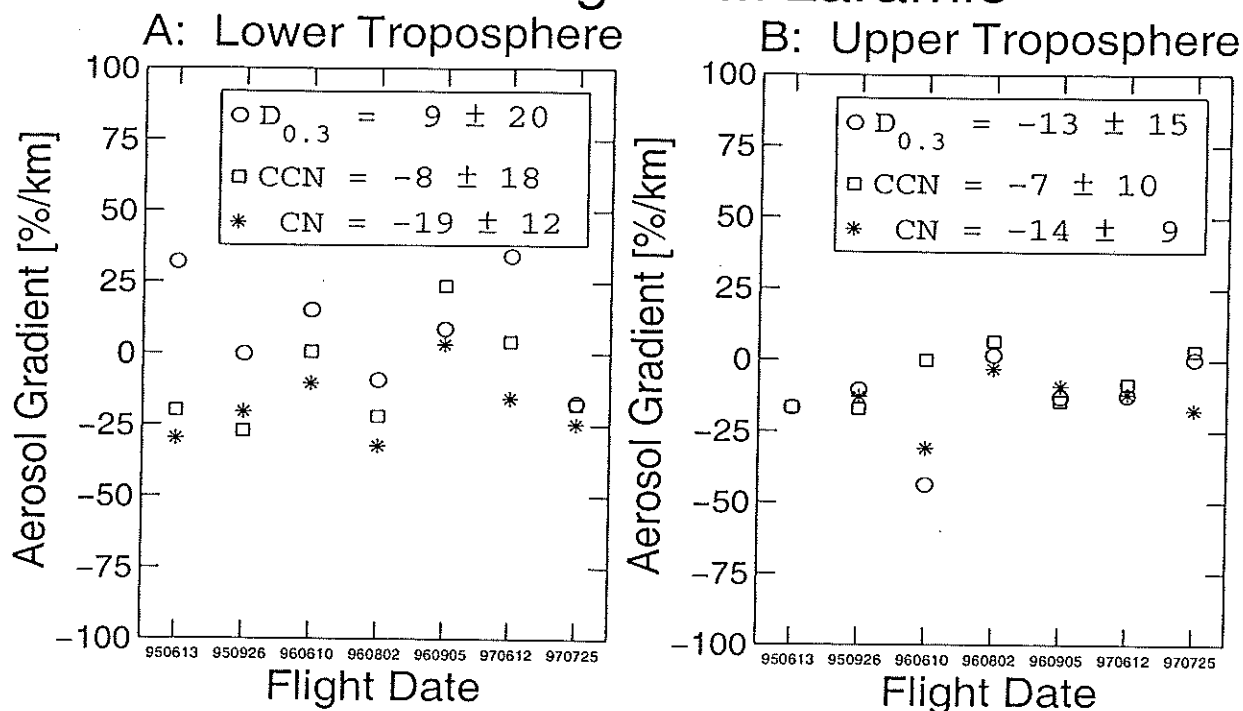


Figure 11. Aerosol ratios for summer and winter flights at Laramie, Wyoming. The average and standard deviation for the lower tropospheric (top line) and upper tropospheric (bottom line) layers are displayed in the legends. The aerosol ratios are computed by averaging aerosol measurements within a layer and then taking the ratio of the aerosol averages.

Summer Flights at Laramie



Winter Flights at Laramie

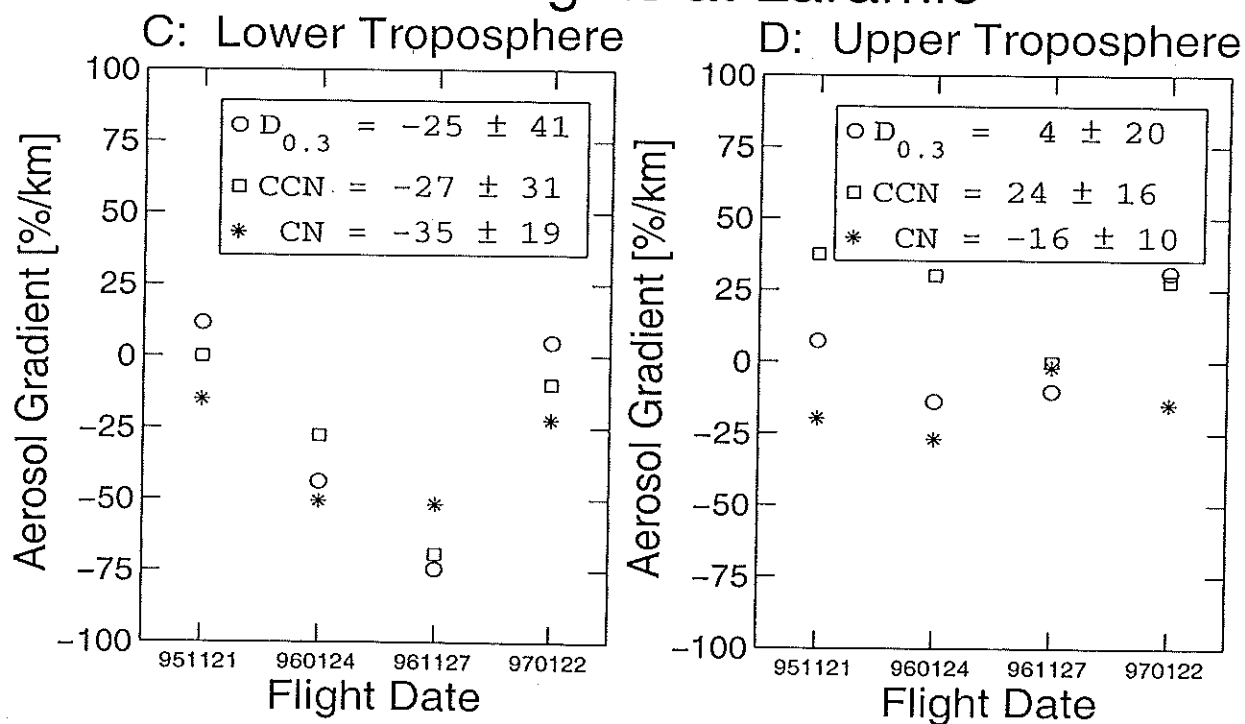


Figure 12. Summer and winter $D_{0.3}$ (circles), CCN (squares), and CN (asterisks) gradients for the lower and upper tropospheric layers. Negative gradients indicate a percentage decrease in concentration with increasing height above the surface. The averages and standard deviations of the layer data presented in each plot are displayed in the legends.

	Summer Balloon Flights at Laramie, Wyoming		Summer Balloon Flights at Lauder, New Zealand	
	Lower Troposphere	Upper Troposphere	Lower Troposphere	Upper Troposphere
$D_{0.3}$ [cm^{-3}]	16 ± 8	1.3 ± 0.8	7.0 ± 1.8	0.9 ± 0.4
CCN [cm^{-3}]	445 ± 157	126 ± 34	964 ± 17	246 ± 49
CN [cm^{-3}]	6837 ± 3842	966 ± 541	5662 ± 4860	445 ± 206
$D_{0.3}/\text{CCN}$	0.041 ± 0.026	0.011 ± 0.006	0.007 ± 0.002	0.004 ± 0.001
CCN/CN	0.09 ± 0.07	0.17 ± 0.09	0.27 ± 0.24	0.59 ± 0.16
$D_{0.3}$ Gradient [%/km]	9 ± 20	-13 ± 15	-30 ± 3	18 ± 30
CCN Gradient [%/km]	-8 ± 18	-7 ± 10	-3 ± 25	2 ± 0.3
CN Gradient [%/km]	-19 ± 12	-14 ± 9	-34 ± 46	-3 ± 8

Table 3. Average aerosol concentrations and standard deviations in the lower and upper troposphere for summer balloon flights at Laramie, Wyoming (7 flights) and Lauder, New Zealand (2 flights). The aerosol ratios are computed by averaging measurements within a layer and then taking the ratio of the aerosol averages. Negative aerosol gradients indicate a decrease in concentration with increasing height above the surface.

CHAPTER 4: Conclusions

1. Summary

A photometric CCN counter was calibrated using a video camera and PC frame grabber card to count droplets. Droplet number is linearly related to the amount of laser light scattered by the droplets. The standard calibration procedure for the CCN counter is repeatable to better than 10% accuracy. The calibration relationship between droplet number and photodetector voltage was verified by a comparison between the CCN counter and a CN counter when sampling monodisperse aerosol. Calibration of the CCN counter is found to depend on supersaturation and to have a slight dependence on the size of CCN that activate to form droplets. The dependence on supersaturation is easily accounted for by using a power law function to relate the calibration slope to supersaturation. The calibration dependence on CCN size is less than 10% at 1% supersaturation. Calibration on ambient atmospheric aerosol appears similar to the standard calibration procedure. Laboratory calibration measurements, compared to field measurements at various locations and within different atmospheric layers, give average photodetector voltage peaks that occur at similar times after an air sample enters the thermal gradient-diffusion chamber. Therefore, it appears that within the diffusion chamber atmospheric CCN behave similar to laboratory produce CCN. Random errors in measured CCN concentration can be computed using Poisson counting statistics and range from 36 to 11% for CCN concentrations in the range of 50 to 500 cm^{-3} . The calibration constant that relates photodetector voltage to CCN concentration is believed to have an accuracy of 10% at 1% supersaturation.

Fourteen, unique, high vertical resolution, midlatitude, continental CCN profiles have been summarized. These CCN profiles were measured with a balloon-borne instrument and have a higher vertical resolution and a greater altitude range than previously available profiles. In addition to the CCN measurements, concurrent aerosol measurements were also made at smaller (CN) and larger ($D > 0.3 \mu\text{m}$) sizes. The high vertical resolution of the balloon profiles shows that aerosol measurements can be classified into distinct atmospheric layers based on the thermodynamic properties of equivalent potential temperature and relative humidity. The profiles reveal that changes in CCN concentration are correlated with changes in the aerosol concentration at other sizes, and are associated with humidity changes. A typical profile consists of a relatively constant CCN concentration within the lower tropospheric layer typically from 0.3 to 2.5 km above the surface, a decrease above the lower tropospheric layer, and a relatively constant CCN concentration in the upper troposphere. Differences from this typical profile occur in the presence of humidity layers, which may be related to cloud processes. Profile changes caused by humidity layers are evident in the three different aerosol size measurements, CN, CCN, $D_{0.3}$.

The average summer lower and upper tropospheric CCN concentration at Laramie, Wyoming (445 ± 157 and 126 ± 34 , respectfully) shows little variability between flights conducted under similar meteorological conditions. Two measurements of CCN profiles above New Zealand indicate concentrations, which are approximately twice as high, in both the lower and upper troposphere, as CCN concentrations in Wyoming. The comparison between Wyoming and New Zealand measurements suggests that geographic location is an important factor in determining CCN concentrations and there relationship

to the smaller (CN) and larger size aerosols ($D_{0.3}$). The CCN/CN ratio increases between the lower and upper troposphere, which suggests that in the upper troposphere, the aerosol spectrum has shifted to larger sizes or aerosols are more soluble. The average summer CCN/CN ratio in Wyoming shows an increase from 0.09 in the lower troposphere to 0.17 in the upper troposphere, while in New Zealand the average summer CCN/CN ratio shows an increase from 0.27 to 0.59. Aerosol gradients within the lower and upper tropospheric layers show relatively small changes within the layers and indicate that smaller sized aerosol decrease the greatest with increasing height above the surface. The decrease in CCN concentration between the lower and upper troposphere and the typical negative gradient in CCN concentration within the lower troposphere suggests a CCN source near the surface.

2. Future Work

Several improvements could be made to the balloon-borne CCN counter to obtain measurements that are more accurate. The thermoelectric coolers do not maintain the temperature difference between the top and the bottom plates as closely as the newer aircraft CCN counters. It seems that the thermoelectric coolers are not as efficient, and hence generate more excess heat on the balloon-borne CCN counter compared to the aircraft CCN counters. By improving the system to cool the bottom plate, it may be possible to obtain measurements above 200 mbar without the possibility of over heating the CCN counter. The sensitivity of the balloon-borne CCN counter is less than the sensitivity of the aircraft CCN counter. The cause for the difference in sensitivity is not apparent. Initially, it was believed that the balloon-borne CCN counter's laser might have been damaged when it was installed; however, the laser was replaced in November 1998

which resulted in an 18% reduction in the calibration (Appendix II). Therefore, it seems unlikely that the laser is the cause for the difference. Major changes and recalibration of the CCN counter are necessary to improve the CCN counter's thermoelectric coolers and sensitivity.

While the improvements discussed above should be incorporated into the design of a new balloon-borne CCN counter, the current balloon-borne CCN counter has some features that need to be preserved in future designs. The passing of air through the CCN counter for 0.3 s before it enters the chamber is very important. It allows air to come to thermal equilibrium with the enclosure temperature of the CCN counter before it enters the thermal-gradient diffusion chamber. This minimizes the possibility of creating transient supersaturations above the steady state supersaturation. Transient supersaturation above the steady state supersaturation also can be produced by creating turbulence when introducing an air sample into the chamber. Turbulence invariably brings an incoming sample in contact with the hotter moist surface thereby generating unpredictable supersaturations [Saxena *et al*, 1970]. To minimize the possible of turbulence when introducing a sample, the current design of having a long straight tube on the chamber's inlet should be preserved. The long straight tube allows for the development of laminar flow, which should be preserved when an air sample enters the chamber.

Another critical advantage of the balloon-borne CCN counter over the new aircraft CCN counts is the long duration of time that the blotting papers remain moist. The blotting papers in the balloon-borne CCN counter remain moist for over 3 hr (Figure 3), while the aircraft CCN counters need to be rewet every hour, and sometimes more often.

Manually rewetting the blotting papers every hour is not possible during a 3 hr balloon flight. The time difference for which the blotting papers stay moist may be related to the difference in the flow rates through the CCN counters. The balloon-borne CCN counter has a flow rate of approximately 2.25 L/min, while the aircraft CCN counters have a flow rate of 3-4 L/min.

The generation of calibration aerosols could be improved by using a currently available model 3075 TSI constant output atomizer. A diffusional dryer can be used to remove water from the generated aerosols. The high concentration of aerosols produced with the atomizer can be diluted using dry filtered air. This type of aerosol generation system will allow better control, compared to the current system, over the concentration of aerosol that enter the CCN counter. It will also ensure that there is no contamination of the air sample by room aerosols. Figure 13 presents example of the aerosol spectra produced with the constant output atomizer. The atomizer produces a single model polydisperse size spectrum. The peaks in Figure 13 are probably an artifact since they are only present in a single measurement and the locations are not consistent between measurements.

The CCN counter's calibration needs to be verified at supersaturations lower than 1% by comparing the CCN counter's concentration to the concentration measured by the TSI CN counter when both instruments are concurrently sampling monodisperse aerosols. This is necessary since droplets are smaller at lower supersaturations; therefore, the video camera system may not be adequate to count all droplets within the video sample volume. The calibration dependence on initial aerosol size needs to be checked at supersaturation lower than 1% since the dependence on aerosol size may be more substantial at lower

supersaturations. Once the calibration at lower supersaturation is varied, the activation of CCN within the thermal-gradient diffusion chamber needs to be compared with Kohler theory. Sampling monodisperse, totally soluble aerosols, over a range of supersaturations, is a check that aerosols activate at supersaturations consistent with Kohler theory.

To address climate change issues, it is important to relate CCN measurements to concurrent aerosol measurements. Aerosol information in climate models is typically represented by lognormal distributions of the aerosol number spectrum and aerosol chemical composition [Ghan *et al.*, 1995]. Each lognormal distribution is derived from the total particle number, the geometric number mean diameter, and the geometric standard deviation. Climate models also typically use a parameterization to relate aerosol number concentration to cloud droplet number concentration [Pan *et al.*, 1998]. CCN measurements can represent the cloud droplet number concentration. This representation is valid if the maximum supersaturation that a parcel experienced during its ascent is the same as the supersaturation in the CCN counter and if the droplets growth is the result of condensation of water vapor alone.

Relationships between CCN measurements and aerosol properties can be used to test and improve climate models. One method of relating CCN measurements to aerosol properties is to develop a relationship between CCN concentration and aerosol volume. There may not be much correlation between CCN concentration at 1% supersaturation and aerosol volume since each is dominated by a different aerosol size mode; however, Boucher and Lohmann [1995] used the relationship between sulfate aerosol mass concentration and CCN concentration at 0.3% supersaturation derived by Berresheim *et*

al [1993] in their modeling of the indirect forcing by CCN. A second method is to relate CCN concentration to aerosol surface area. While aerosol surface area is not typically computed in climate models, a comparison could be used to test climate models. A third method, which is the most interesting and difficult, is to relate the CCN concentration to the aerosol number distribution. Each of these methods for relating CCN concentration to aerosol properties should be investigated. Measuring the aerosol number concentration is difficult with the balloon borne instruments because of a lack of size resolution in the nucleation mode ($<0.30\ \mu\text{m}$ diameter). A determination should be made to see if the balloon aerosol instruments could be used to parameterize the aerosol number spectrum sufficiently to allow a useful relationship to be developed between the aerosol number spectrum and CCN concentration. CCN measurements at lower supersaturation, instead of 1% supersaturation, will probably have better correlation with the aerosol properties measured using the balloon-borne instruments. Thus, an additional measurement at a lower supersaturation will be helpful in relating CCN measurements to aerosol properties.

Polydisperse NaCl Aerosol

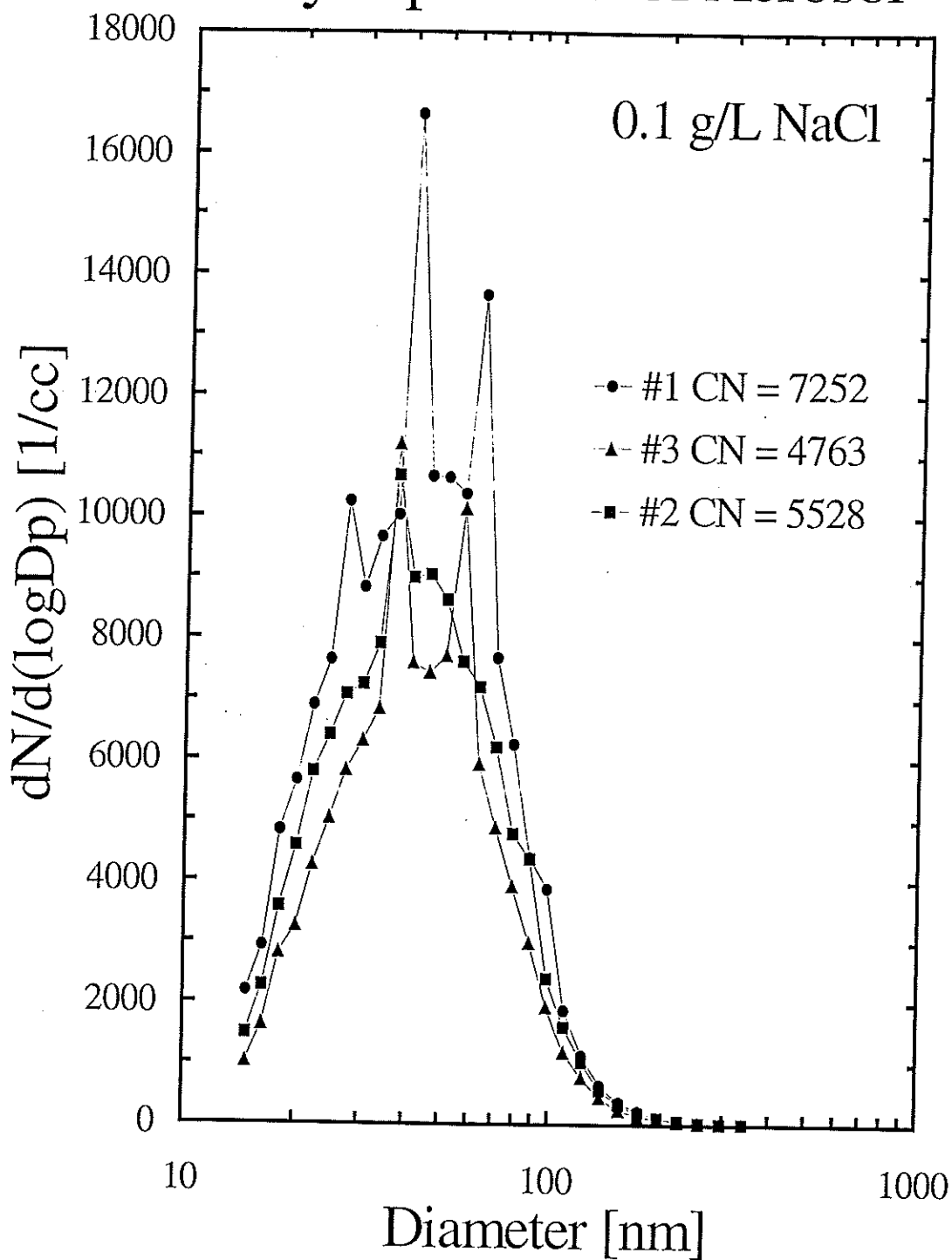


Figure 13. Examples of the aerosol size spectrum generated using a solution of 0.1 g/L of NaCl in a model 3075 TSI constant output atomizer. Legend gives the total number concentration, in cm^{-3} , for each aerosol size spectrum.

References

- Albrecht, B. A.; Aerosol, cloud microphysics, and fractional cloudiness, *Science*, 245, 1227-1230, 1989.
- Auer A. H., Determination of condensation nuclei spectra and supersaturation values in Yellowstone National Park, *J. Rech. Atmos.*, 3, 289-295, 1966.
- Bartlett, B. M., and G. P. Ayers, Static diffusion cloud chamber, *J. Rech. Atmos.*, 15, 231-233, 1981.
- Berresheim, H., F. L. Eisele, D. J. Tanner, L. M. McInnes, D. C. Ramsey-Bell, and D. S. Covert, Atmospheric sulfur chemistry and cloud condensation nuclei (CCN) concentrations over the northeastern pacific coast, *J. Geophys. Res.*, 98, 12,701-12,711, 1993.
- Bigg, E. K., J. L. Gras, and C. Evans, Origin of Aitken Particles in Remote Regions of the Southern Hemisphere, *J. Atmos. Chem.*, 1, 203-214, 1984.
- Birmili, W., F. Stratmann, A. Wiedensohler, D. Covert, L. M. Russell, and O. Berg, Determination of differential mobility analyzer transfer functions using identical instruments in series, *Aerosol Sci. Technol.*, 27, 215-223, 1997.
- Boucher, O., and T. L. Anderson, General circulation model assessment of the sensitivity of direct climate forcing by anthropogenic sulfate aerosols to aerosol size and chemistry, *J. Geophys. Res.*, 100, 26,117-26,134, 1995.
- Boucher, O., and U. Lohmann, The sulfate-CCN-cloud albedo effect A sensitivity study with two general circulation models, *Tellus*, 47B, 281-300, 1995.
- Charlson, R. J. and J. Heintzenberg, *Aerosol Forcing of Climate*, pp 197-296, John Wiley & Sons, New York, 1995.
- Charlson, R. J., S. E. Schwartz, J. M. Hales, R. D. Cess, J. A. Coakley, Jr., J. E. Hansen, and D. J. Hofmann, Climate forcing by anthropogenic aerosols, *Science*, 255, 423-430, 1992.
- Chuang, C. C., J. e. Penner, and L. L. Edwards, Nucleation scavenging of smoke particles and simulated drop size distributions over large biomass fires, *J. Atmos. Sci.*, 49, 1264-1275, 1992.
- Chuang, C. C., J. E. Penner, K. E. Taylor, A. S. Grossman, and J. J. Walton, An assessment of the radiative effects of anthropogenic sulfate, *J. Geophys. Res.*, 102, 3761-3778, 1997.
- Chylek, P. and J. G. D. Wong, Erroneous use of the modified Kohler equation in cloud and aerosol physics applications, *J. Atmos. Sci.*, 55, 1473-1477, 1998.
- Clarke, A. D., Atmospheric nuclei in the remote free-troposphere, *J. Atmos. Chem.*, 14, 479-488, 1992.
- Clarke, A. D., Atmospheric nuclei in the Pacific Midtroposphere: Their nature, concentration, and evolution, *J. Geophys. Res.*, 98, 20,633-20,647, 1993.
- Covert, D. S., J. L. Gras, A. Wiedensohler, and F. Stratmann, Comparison of directly measured CCN with CCN modeled from the number-size distribution in the marine boundary layer during ACE 1 at Cape Grim, Tasmania, *J. Geophys. Res.*, 103, 16,597-16,608, 1998.
- Delene, D. J., T. Deshler, P. Wechsler, and G. A. Vali, A balloon-borne cloud condensation nuclei counter, *J. Geophys. Res.*, 103, 8927-8934, 1998.

- de Oliveira, J. C. P. and G. Vali, Calibration of a photoelectric cloud condensation nucleus counter, *Atmos. Res.*, 38, 237-248, 1995.
- Deshler, T., D. J. Hofmann, B. J. Johnson, and W. R. Rozier, Balloonborne measurements of the Pinatubo aerosol size distribution and volatility at Laramie, Wyoming during the summer of 1991, *Geophys. Res. Lett.*, 19, 199-202, 1992.
- Eagan, R. C., P. V. Hobbs, and L. F. Radke, Measurements of cloud condensation nuclei and cloud droplet size distributions in the vicinity of forest fires, *J. Appl. Meteorol.*, 13, 553-557, 1974.
- Fitzgerald, J. W., Non-steady-state supersaturations in thermal diffusion chambers, *J. Atmos. Sci.*, 27, 70-72, 1970.
- Ghan, S. J., C. C. Chuang, and J. E. Penner, A parameterization of cloud droplet nucleation. Part I: single aerosol type, *Atmos. Res.*, 30, 197-221, 1993.
- Ghan, S. J., C. C. Chuang, R. C. Easter, J. E. Penner, A parameterization of cloud droplet nucleation. Part II: multiple aerosol types, *Atmos. Res.*, 36, 39-54, 1995.
- Gras, J. L., CN, CCN and particle size in Southern Ocean air at Cape Grim, *Atmos. Res.*, 35, 233-251, 1995.
- Haywood, J. M., and K. P. Shine, The effect of anthropogenic sulfate and soot aerosol on the clear sky planetary radiation budget, *Geophys. Res. Lett.*, 22, 603-606, 1995.
- Han, Q., W. B. Rossow, and A. A. Lacis, Near-global survey of effective droplet radii in liquid water clouds using ISCCP data, *J. Clim.*, 465-497, 1994.
- Hegg, D. A., Heterogeneous production of cloud condensation nuclei in the marine atmosphere, *Geophys. Res. Lett.*, 17, 2165-2168, 1990.
- Hegg, D. A., Particle production in clouds, *Geophys. Res. Lett.*, 18, 995-998, 1991.
- Hegg, D. A., L. F. Radke, and P. V. Hobbs, measurements of Aitken nuclei and cloud condensation nuclei in the marine atmosphere and their relation to the DMS-cloud-climate hypothesis, *J. Geophys. Res.*, 96, 18,727-18,733, 1991.
- Hegg, D. A., R. J. Rerek, and P. V. Hobbs, Cloud condensation nuclei over the Arctic Ocean in early spring, *J. Appl. Meteorol.*, 34, 2076-2082, 1995.
- Hindman, E. E., P. V. Hobbs, and L. F. Radke, Cloud condensation nuclei from a paper mill. Part I: measured effects on clouds, *J. Appl. Meteorol.*, 16, 745-752, 1977.
- Hobbs, P. V., *Aerosol--Cloud--Climate Interactions*, pp 33-73, Academic Press, Inc., San Diego, CA, 1993.
- Hobbs, P. V., L. F. Radke, and S. E. Shumway, Cloud condensation nuclei from industrial sources and their apparent influence on precipitation in Washington State, *J. Atmos. Sci.*, 27, 81-89, 1970.
- Hobbs, P. V., D. A. Bowdle, and L. F. Radke, Particles in the lower troposphere over the High Plains of the United States. Part II: Cloud Condensation Nuclei, *J. Climate and Appl. Meteorol.*, 24, 1358-1369, 1985.
- Hofmann, D. J., Twenty years of balloon-borne tropospheric aerosol measurements at Laramie, Wyoming, *J. Geophys. Res.*, 98, 12,753-12,766, 1993.
- Hofmann, D. J. and T. Deshler, Stratospheric cloud observations during formation of the Antarctic ozone hole in 1989, *J. Geophys. Res.*, 96, 2897-2912, 1991.
- Holton, J. R., P. H. Haynes, M. E. McIntyre, A. R. Douglass, R. B. Rood, and L. Pfister, Stratosphere-Troposphere Exchange, *Rev. Geophys.*, 33, 403-439, 1995.

- Hoppel, W. A., and T. A. Wojciechowski, Description and discussion of the NRL TGDCC, *J. Rech. Atmos.*, 15, 209-213, 1981.
- Hoppel, W. A., J. E. Dinger, and R. R. Ruskin, Vertical profiles of CCN at various geographical locations, *J. Atmos. Sci.*, 30, 1410-1420, 1973.
- Horvath, H., R. L. Gunter, and S. W. Wilkison, Determination of the coarse mode of the atmospheric aerosol using data from a forward-scattering spectrometer probe, *Aerosol Sci. Tech.*, 12, 964-980, 1990.
- Hudson, J. G., Observations of anthropogenic cloud condensation nuclei, *Atmos. Environ.*, 25A, 2449-2455, 1991.
- Hudson, J. G., Cloud condensation Nuclei near marine Cumulus, *J. Geophys. Res.*, 98, 2693-2702, 1993a.
- Hudson, J. G., Cloud Condensation Nuclei, *J. Appl. Meteorol.*, 32, 596-607, 1993b.
- Hudson, J. G., and P. Squires, Continental surface measurements of CCN flux, *J. Atmos. Sci.*, 35, 1289-1295, 1978.
- Hudson, J. G., and P. R. Frisbie, Surface cloud condensation nuclei and condensation nuclei measurements at Reno, Nevada, *Atmos. Environ.*, 25A, 2285-2299, 1991.
- Hudson, J. G., and P. R. Frisbie, Cloud condensation nuclei near Marine Stratus, *J. Geophys. Res.*, 96, 20,795-20,795, 1991b.
- Hudson, J. G., and G. Svensson, Cloud microphysical relationships in California Marine Stratus, *J. Appl. Meteorol.*, 34, 2655-2666, 1995.
- Hudson, J. G., and Y. Xie, Cloud condensation nuclei measurements in the high troposphere and in jet aircraft exhaust., *Geophys. Res. Lett.*, 25, 1395-1398, 1998.
- Hudson, J.G., Y. Xie, and S. S. Yum, Vertical distributions of cloud condensation nuclei spectra over the summertime Southern Ocean, *J. Geophys. Res.*, 103, 16,609-16,624, 1998.
- Jennings, S. G., *Aerosol Effects on Climate*, pp 275-297, The University of Arizona Press, Tucson & London, 1993.
- Jennings, S. G., and C. D. O'Dowd, Volatility of aerosol at Mace Head, on the west coast of Ireland, *J. Geophys. Res.*, 95, 13,937-13,948, 1990.
- Jones, A., D. L. Roberts, and A. Slingo, A climate model study of indirect radiative forcing by anthropogenic sulphate aerosols, *Nature*, 370, 450-453, 1994.
- Katz, J. L., and P. Mirabel, Calculation of supersaturation profiles in thermal diffusion cloud chambers, *J. Atmos. Sci.*, 32, 646-652, 1975.
- Kent, G. S., M. P. McCormick, and S. K. Schaffner, Global Optical Climatology of the Free Tropospheric Aerosol from 1.0-um Satellite Occultation Measurements, *J. Geophys. Res.*, 96, 5249-5267, 1991.
- Knutson, E. O. and K. T. Whitby, Aerosol classification by electric mobility: Apparatus, theory, and applications, *J. Aerosol Sci.*, 6, 443-451, 1975.
- Lala, G. G., J. E. Jiusto, An automatic light scattering CCN counter, *J. Appl. Meteorol.*, 16, 413-418, 1977.
- Lala, G. G., An automatic light scattering CCN counter, *J. Rech. Atmos.*, 15, 259-262, 1981.
- Langner, J. and H. Rodhe, A global three-dimensional model of the tropospheric sulfur cycle, *J. Atmos. Chem.*, 13, 225-263, 1991.

- Langner, J., H. Rodhe, P. J. Crutzen, and P. Zimmermann, Anthropogenic influence on the distribution of tropospheric sulphate aerosol, *Nature*, 359, 712-715, 1992.
- Lin, X., W. L. Chameides, C. S. Kiang, A. W. Stelson, and H. Berresheim, A model study of the formation of cloud condensation nuclei in remote marine areas, *J. Geophys. Res.*, 97, 18,161-18,171, 1992.
- Liu, P. S. K., W. R. Leitch, C. M. Banic, and S. M. Li, Aerosol observations at Chebogue Point during the 1993 North Atlantic Regional Experiment: Relationships among cloud condensation nuclei, size distribution, and chemistry, *J. Geophys. Res.*, 101, 28,971-28,990, 1996.
- Meehl, G. A., W. M. Washington, D. J. Erickson III, B. P. Briegleb, and P. J. Jaumann, Climate change from increased CO₂ and direct and indirect effects of sulfate aerosols, *Geophys. Res. Lett.*, 23, 3755-3758, 1996.
- Minnis, P., E. f. Harrison, L. L. Stowe, G. G. Gibson, F. M. Denn, d. R. Doelling, and W. L. Smith, Jr., Radiative climate forcing by the Mount Pinatubo Eruption, *Science*, 259, 1411-1415, 1993.
- Mohnen, V. A., Stratospheric Ion and Aerosol Chemistry and Possible Links with Cirrus Cloud Microphysics--A Critical Assessment, *J. Atmos. Sci.*, 47, 1933-1947, 1990.
- O'Dowd, C. D., J. A. Lowe, M. H. Smith, B. Davison, C. N. Hewitt, and R. M. Harrison, Biogenic sulphur emissions and inferred non-sea-salt-sulphate cloud condensation nuclei in and around Antarctica, *J. Geophys. Res.*, 102, 12,839-12,854, 1997.
- Pan, W., M. a. Tatang, g. J. McRae, and R. g. Prinn, Uncertainty analysis of indirect radiative forcing by anthropogenic sulfate aerosols, *J. Geophys. Res.*, 103, 3815-3823, 1998.
- Parungo, F., J. F. Boatman, H. Sievering, S. W. Wilkison, and B. B Hicks, Trends in global marine cloudiness and anthropogenic sulfur, *J. Clim.*, 7, 434-440, 1994.
- Penner, J. E., R. J. Charlson, J. M. Hales, N. S. Laulainen, R. Leifer, T. Novakov, J. Ogren, L. F. Radke, S. E. Schwartz, and L. Travis, Quantifying and minimizing uncertainty of climate forcing by Anthropogenic aerosols, *Bull. Amer. Meteor. Soc.*, 75, 375-400, 1994.
- Perry, K. D., and P. V. Hobbs, Further evidence for particle nucleation in clear air adjacent to marine cumulus clouds, *J. Geophys. Res.*, 99, 22,803-22,818, 1994.
- Philippin, S. and E. A. Betterton, Cloud condensation nuclei concentrations in Southern Arizona: Instrumentation and early observations, *Atmos. Res.*, 43, 263-275, 1997.
- Pinnick, R. G., S. G. Jennings, and G. Fernandez, Volatility of aerosols in the arid southwestern United States, *J. Atmos. Sci.*, 44, 562-576, 1987.
- Pruppacher, H. R., J. D. Klett, *Microphysics of Clouds and Precipitation*, pp 287-289, Kluwer Academic Publishers, Boston, 1997.
- Radke, L. F., and P. V. Hobbs, Humidity and particle fields around some small cumulus clouds, *J. Atmos. Sci.*, 48, 1190-1193, 1991.
- Raga, G. B., and P. R. Jonas, Vertical distribution of aerosol particles and CCN in clear air around the British Isles, *Atmos. Environ.*, 29, 673-684, 1995.
- Roberts G, R. Flagan, G. Lala, and M. Andreae, Photodetector output calibration of a photometric static thermal-gradient cloud condensation nuclei counter, paper presented at 16th Annual Conference of the American Association for Aerosol Research, Denver, Colorado, 1997.

- Rood, M. J., D. S. Covert, and T. V. Larson, Temperature and humidity controlled nephelometry: Improvements and calibration, *Aerosol Sci. Technol.*, 7, 57-65, 1987.
- Rogers, C. F., J. G. Hudson, W. C. Kocmond, Measurements of cloud condensation nuclei in the stratosphere around the plume of Mount St. Helens, *Science*, 211, 824-825, 1981.
- Rogers, R. R. and M. K. Yau, *A short course in cloud physics*, pp. 99-120, Elsevier Science Inc., New York, 1989.
- Rosen, J. M., The vertical distribution of dust to 30 km, *J. Geophys. Res.*, 69, 4673-4676, 1964.
- Rosen, J. M., The boiling point of stratospheric aerosols, *J. Appl. Meteorol.*, 10, 1044-1046, 1971.
- Rosen, J. M. and D. J. Hofmann, Balloonborne measurements of Condensation Nuclei, *J. Appl. Meteorol.*, 16, 56-62, 1977.
- Salk (Suck) S. H., R. E. Thurman, and C. H. Kim, Growth of ultrafine particles by brownian coagulation, *Atmos. Environ.*, 20, 773-777, 1986.
- Saxena, V. K., J. N. Burford, and J. L. Kassner, Jr., Operation of a thermal diffusion chamber for measurements on cloud condensation nuclei, *J. Atmos. Sci.*, 27, 73-80, 1970.
- Saxena, V. K., and J. D. Grovenstein, The role of clouds in the enhancement of cloud condensation nuclei concentrations, *Atmos. Res.*, 31, 71-89, 1994.
- Saxena, V. K., Bursts of cloud condensation nuclei (CCN) by dissipating clouds at Palmer Station, Antarctica, *Geophys. Res. Lett.*, 23, 69-72, 1996.
- Singh, H. B., *Composition, Chemistry, and Climate of the Atmosphere*, Chapter 5, Van Nostrand Reinhold, New York, 1995.
- Squires, P., and S. Twomey, A comparison of cloud nucleus measurements over central North America and the Caribbean Sea, *J. Atmos. Sci.*, 23, 401-404, 1966.
- Schafer, B., H. W. Georgii, Airborne measurements of condensation nuclei and cloud condensation nuclei above the Alpine Foothills, *Beitr. Phys. Atmosph.*, 67, 225-340, 1994.
- Silvente, E., and M. Legrand, Ammonium to sulphate ratio in aerosol and snow of Greenland and Antarctic regions, *Geophys. Res. Lett.*, 20, 687-690, 1993.
- Taylor, K. E., and J. E. Penner, Response of the climate system to atmospheric aerosols and greenhouse gases, *Nature*, 369, 734-737, 1994.
- Twomey, S., The nuclei of natural cloud formation Part I: the chemical diffusion method and its application to atmospheric nuclei, *Geofis. Pur. Appl.*, 43, 227-250, 1959.
- Twomey, S., *Atmospheric Aerosols*, Elsevier, New York, 1977.
- Twomey, S., Aerosols, Clouds and Radiation, *Atmos. Environ.*, 25A, 2435-2442, 1991.
- Twomey, S., and T. a. Wojciechowski, Observations of the geographical variation of cloud nuclei, *J. Atmos. Sci.*, 26, 684-688, 1969.
- Wang, P., P. Minnis, and G. K. Yue, Extinction coefficient (1 μm) properties of high-altitude clouds from solar occultation measurements (1985-1990): Evidence of volcanic aerosol effect, *J. Geophys. Res.*, 100, 3181-3199, 1995.
- Wigley, T. M. L., Possible climate change due to SO_2 -Derived cloud condensation nuclei, *Nature*, 339, 365-367, 1989.

Willeke K., P. A. Baron, *Aerosol Measurement: Principles, Techniques, and Applications*, pp. 48-49, Van Nostrand Reinhold, New York, 1993.

Appendix I:

1. Aerosol Volatility Measurements

Upon balloon descent, the aerosol inlet was heated to 160 °C to investigate the volatility of aerosols. Heating the air intake to 160 °C will evaporate sulfuric acid from the aerosol droplets within the air sample [Pinnick *et al.*, 1987; Rood *et al.*, 1987; Jennings and O'Dowd, 1990]. Aerosol volatility at 160 °C indicates that sulfuric acid aerosols have not been neutralized by ammonia (NH₃). O'Dowd *et al.* [1997] presented aerosol volatility measurements made in the South Atlantic and Antarctic Oceans that indicate a deficit of ammonia in polar air masses compared with maritime air masses. Silven and Legrand [1993] concluded from their measurements in Greenland that NH₃ is unable to neutralize the acidity of the high latitude atmosphere. These studies, along with Clarke's [1993] observation in the remote Pacific, suggest that tropospheric air above Laramie, Wyoming could be deficient in ammonia, which would allow sulfuric acid droplets to exist.

Figure 14 presents the summer Laramie, Wyoming descent (heated) aerosol concentrations and summarizes the ratio of the heated (160 °C) descent concentration to the 40 °C ascent concentration. The aerosol number ratios include measurements from all atmospheric layers, along with CCN measurements below the detection limit. For measurements below the detection limit ($\sim 20 \text{ cm}^{-3}$), the CCN concentration is determined using any detectable peak no matter where it occurs within the sample time or if no peak is detectable the concentration is set to 1 cm^{-3} . The median ratio is largest for the CN aerosol, decreases for the CCN aerosol, and is lowest for the D_{0.3} aerosols. This

indicates that heating the air to 160 °C had more of an effect on the larger size aerosols than on the smaller size aerosols. The inlet heater probably reduced the size of aerosols resulting in larger size aerosols not being large enough to be counted with the OPC, while smaller aerosols still have nonvolatile nucleus large enough to be activated within the CN counter.

Summer Flights at Laramie

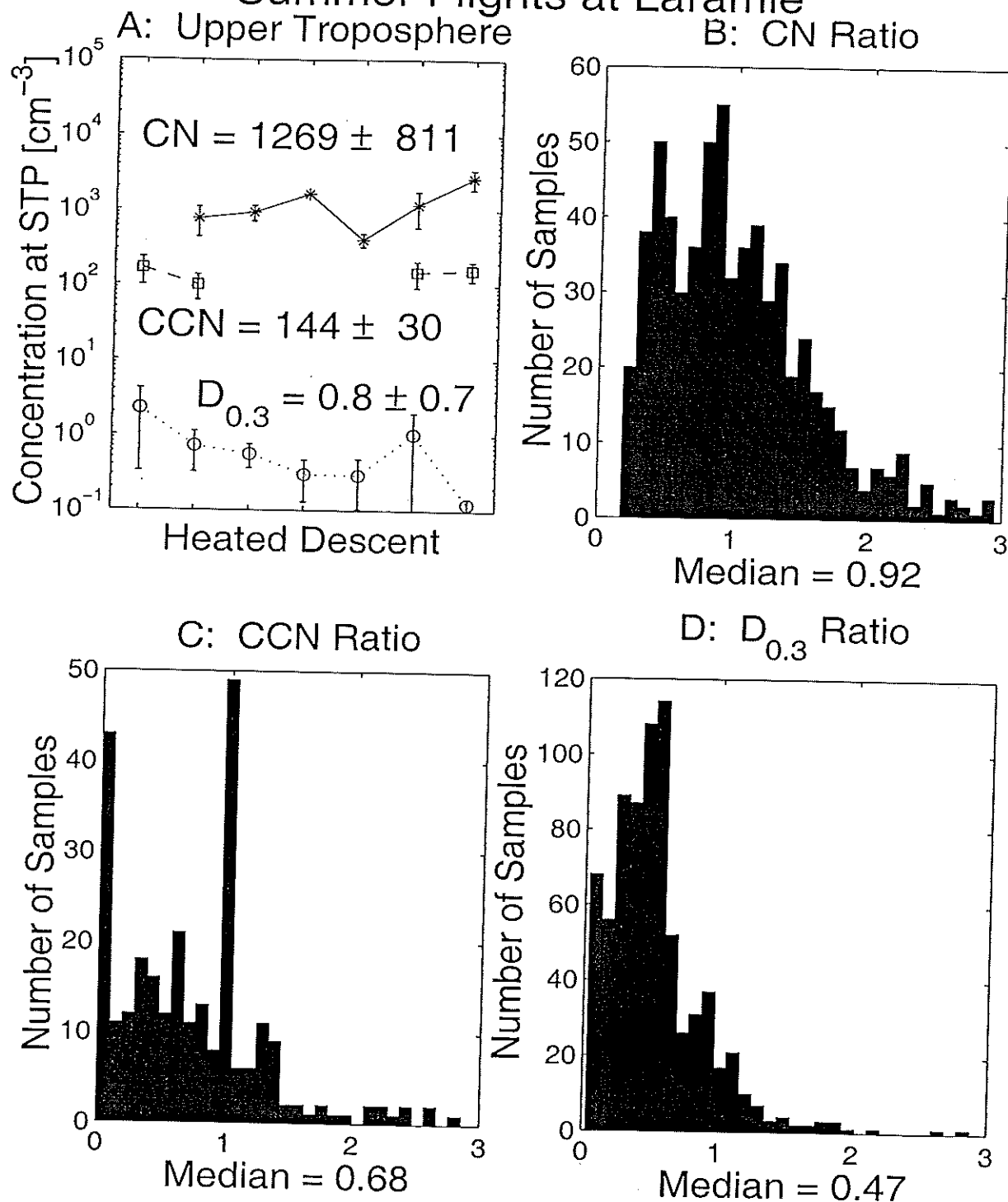


Figure 14. Plot showing the average upper tropospheric $D_{0.3}$ (circles), CCN (squares), and CN (asterisks) concentrations for each summer balloon descent profile obtain in Laramie, Wyoming. Histograms showing the ratio of heated (160°C) descent to 40°C ascent aerosol concentration ratios for all summer flights at Laramie, Wyoming.

Appendix II

1. CCN Counter Calibration Procedure

Calibration of the balloon-borne CCN counter consists of relating the measured photodetector voltage, resulting from the scattering of laser light by droplets, to the number concentration of droplets, and hence the number concentration of CCN. This relationship is determined by simultaneously measuring the photodetector voltage and using a video camera to image droplets within CCN counter's static thermal-gradient diffusion chamber. *Delene et al.*, [1998] presents background information on the calibration of the CCN counter. Below are listed the detail steps to follow when calibrating the CCN counter. A complete calibration at one supersaturation consists of six runs of 100 samples each. Each calibration run begins by wetting the top and bottom pads and checking the alignment of the video camera. An accurate calibration requires very close attend to the video camera alignment and lens focus setting. Video camera alignment consists of ensuring that the video camera is level and centered on the inlet tube. A missed aligned camera or an incorrectly set focus could easily results in a calibration that is incorrect by more than 10%.

1. Use a Q-tip with 2-Propanol to clean the laser, photodetector, and video camera windows. Also, clean the top and bottom plates of the chamber. It is best to clean the chamber the day before doing a calibration and after finishing using the CCN counter for the day. This allows time for the 2-Propanol to evaporate.
2. Remove the balloon-borne CCN counter from its plastic enclosure box
3. Bolt the CCN counter to the calibration bench.
4. Attach the video camera and lens to the calibration bench.

5. Turn on the video camera.
6. Turn on the TV monitor.
7. Turn on the PC computer, start windows, and run the calibration program "WINCCN4".
8. Check the dimensions of the rectangle that defines the video sample volume by selecting the set/rectangle bottom. The dimension should be, top = 240, left = 95, bottom = 360, and right = 405.
9. Display the video sample box by selecting the "Image Start" button.
10. Align video camera with the CCN counter. This requires adjusting the location of the video camera's lens so it is as close as possible to the CCN chamber window. The center of the video sample volume needs to be in the exact center of the inlet tube opening. The video camera needs to be checked with a small level to ensure that it is level.
11. Check that the video-sampling window encloses the top and bottom of the laser beam. This requires placing the "Ruler Top" on the chamber and connecting the CCN counter to power supply. After the video-sampling window is aligned, disconnect the CCN counter from its power supply and remove the "Ruler Top". The alignment of the video camera is very important and may require several adjustments.
12. Adjust the focus of the video lens by placing a Q-tip in the center of the chamber. Focus the lens on a Q-tip hair that is in the exact center of the chamber. A lamp may be used to illuminate the Q-tip hair. Q-tip hairs will appear dim when out of focus. The focus setting is very critical and difficult to set correctly.

13. Connect the "Balloon-borne CCN Counter 9-pin Cable" from the PC's comm port #1 to the "Storage" input on the CCN counter.
14. Connect the PC's comm port #2 to the "Console" input on the CCN counter.
15. Start the Windows Terminal Program. Select File/Open and choose the "BCCN.TRM" file.
16. Prepare a 0.1 g/L solution of NaCl and distilled water.
17. Fill humidifier half full of solution.
18. Place humidifier in corner next to the aerosol-mixing chamber. Turn on the humidifier and set "Mist Output" to ~80%.
19. Place PVC drying chamber tube on top of humidifier output. Turn on clear/dry air supply.
20. Connect the PVC aerosol output (top of PVC tube) to the aerosol/sheath air-mixing chamber.
21. Connect the mixing chamber to the CCN counter's air intake.
22. Turn on the ceiling pump. Switch is located on the back wall near to the hood.
23. Prepare two blotter pads by allowing them to sit in distilled water on a dish for 10 minutes. Only touch the edge of the pads with your fingers.
24. Place pads on the bottom and the top plates of chamber. Secure the top plate to chamber.
25. Connect CCN counter to power supply.
26. Start the Windows calibration program by selection the "Run" button. If the button is not in bold font, stop the video sample window by selecting the "Image Stop" window.

27. Set CCN counter's supersaturation using the terminal window.
28. Start the CCN counter by enter "10" in the terminal window.
29. Note the CCN counter supersaturation.
30. Note the "DN Threshold" value given in the Message window.
31. Select a low concentration of CCN (~10 droplets counted) by adjusting the ball value on the outlet of the drying chamber.
32. Check that the baseline voltage is less than -5.5. If not, stop and rewet pads.
33. Check that droplets are visible in the video sample box.
34. Check that all droplets within the video sample box are within focus. Out of focus droplet will appear large with dim centers. If there is out of focus droplet, stop and readjust the lens focus.
35. Increase the aerosol supply about every 20 samples. Don't exceed a count of 50 droplets.
36. After sample number 100 is completed, stop the calibration by pressing ctrl-D in the terminal window.
37. Close calibration program window.
38. Turn off CCN counter by disconnecting it from the power supply.
39. Calibration data is located in C:/delene/ccn/winccn4/ccn_cal.out. Copy this file to new directory and filename.
40. Use Excel template to analyze the calibration data.
41. To begin another calibration run, rewet pads and check the video camera alignment. Proceed to step 25.

2. Balloon-borne CCN Counter's Calibration History

Figure 15 presents the calibration constant of the balloon-borne CCN counter using the voltage peak method. The calibration constant is defined to be the calibration slope (e.g. Figure 2) divided by the video sample volume. The CCN counter's laser was replaced in November 1997, resulting in a 17% decrease in the calibration of the CCN counter. The thermal-gradient diffusion chamber was disassembled in February 1998 to replace the differential thermocouple. The CCN counter's differential thermocouple was tested in December 1997, before field measurements in New Zealand, and after being replaced in late February 1998. The tests consisted of measuring the temperature difference between the top and the bottom plates using a laboratory standard differential thermocouple. The differential thermocouple was placed within the thermal-gradient diffusion chamber with one lead placed on the top blotter paper and the other lead placed on the bottom blotter paper. The tests confirmed that the CCN counter's prescribed temperature difference is accurate. A new video camera, with a different video sample volume, resulted in an 18% decrease in the CCN counter's calibration constant as compared to the old video camera. Since the calibration using the new video camera is more accurate (see chapter 2), the calibration difference between the old and new video camera is used to adjust the calibration constant when processing field data taken before November, 1997. The calibration difference between 0.5 g/L of NaCl and 0.1 g/L of NaCl (Figure 15) is probably due to systematic difference in the alignment and setup of the video camera system.

Balloon-Borne CCN Counter Calibration

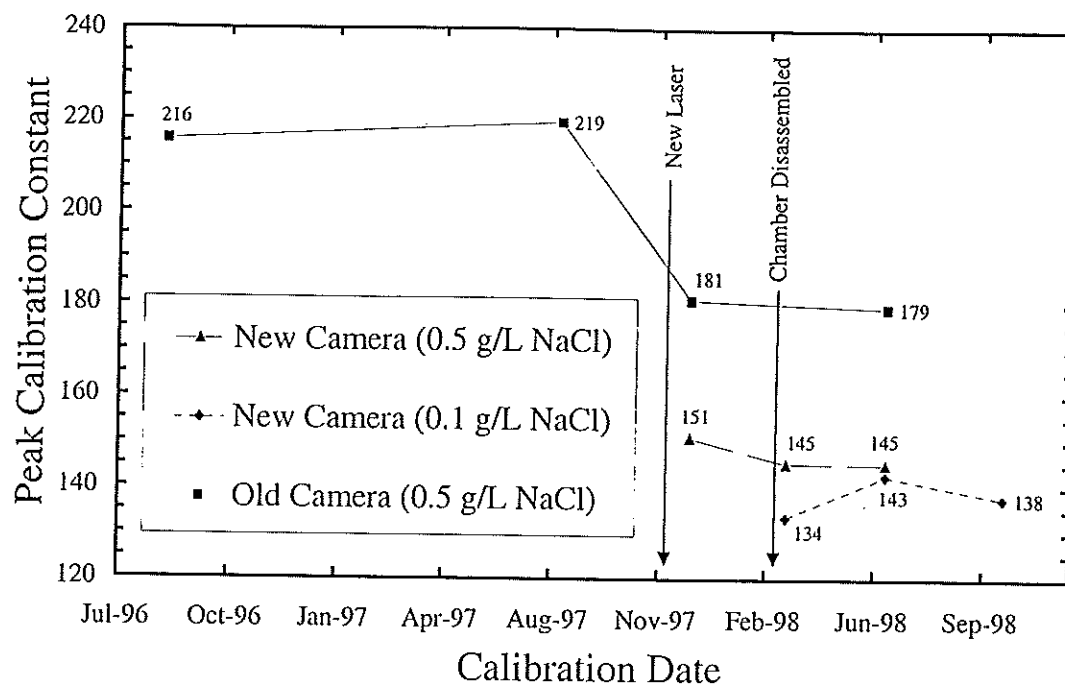


Figure 15. Calibration constants for the CCN counter using the peak calibration method. The old video camera calibration constant is based on a 0.0314 cm^3 video sample volume and the new video camera calibration constant is based on a 0.0707 cm^3 video sample volume. The legend indicates the concentration of the NaCl solution using in the vaporizer to produce the calibration aerosol.

Appendix III:

1. CCN Counter Data Processing

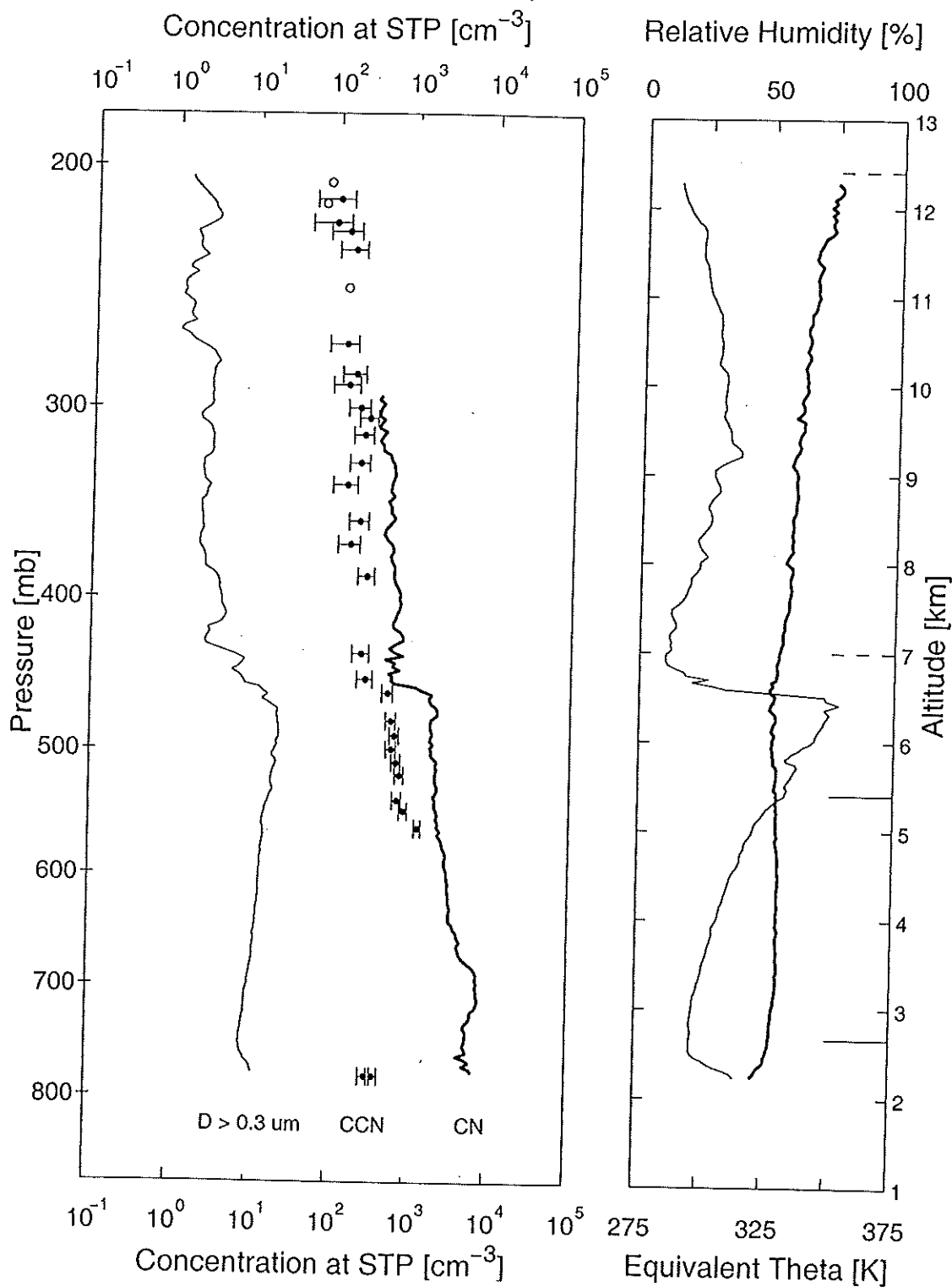
During balloon flights, the photodetector voltage, top plate temperature, temperature difference between the top and bottom plate, laser current, laser power, ambient pressure, CCN counter's state, and enclosure temperature of the CCN counter are stored at 1 Hz on a nonvolatile data module. Along with storing the CCN counter's data, the data module is also used to backup data from the balloon package aerosol instruments. A BASIC program, "read.bas", uses the comm port on a PC to download the data module. A C processing code, "ccn", extracts the balloon package data to an ASCII file (B*.ra1) and produces several ASCII text files containing the CCN processed data. The processing code produces a "readme" file that contains processing notes and a description of each data file produced. A Matlab code, "ccn.m", is used to analyze the balloon flight data and produce standard data plots. The Matlab code combines the CCN data with processed data from the balloon package aerosol instruments. The Matlab analysis program uses a description file, "balloon_*.m", to provide balloon flight information, input data file locations, and information about what plots to produce. The description file needs to be edited when additional balloon flights are added to the data set. After each plot is displayed on the screen, an encapsulated postscript file is produce that can be printed or imported into a word processor, such as "Microsoft Word"

2. Standard Plot of all Balloon Flights

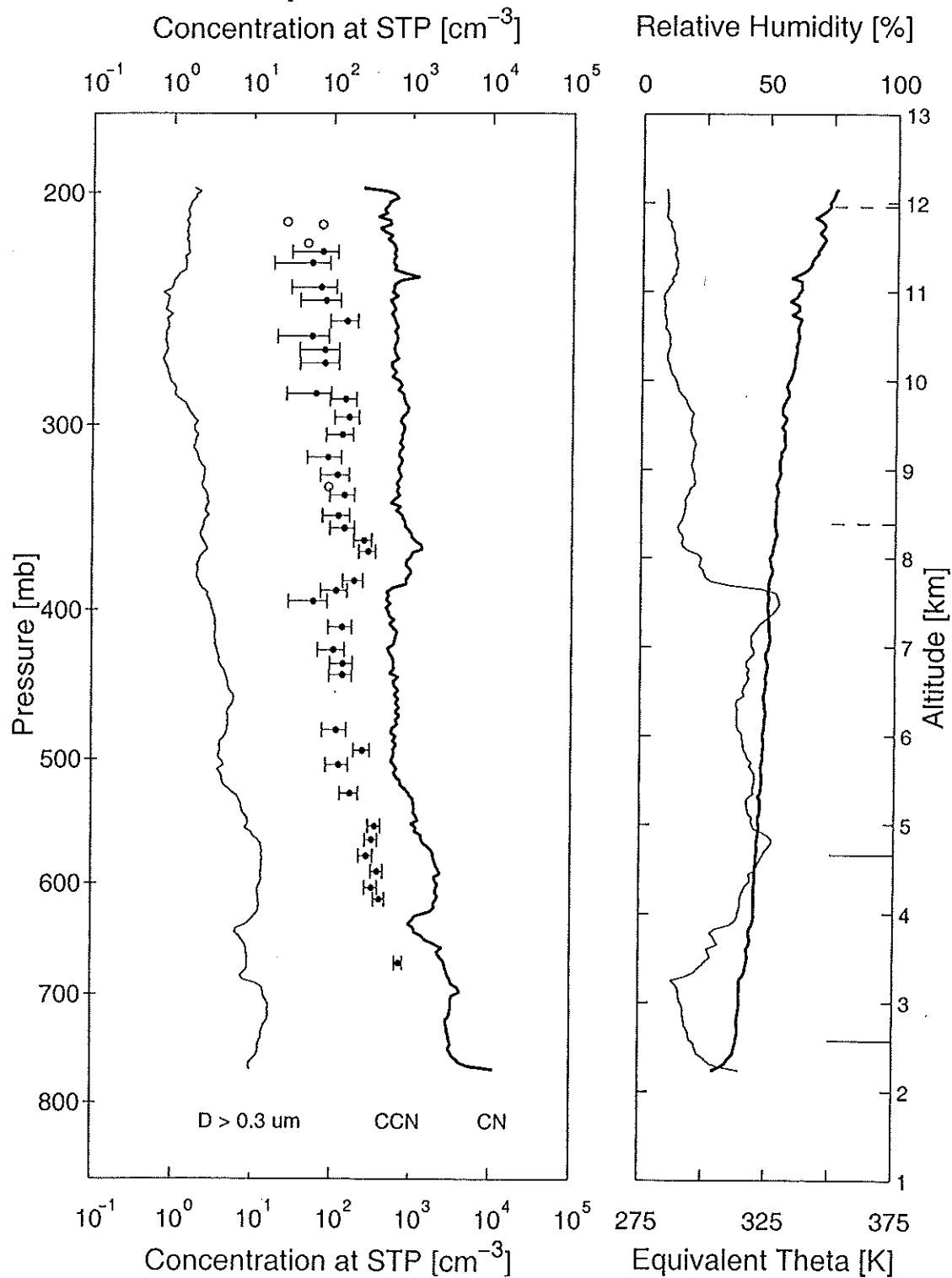
The Matlab code, "ccn.m", produces several standard plots that combine the CCN, CN and optical aerosol concentrations. Shown on the following pages are the balloon profiles for all fourteen flights that have CCN data. Each plot gives the optical aerosol concentration for aerosols larger than $0.3\ \mu\text{m}$ in diameter ($D_{0.3}$, thin line), the CCN concentration (circles), and the CN concentration ($D > 0.01\ \mu\text{m}$, thick line). Open circles represent measurements below the detection limit of the CCN counter. The concentration measured by each aerosol instrument has been corrected to standard temperature and pressure (STP). This gives a concentration which is similar to mixing ratio where the change in concentration due to changes in pressure and temperature have been removed. Equivalent potential temperature (thick line) and relative humidity (thin line) are shown in the right-hand panel. The lines on the right side of the right-hand panel denote the lower (solid lines) and upper (dashed lines) tropospheric layers.

a

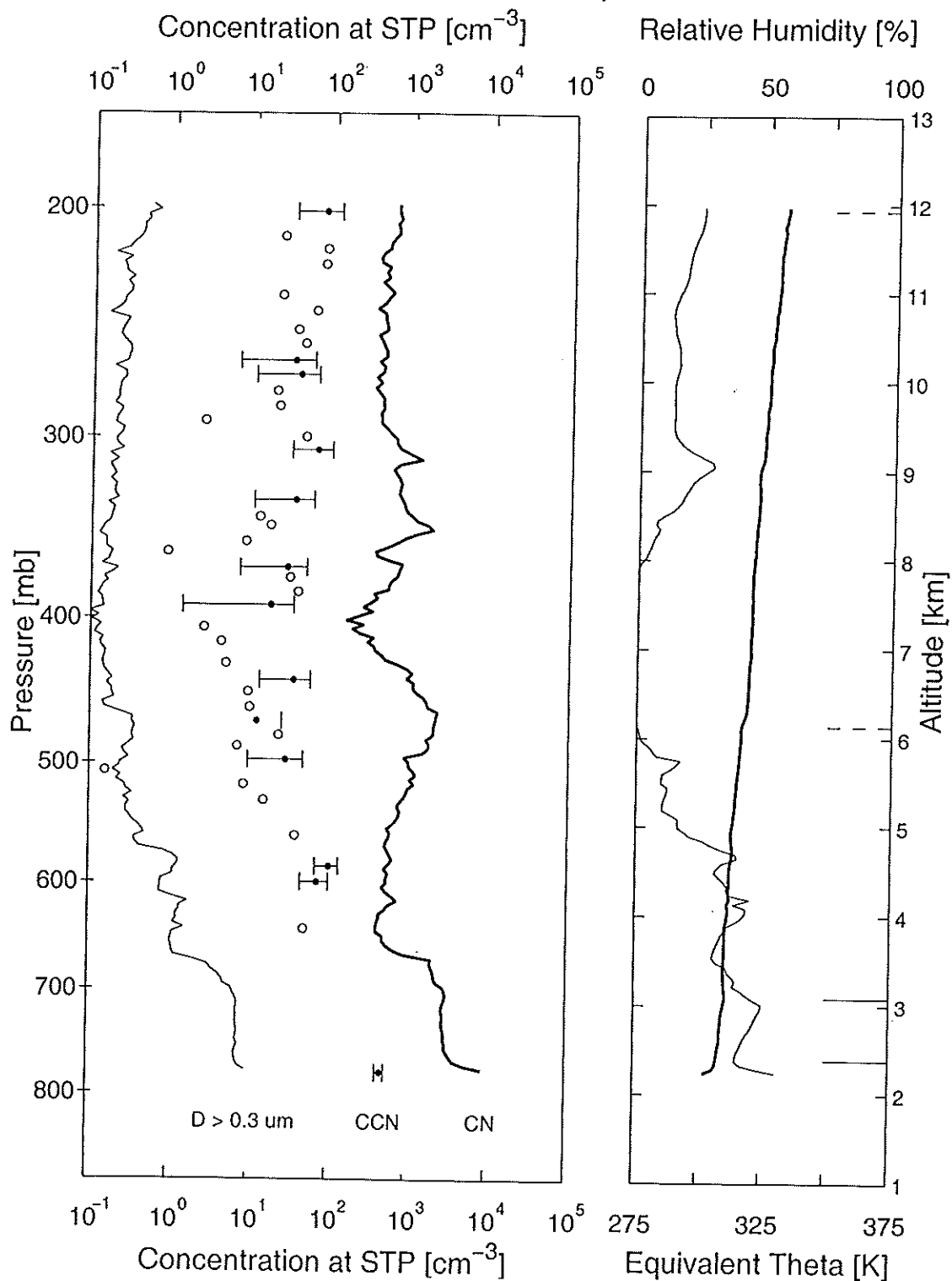
June 13, 1995



b September 26, 1995

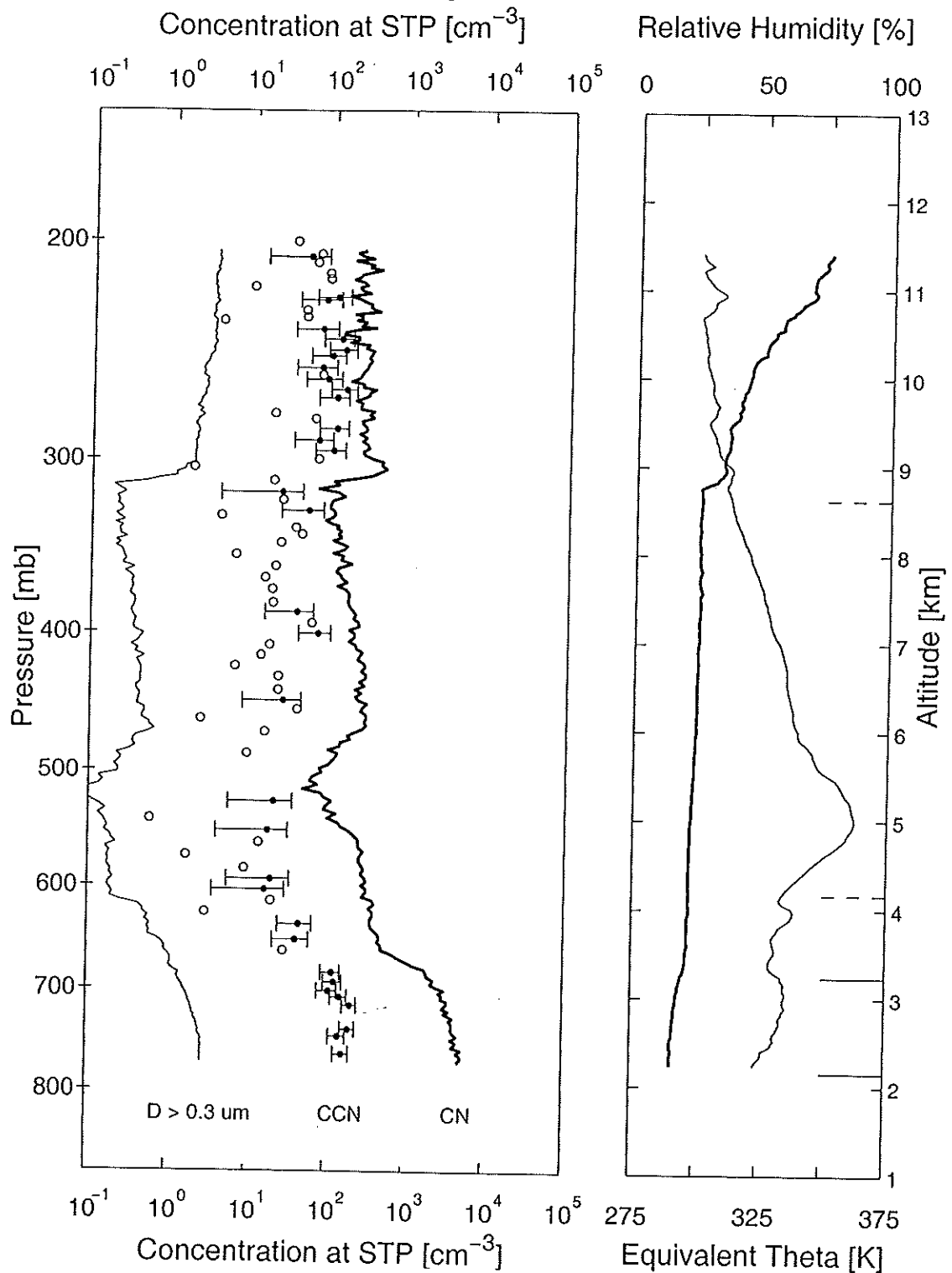


C November 21, 1995



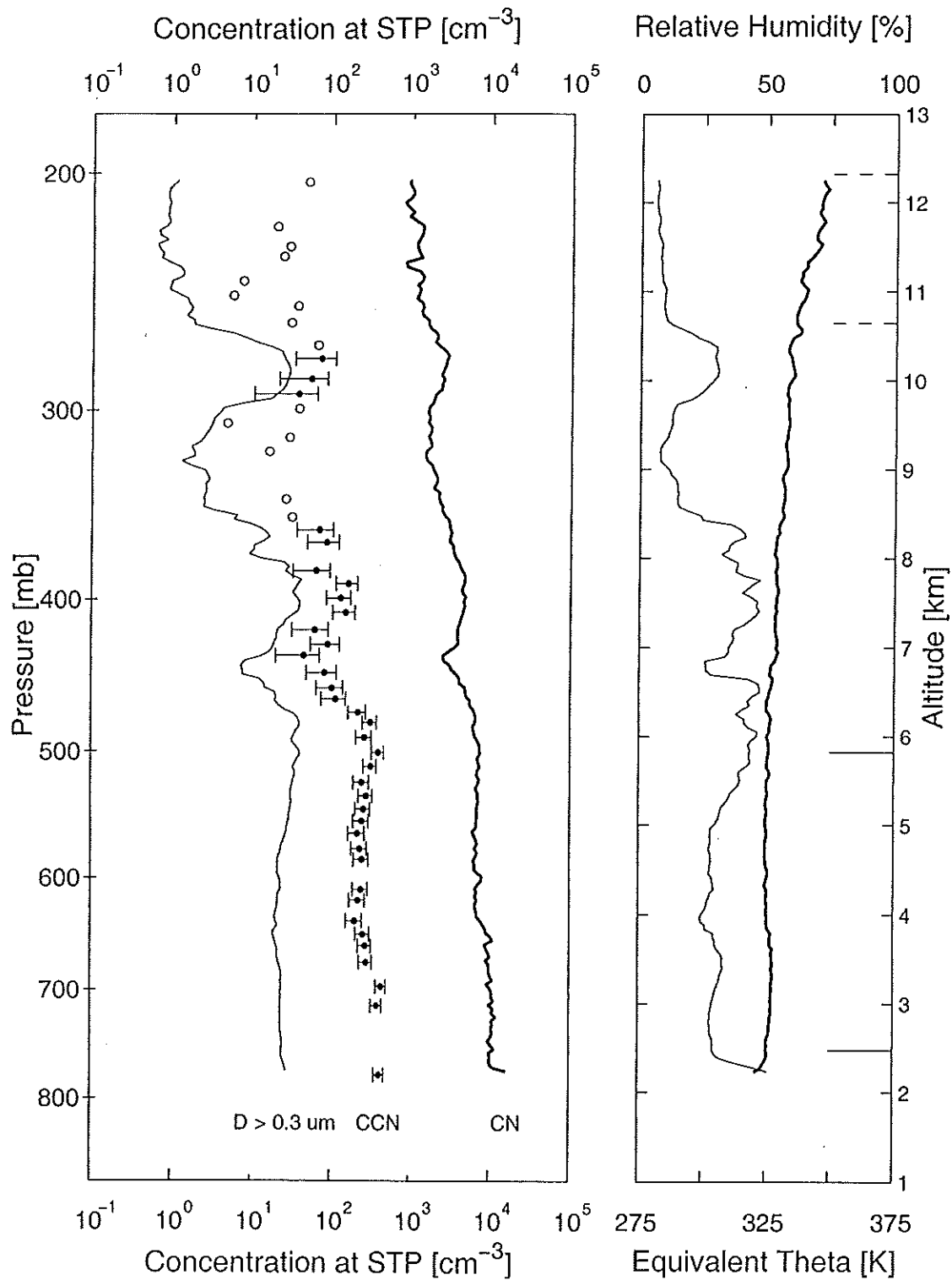
d

January 24, 1996



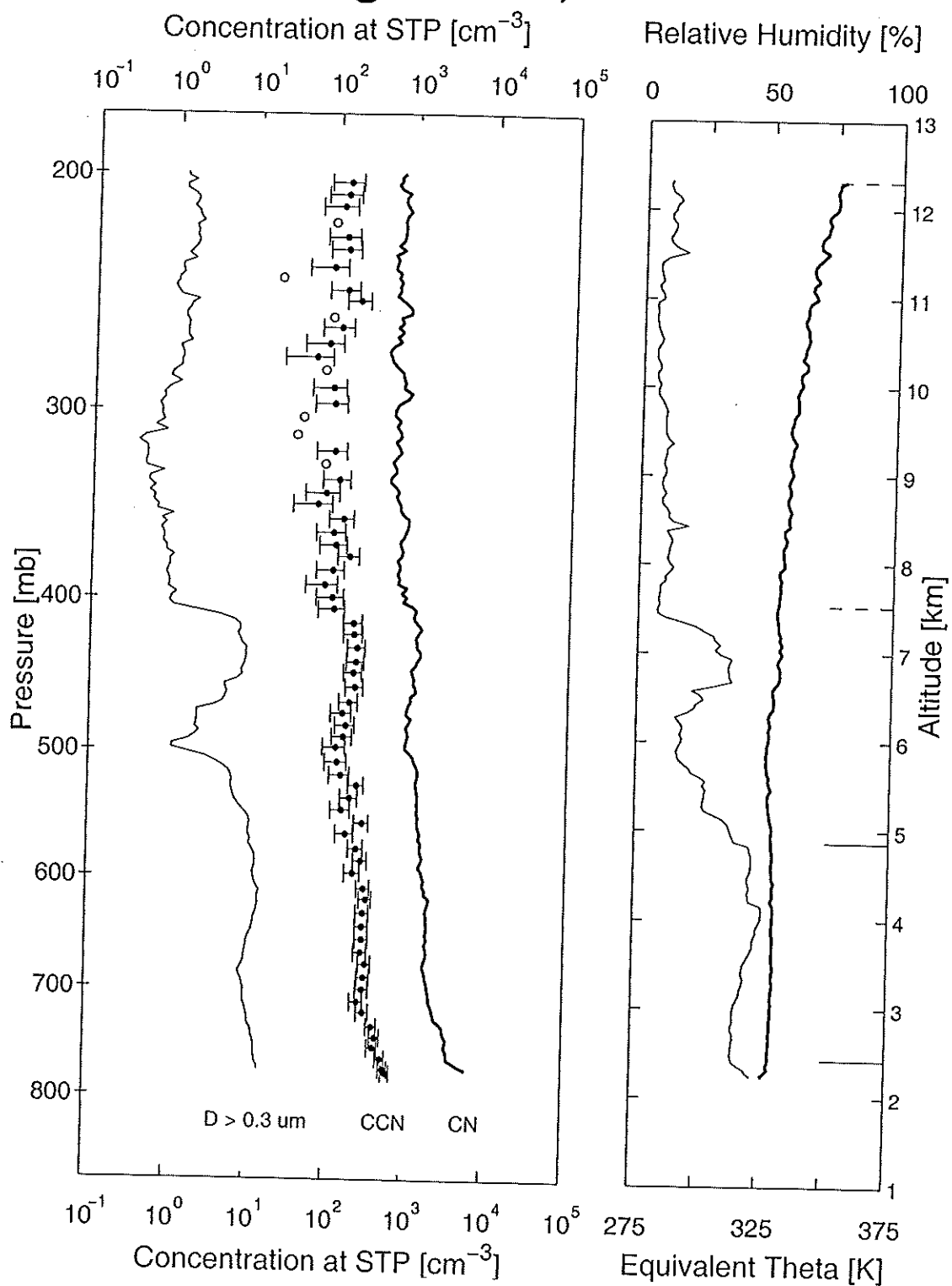
e

June 10, 1996



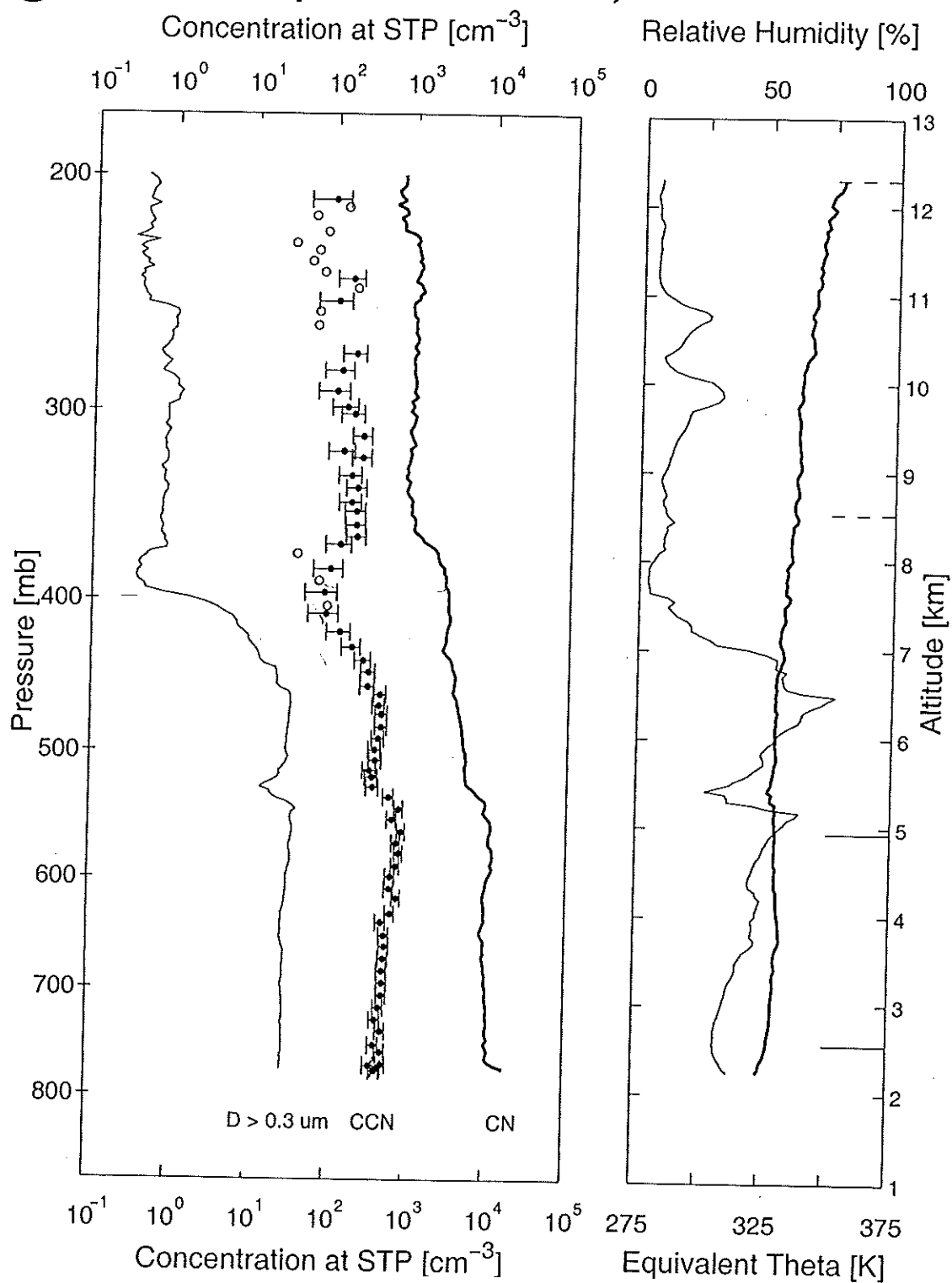
f

August 02, 1996



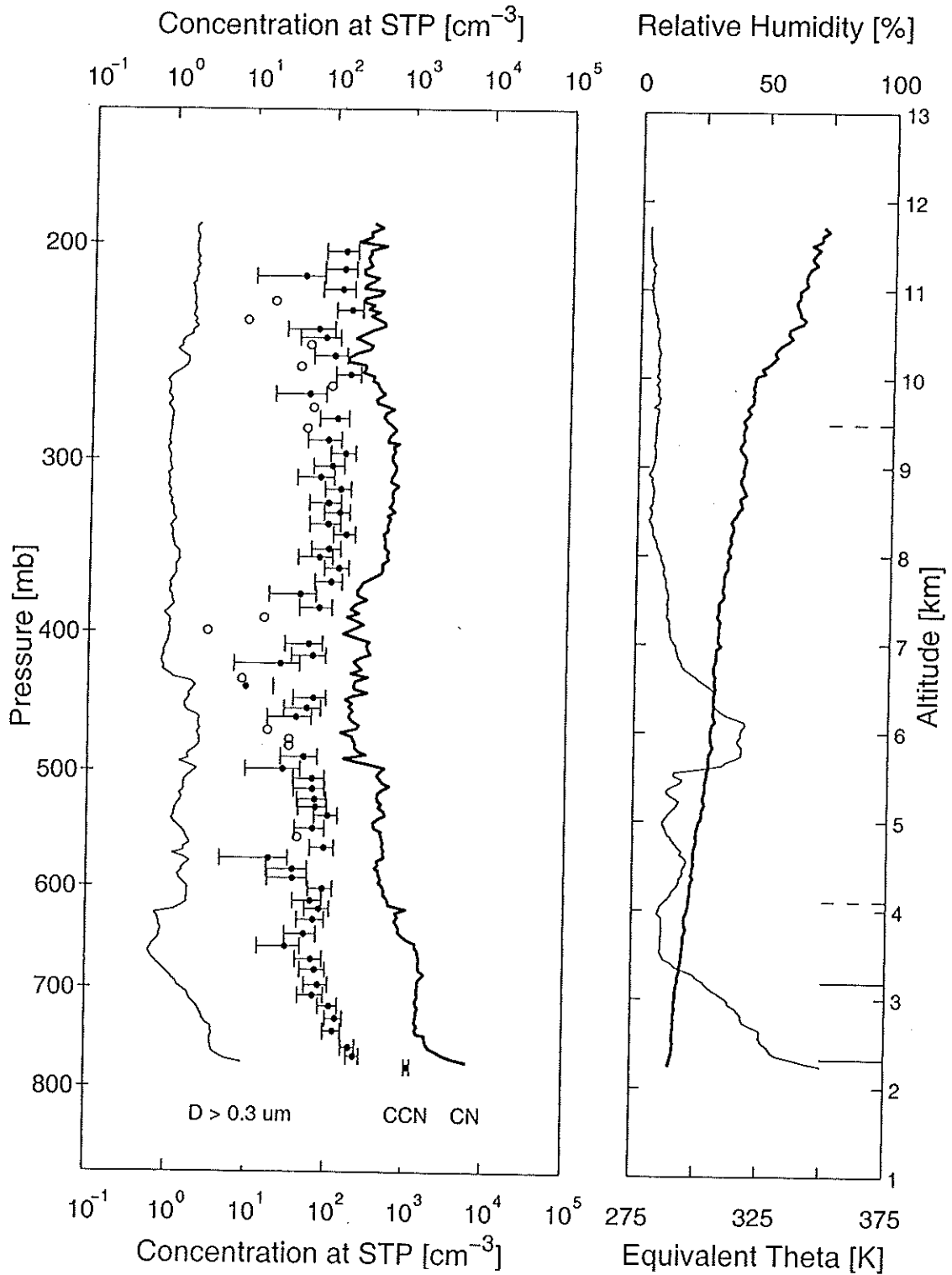
g

September 05, 1996



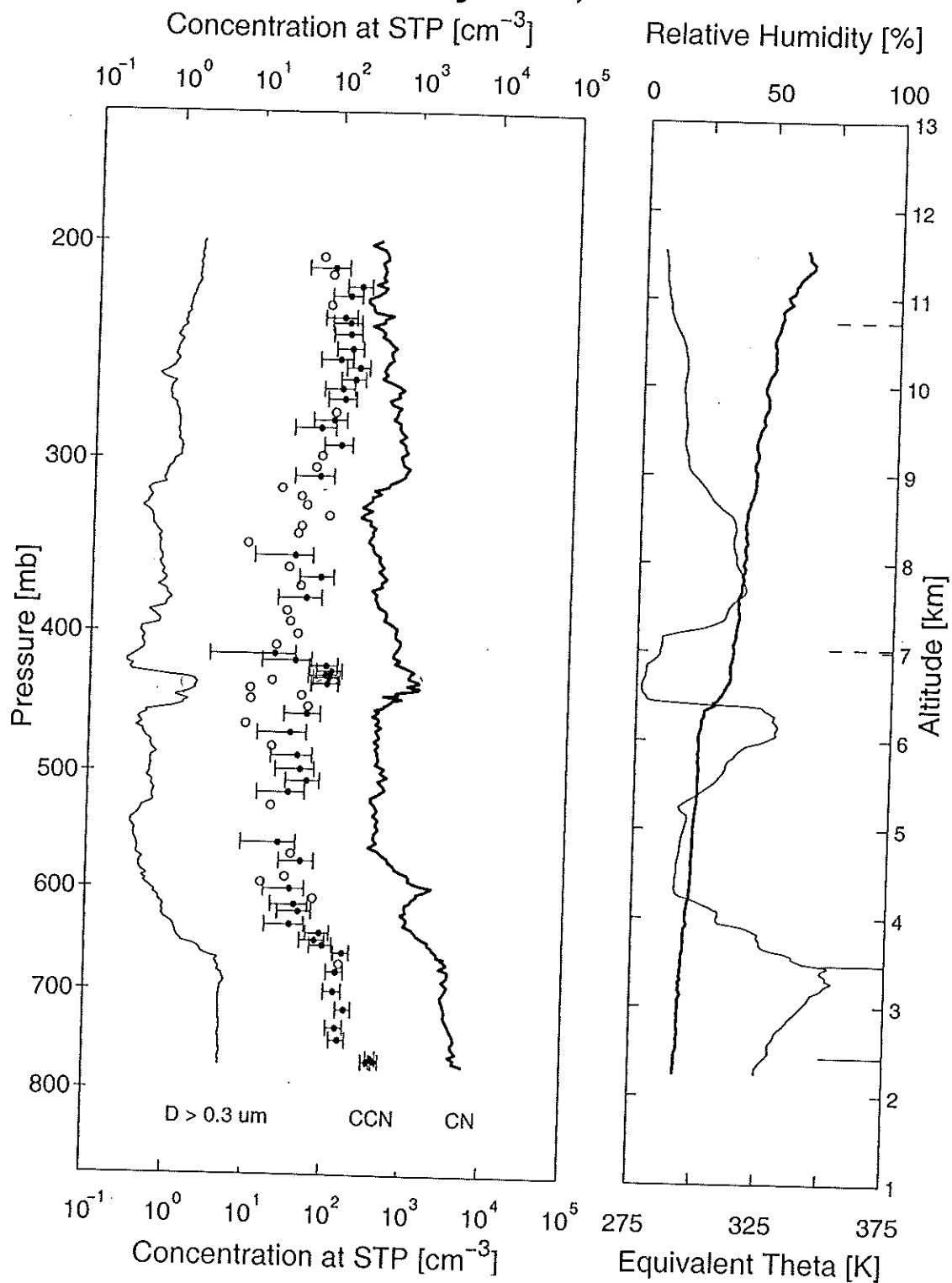
h

November 27, 1996



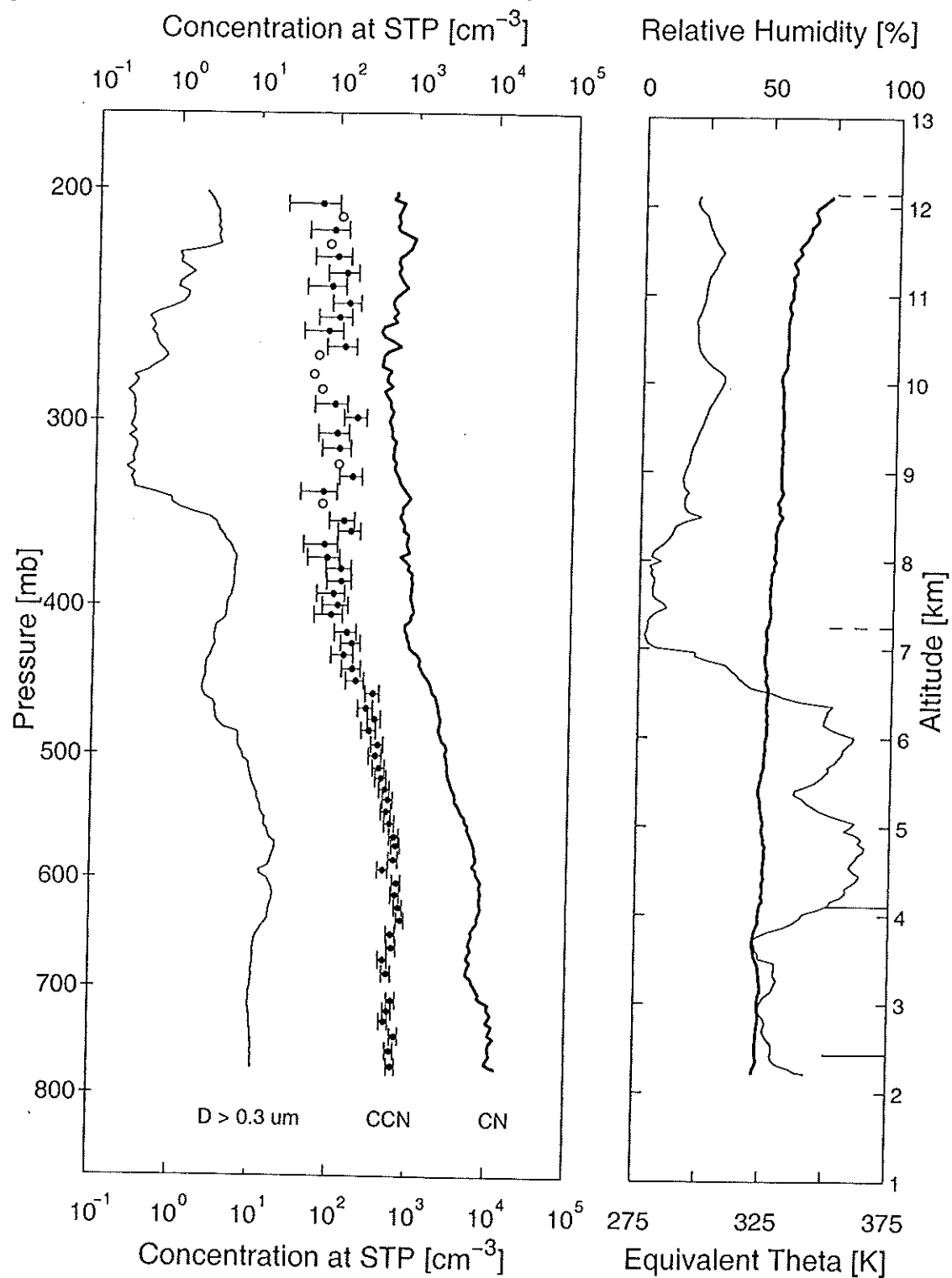
i

January 22, 1997



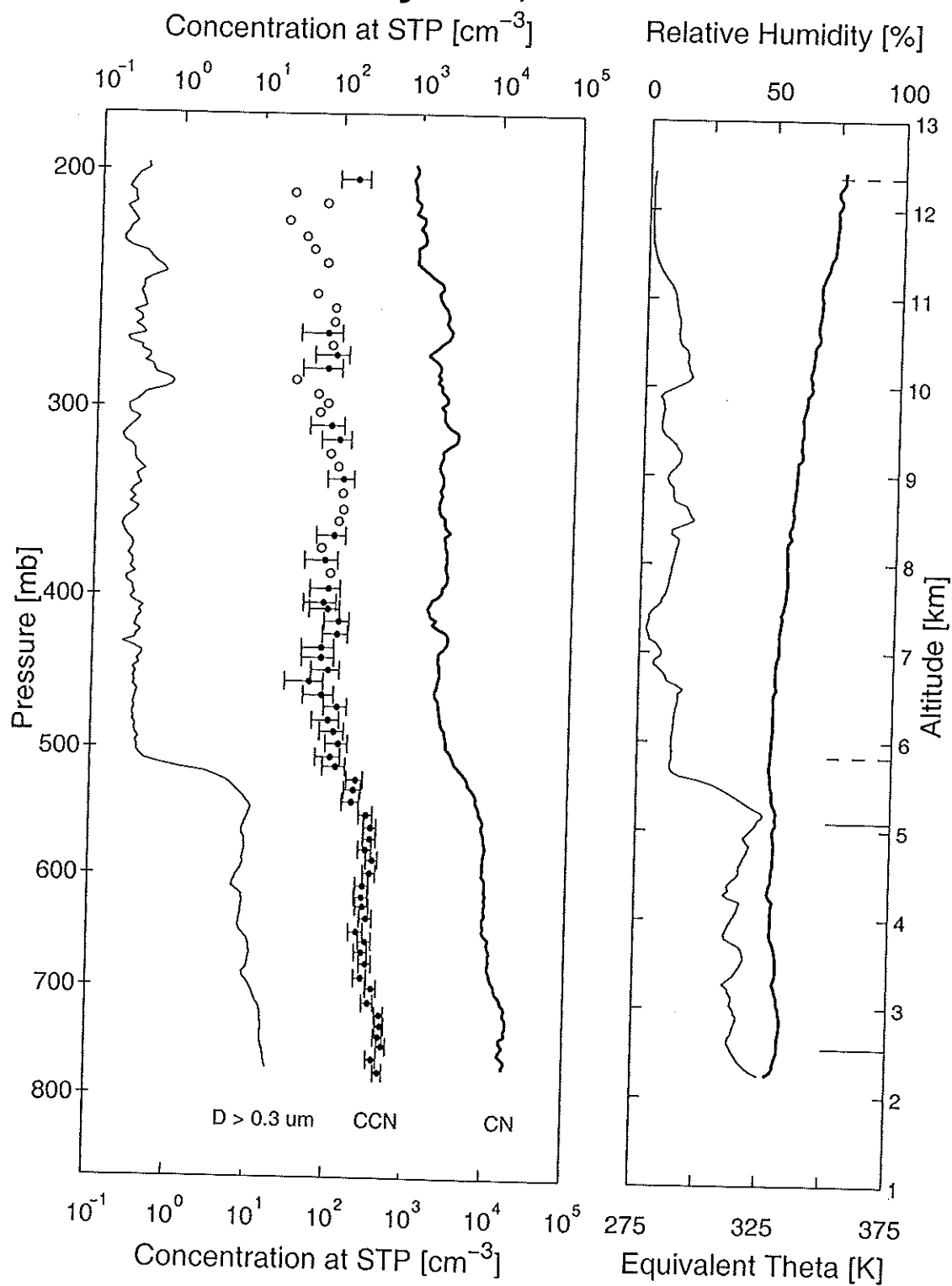
j

June 12, 1997

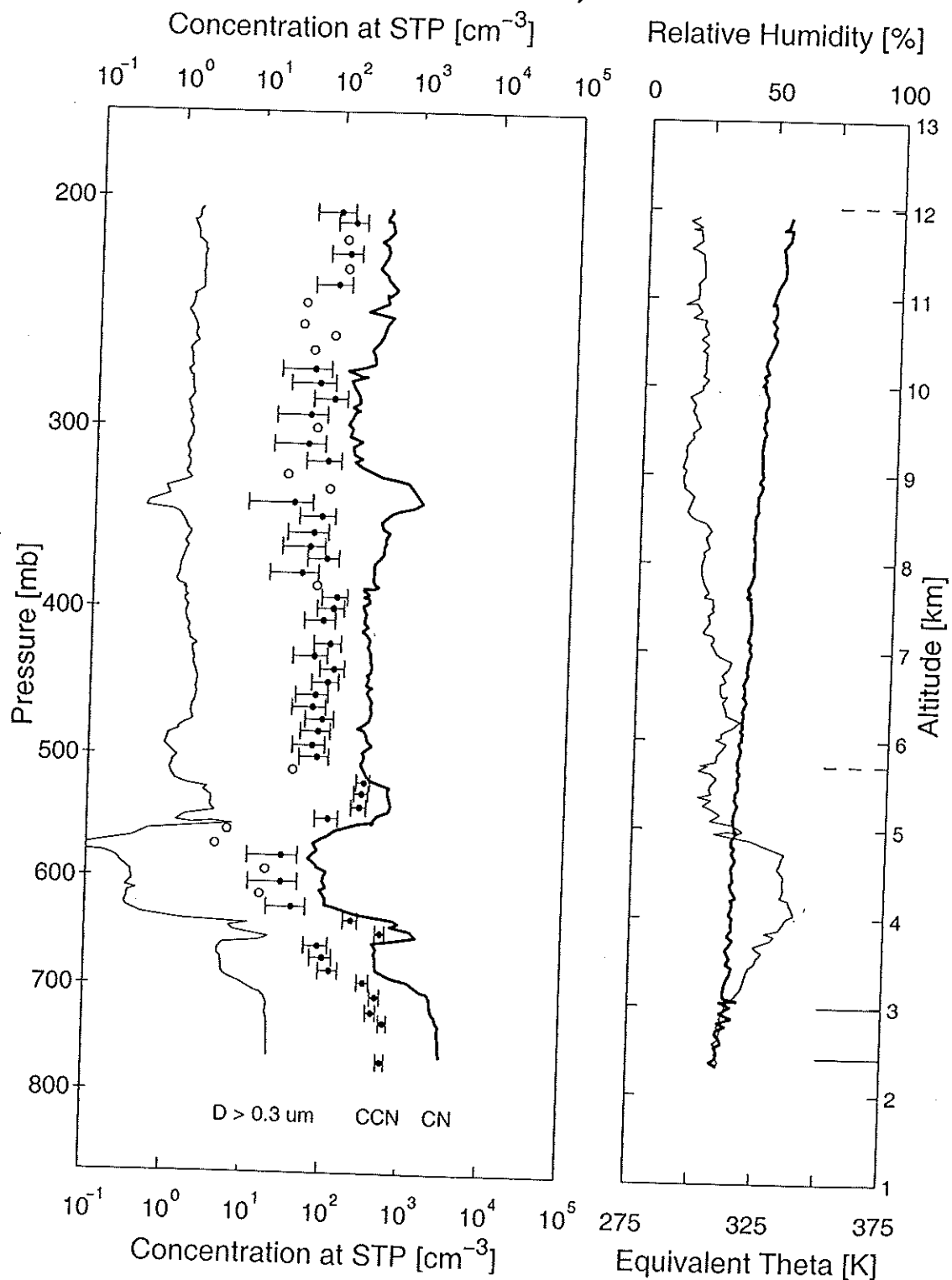


k

July 25, 1997

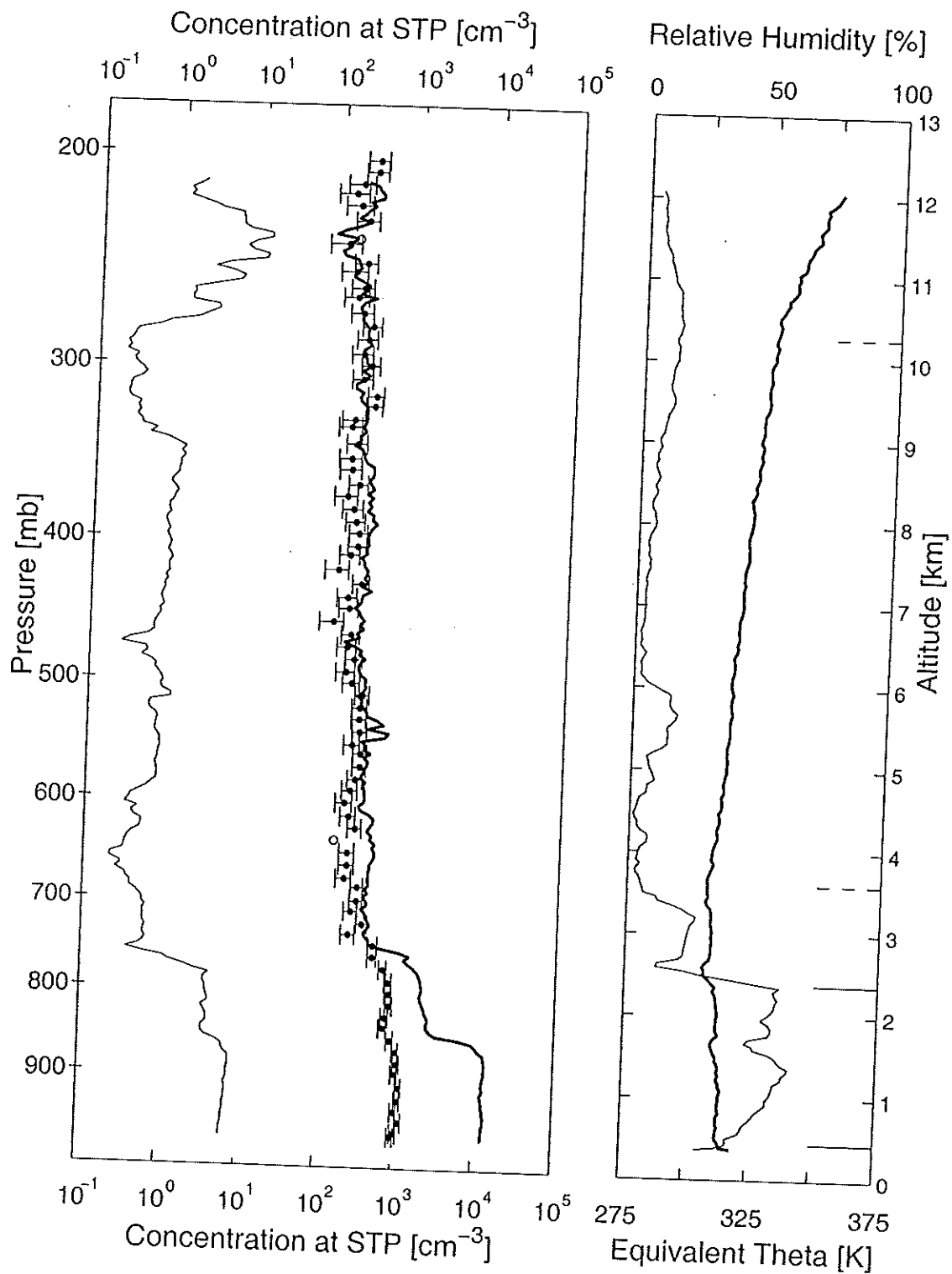


October 22, 1997



m

January 22, 1998



n

February 03, 1998

